

# **Role of integrin-linked kinase (ILK) in VEGFR3 signaling and lymphatic vascular growth**

Inaugural-Dissertation

for the attainment of the title of doctor  
in the Faculty of Mathematics and Natural Sciences  
at the Heinrich Heine University Düsseldorf

presented by

**Sofia Urner**

from Kostanay, Kazakhstan

Düsseldorf, November 2017

From the Institute of Metabolic Physiology  
at the Heinrich Heine University Düsseldorf

Published by permission of the  
Faculty of Mathematics and Natural Sciences at  
Heinrich Heine University Düsseldorf

Supervisor: Prof. Dr. Eckhard Lammert  
Co-supervisor: Prof. Dr. Axel Gödecke

Date of the oral examination: 19.02.2018

## Table of Content

<b>I. List of abbreviations</b> .....	<b>VI</b>
<b>1. Summary</b> .....	<b>1</b>
<b>2. Zusammenfassung</b> .....	<b>2</b>
<b>3. Introduction</b> .....	<b>4</b>
3.1. The lymphatic vasculature .....	4
3.1.1. Physiological relevance and organization of the lymphatic vasculature.....	4
3.1.2. Clinical relevance of the lymphatic vasculature .....	6
3.1.3. Embryonic development of the lymphatic vasculature .....	8
3.2. Vascular endothelial growth factor receptor 3 (VEGFR3).....	10
3.2.1. The vascular endothelial growth factor receptor (VEGFR) family .....	10
3.2.2. Ligand-induced VEGFR3 signaling.....	11
3.2.3. Mechano-induced VEGFR3 signaling.....	12
3.3. Integrin-linked kinase (ILK) .....	15
3.3.1. Physiological function of ILK.....	15
3.3.2. The ILK/PINCH/parvin (IPP) complex.....	17
3.4. Aims of the study.....	19
<b>4. Experimental procedures</b> .....	<b>21</b>
4.1. Mouse models .....	21
4.1.1. Genotyping.....	22
4.2. <i>Ex vivo</i> and <i>in vivo</i> methods.....	23
4.2.1. Magnetic-activated cell sorting (MACS).....	23
4.2.2. Corneal angiogenesis assays .....	24
4.2.3. Myocardial infarction .....	25
4.3. <i>In vitro</i> methods.....	26
4.3.1. Cell culture and transfections .....	26
4.3.2. <i>In vitro</i> proliferation assays .....	27
4.4. Molecular biological methods.....	28
4.4.1. Quantitative real-time PCR .....	28
4.5. Biochemical methods .....	30
4.5.1. Co-immunoprecipitation (Co-IP) .....	30
4.5.2. Western Blotting.....	30
4.5.3. ELISA.....	32
4.6. Histochemical methods .....	33
4.6.1. Whole-mount stainings .....	33
4.6.2. Immunohistochemistry.....	34

---

4.6.3. Proximity ligation assays (PLA) .....	35
4.6.4. Imaging and image analysis .....	36
4.7. Statistics .....	37
4.8. Personal contributions.....	37
<b>5. Results.....</b>	<b>39</b>
5.1. Role of ILK in lymphatic vascular growth during mouse embryonic development.....	39
5.1.1. ILK controls lymphatic vascular expansion and LEC proliferation during mouse embryonic development.....	40
5.1.2. ILK controls VEGFR3 rather than VEGFR2 signaling in LECs during mouse embryonic development.....	41
5.2. Role of caveolin-1 in lymphatic vascular growth during mouse embryonic development	44
5.2.1. Caveolin-1 is not required to control lymphatic vascular expansion, LEC proliferation and VEGFR3 signaling during mouse embryonic development.....	44
5.3. Role of $\beta$ 1 integrin in ILK-regulated lymphatic vascular growth during mouse embryonic development.....	47
5.3.1. ILK controls interactions between VEGFR3 and $\beta$ 1 integrin in LECs during mouse embryonic development.....	47
5.3.2. The effect of <i>Ilk</i> deletion on lymphatic vascular expansion during mouse embryonic development depends on $\beta$ 1 integrin .....	48
5.4. Role of $\alpha$ -parvin in lymphatic vascular growth during mouse embryonic development....	52
5.4.1. $\alpha$ -parvin is involved in controlling lymphatic vascular expansion and LEC proliferation during mouse embryonic development.....	53
5.5. Role of ILK in the adult mouse lymphatic vasculature .....	56
5.5.1. ILK controls lymphatic vascular expansion in the avascular adult mouse cornea..	56
5.5.2. ILK controls lymphatic vascular expansion, LEC proliferation and VEGFR3 signaling in the adult mouse skin.....	58
5.5.3. ILK controls lymphatic vascular expansion after myocardial infarction (MI) in the adult mouse heart .....	60
5.6. Role of ILK in adult human LECs .....	62
5.6.1. ILK controls LEC proliferation and VEGFR3 signaling in adult human LECs.....	63
5.6.2. ILK controls interactions between VEGFR3 and $\beta$ 1 integrin in adult human LECs	64
5.6.3. ILK dissociates from $\beta$ 1 integrin upon mechanical stimulations of adult human LECs .....	65
<b>6. Discussion .....</b>	<b>68</b>
6.1. Role of ILK in VEGFR3 signaling, LEC proliferation and lymphatic vascular growth .....	68
6.1.1. Role of ILK in regulating LEC proliferation and lymphatic vascular growth.....	68
6.1.2. Role of ILK in regulating VEGFR3 signaling.....	70
6.1.3. Role of ILK in regulating lymphatic vascular growth after MI.....	71
6.2. Underlying mechanism of the regulatory function of ILK in VEGFR3 signaling and lymphatic vascular growth.....	72

6.2.1. Role of caveolin-1 .....	73
6.2.2. Role of $\beta$ 1 integrin.....	73
6.2.3. Role of $\alpha$ -parvin.....	75
6.2.4. Role of mechanical stretch.....	76
6.3. Conclusion.....	77
<b>7. Publications .....</b>	<b>78</b>
<b>8. References .....</b>	<b>79</b>
<b>9. Supplementary information .....</b>	<b>90</b>
<b>Statutory declaration.....</b>	<b>91</b>
<b>Danksagung .....</b>	<b>92</b>

## I. List of abbreviations

### A

AF	Alexa Fluor
ANOVA	Analysis of variance

### B

B2M	Beta-2-microglobulin
bp	Base pair
BCA	Bicinchoninic acid
BrdU	5-bromo-2'-deoxyuridine
BSA	Bovine serum albumin

### C

Ca <sup>2+</sup>	Calcium
Cav1	Caveolin-1
CCBE1	Collagen- and calcium-binding EGF domains 1
cDNA	Complementary DNA
CH-ILKBP	Calponin homology (CH) domain-containing ILK-binding protein
Co-IP	Co-immunoprecipitation
Com	Common
COUP-TFII	COUP transcription factor 2
C <sub>T</sub>	Cycle threshold
CV	Cardinal vein

### D

DAPI	4',6-Diamidino-2-Phenylindole
DNA	Deoxyribonucleic acid

### E

E	Embryonic day
EBM-2	Endothelial cell basal medium
ECG	Electrocardiography
ECL	Enhanced Chemiluminescence
ECM	Extracellular matrix
EGM-2 MV	Endothelial cell growth factor medium MV2
ELISA	Enzyme-linked immunosorbent assay

**F**

FITC	Fluorescein isothiocyanate
Flk1	Fetal liver kinase 1
Flt1	fms-like tyrosine kinase1
Flt4	fms-like tyrosine kinase 4
Fwd	Forward

**G**

GAPDH	Glyceraldehyde 3-phosphate dehydrogenase
-------	--

**H**

h	Hour
HA	Human influenza hemagglutinin
HBSS	Hank's Balanced Salt Solution
HCl	Hydrogen chloride
HEPES	4-(2-hydroxyethyl)-1-piperazineethanesulfonic acid
HRP	Horseradish peroxidase

**I**

IgG	Immunoglobulin G
ILK	Integrin-linked kinase
IPP	ILK/PINCH/parvin
ISV	Intersomitic vessel

**J**

jls	Jugular lymph sac
-----	-------------------

**K**

K.O.	Knockout
------	----------

**L**

LAD	Left anterior descending coronary artery
LECs	Lymphatic vascular endothelial cells
LSM	Laser scan microscopy

**M**

M	Molar
MACS	Magnetic-activated cell sorting
Mg <sup>2+</sup>	Magnesium
MI	Myocardial infarction
min	Minute
MOPS	3-(N-morpholino)propanesulfonic acid

**N**

NaCl	Sodium chloride
NDS	Normal donkey serum
NaF	Sodium fluoride
NaN <sub>3</sub>	Sodium azide
Na <sub>3</sub> VO <sub>4</sub>	Sodium orthovanadate

**O**

OCT	Optimal cutting temperature
o/n	Over night

**P**

PBS	Phosphate-buffered saline
PECAM-1	Platelet endothelial cell adhesion molecule
PCR	Polymerase chain reaction
PFA	Paraformaldehyde
pH3	Phospho-Histone H3
PI3K	Phosphoinositide 3-kinase
PIGF	Placental growth factor
PKC	Protein kinase C
PLA	Proximity ligation assay
PINCH	Particularly interesting new cysteine-histidine-rich protein
PPIA	Peptidylprolyl isomerase A
pTD	Primordial thoracic duct
p-Tyr	Phosphorylated tyrosine

**R**

Rev	Reverse
rpm	Revolutions per minute
RNA	Ribonucleic acid
RT	Room temperature
RTK	Receptor tyrosine kinase

**S**

Sec	Seconds
SEM	Standard error of the mean
siRNA	Silencing interfering RNA
SMCs	Smooth muscle cells

**T**

Tyr	Tyrosine
-----	----------

**U**

U	Unit
---	------

**V**

V	Volt
VECs	Vascular endothelial cells
VEGF	Vascular endothelial growth factor
VEGFR1	Vascular endothelial growth factor receptor 1
VEGFR2	Vascular endothelial growth factor receptor 2
VEGFR3	Vascular endothelial growth factor receptor 3
Vol	Volume

**W**

WMS	Whole-mount staining
-----	----------------------

## 1. Summary

The lymphatic vasculature is part of the circulatory system, and critically required for the maintenance of fluid homeostasis in the body. Dysfunctional lymphatic vasculature therefore is associated with pathological conditions like lymphedema. Further, several recent studies provided evidence that lymphatic vascular remodeling is highly associated with cardiovascular disease, such as myocardial infarction (MI). Therefore, it is essential to understand the underlying regulatory processes of lymphatic vascular growth.

Lymphatic vascular growth is critically regulated by the vascular endothelial growth factor receptor 3 (VEGFR3), which is highly expressed by lymphatic endothelial cells (LECs). VEGFR3 signaling can be ligand-induced, such as by binding of the vascular endothelial growth factor (VEGF)-C or -D, as well as mechano-induced via  $\beta$ 1 integrin. As a consequence, VEGFR3 tyrosine phosphorylation is induced, which leads to LEC survival, migration, and proliferation. In this study, we focused on analyzing the role of integrin-linked kinase (ILK), which is known to bind to  $\beta$ 1 integrin, in VEGFR3 signaling and lymphatic vascular growth. We analyzed mouse embryos with endothelial cell-specific *Ilk*-deficiency, adult mice with tamoxifen-induced LEC-specific deletion of *Ilk*, and adult human LECs upon silencing of *ILK*. Surprisingly, we found that ILK is a critical inhibitor of VEGFR3 tyrosine phosphorylation, LEC proliferation and lymphatic vascular expansion. Our results further indicate that ILK prevents VEGFR3 and  $\beta$ 1 integrin interaction, thereby inhibiting  $\beta$ 1 integrin-mediated VEGFR3 signaling, as supported by our genetic rescue experiments, in which we analyzed mouse embryos with endothelial cell-specific deletion of both *Ilk* and *Itgb1*. Since ILK is often described as the central component of the ILK/PINCH/parvin (IPP) complex, we also investigated mouse embryos with endothelial cell-specific deletion of *Parva*, which indicate that  $\alpha$ -parvin is also involved in regulating LEC proliferation and lymphatic vascular growth during embryonic development. Next, we aimed to define the physiological mechanism of how ILK regulates VEGFR3 signaling. We used adult human LECs for mechanical stretch experiments, which revealed that ILK dissociates from  $\beta$ 1 integrin upon stretch, while interactions between VEGFR3 and  $\beta$ 1 integrin increase. Finally, we analyzed the role of ILK in lymphatic vascular growth during pathological conditions, and found that ILK also controls cardiac lymphatic vascular expansion following MI.

In summary, my thesis is the first study to describe that ILK plays an essential role in regulating VEGFR3 signaling, LEC proliferation, and thus lymphatic vascular growth during developmental, physiological and pathological conditions. In addition, it provides a new mechanism of how  $\beta$ 1 integrin-mediated VEGFR3 signaling might be kept in balance in order to prevent lymphatic vascular overgrowth.

## 2. Zusammenfassung

Das Lymphgefäßsystem ist essentiell für die Aufrechterhaltung der Flüssigkeitshomöostase im Körper. Nicht-funktionierende Lymphgefäße sind deshalb mit pathologischen Zuständen, wie der Entwicklung eines Lymphödems, verbunden. Des Weiteren zeigten aktuelle Studien, dass Lymphgefäßveränderungen mit kardiovaskulären Erkrankungen, insbesondere dem Herzinfarkt, zusammenhängen. Daher ist das Verständnis der regulatorischen Prozesse des Lymphgefäßwachstums von großer Wichtigkeit.

Das Lymphgefäßwachstum wird über den hauptsächlich in lymphatischen Endothelzellen (LECs) exprimierten vaskulären endothelialen Wachstumsrezeptor 3 (VEGFR3) reguliert. Die Signalaktivität des VEGFR3 kann entweder durch Bindung von Liganden wie den vaskulären endothelialen Wachstumsfaktoren (VEGF)-C oder -D induziert werden oder durch mechanische Stimulation, bei der  $\beta 1$  Integrine involviert sind. Als Folge wird die Tyrosin Phosphorylierung von VEGFR3 induziert, welche dazu führt, dass LECs überleben, migrieren sowie proliferieren. In dieser Arbeit wurde insbesondere die Rolle der ‚integrin-linked kinase‘ (ILK) in der Signalaktivierung von VEGFR3 sowie im Lymphgefäßwachstum untersucht. Hierfür haben wir Mausembryonen mit einer endothelialen Deletion des *Ilk* Gens, adulte Mäuse mit einer durch Tamoxifen induzierten *Ilk* Deletion in LECs sowie adulte humane LECs mit ausgeschaltetem *ILK* untersucht. Erstaunlicherweise konnten wir dabei ILK als einen kritischen Inhibitor der VEGFR3 Signalaktivität, LEC Proliferation sowie des Lymphgefäßwachstums identifizieren. Desweiteren deuten unsere Ergebnisse darauf hin, dass ILK die Interaktionen zwischen VEGFR3 und  $\beta 1$  Integrin verhindert, wodurch die  $\beta 1$  Integrin-induzierte VEGFR3 Signalaktivität unterdrückt wird. Dies wurde insbesondere durch genetische Experimente verdeutlicht, in denen wir Mausembryonen mit endothelialer Deletion von *Ilk* sowie *Itgb1* untersuchten. Da ILK ein Bestandteil des ILK/PINCH/parvin (IPP) Komplexes ist, haben wir zusätzlich Mausembryonen mit endothelialer Deletion des *Parva* Gens untersucht. Diese zeigten, dass auch  $\alpha$ -parvin in die Regulation der LEC Proliferation sowie des Lymphgefäßwachstums involviert ist. Um zu verstehen, in welchem physiologischen Kontext ILK die VEGFR3 Signalaktivität reguliert, haben wir außerdem humane LECs mechanisch gestreckt, welches dazu geführt hat, dass ILK vom  $\beta 1$  Integrin dissoziierte, während jedoch die Interaktionen zwischen VEGFR3 und  $\beta 1$  Integrin erhöht wurden. Zuletzt haben wir die Rolle von ILK ebenfalls im Lymphgefäßwachstum unter pathologischen Bedingungen untersucht und fanden heraus, dass ILK auch das Wachstum der Herzlymphgefäße nach einem Herzinfarkt reguliert.

Zusammenfassend beschreibt meine Arbeit zum ersten Mal eine essentielle Rolle von ILK in der Regulierung der VEGFR3 Signalaktivität, LEC Proliferation sowie des

Lymphgefäßwachstums unter embryonalen, physiologischen und pathologischen Gegebenheiten. Darüber hinaus schlägt sie einen neuartigen Mechanismus vor, wie  $\beta$ 1 Integrin-vermittelte VEGFR3-Signale im Gleichgewicht gehalten werden, um ein exzessives Lymphgefäßwachstum zu verhindern.

### 3. Introduction

#### 3.1. The lymphatic vasculature

##### 3.1.1. Physiological relevance and organization of the lymphatic vasculature

The lymphatic vasculature is a specialized part of the circulatory system, which is complemented by the blood vasculature. Diverse blood vessel types form a closed blood vascular system, in which arteries and veins are responsible for the transport of blood, while blood capillaries are required for the exchange of oxygen, nutrients, hormones and waste products. During the exchange phase some fluid, which cannot be fully taken up again by blood capillaries, remains in the extracellular or interstitial spaces, and needs to be drained by the lymphatic vasculature (Wiig and Swartz 2012). In contrast to the blood vasculature, the lymphatic vasculature is an open vascular system, in which the blind-ending lymphatic capillaries are responsible for the uptake of interstitial fluid (Figure 1). This fluid, collectively called lymph, is transported through pre-collecting and collecting lymphatic vessels, and returned back to the blood vascular system (Schulte-Merker et al. 2011). Therefore, the lymphatic vasculature plays an essential role in maintaining fluid homeostasis in the body.

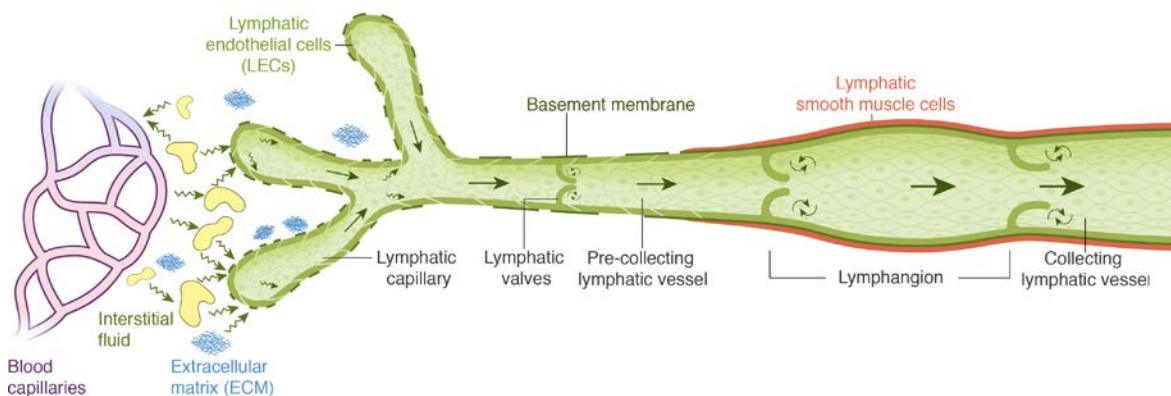


**Figure 1: The lymphatic vasculature.** Due to leakage from blood capillaries some fluid remains in extracellular or interstitial spaces, and is taken up by lymphatic capillaries. The uptake of fluid is supported by the special morphology of lymphatic capillaries: they are composed of lymphatic endothelial cells (LECs) that are connected to the extracellular matrix (ECM), and lack both a continuous basement membrane and mural cells. This fluid, referred to as lymph, is then transported through pre-collecting and collecting lymphatic vessels, and returned to the blood vasculature. Lymphatic valves subdivide collecting lymphatic vessels into lymphangions, and prevent backflow of lymph during transport, thereby ensuring unidirectional lymph flow. Modified from (Uerner et al. in press 2017).

In addition, the lymphatic vasculature is involved in the immune response, since it transports antigens and immune cells through interconnected lymph nodes (reviewed in (Randolph et al. 2017)). Further, specialized lymphatic vessels in the villi of the intestine, known as lacteals, are required for the uptake of dietary lipids and fat-soluble vitamins (Choe et al. 2015). Due to their high relevance, lymphatic vessels can be found in almost all organs of the body, except in avascular tissues like the cornea, as well as some vascularized tissues like the retina (Nakao et al. 2012). Until recently, also the central nervous system was considered to be free of lymphatic vessels. However, independent studies lately proved the existence of functional lymphatic vessels in the brain, reinforcing its essential function in fluid drainage and immune surveillance (Aspelund et al. 2015; Louveau et al. 2015).

The lymphatic vasculature can hierarchically be subdivided into lymphatic capillaries, pre-collecting and collecting lymphatic vessels, which are morphologically different due to their diverse roles. All of them, however, are lined by lymphatic endothelial cells (LECs), which surround the lymphatic lumen (Figure 1). Lymphatic capillaries, or initial lymphatic vessels, that form the blind-ending compartments of the lymphatic vasculature, have a unique structure, which contributes to their function of interstitial fluid uptake (Figure 2A). Lymphatic capillaries have a wide lumen, and are covered with only a discontinuous basement membrane without any mural cells, such as pericytes or smooth muscle cells (SMCs) (Leak 1970). The LECs of lymphatic capillaries are oak leaf-shaped, and have overlapping cell edges with discontinuous button-like junctions (Baluk et al. 2007; Murfee et al. 2007). Further, they are connected to the extracellular matrix (ECM) via anchoring filaments and integrins (Leak and Burke 1968; Gerli et al. 2000). This morphological structure allows the lymphatic capillaries to sense changes in the surrounding fluid pressure, and to enable uptake of interstitial fluid together with antigens, macromolecules and small cells through intercellular spaces (Leak 1976). Interstitial fluid uptake by lymphatic capillaries also depends on a pressure gradient between the interstitial fluid pressure and the intraluminal pressure of lymphatic capillaries (Breslin 2014). Lymphatic capillaries converge into pre-collecting lymphatic vessels, which morphologically are a mixture of lymphatic capillaries and collecting lymphatic vessels. The latter are covered with a continuous basement membrane, and the elongated LECs are connected via zipper-like junctions that prevent leakage of lymph during transport (Figure 2B) (Baluk et al. 2007; Yao et al. 2012). Further, collecting lymphatic vessels are surrounded by lymphatic SMCs, which represent an intrinsic pump ensuring movement of lymph by phasic contractions (Benoit et al. 1989; von der Weid and Zawieja 2004). Lymph transport is also supported by compression of lymphatic vessels from surrounding tissues that act

as extrinsic pumps (Zawieja 2009). Both, pre-collecting and collecting lymphatic vessels further display intraluminal valves that separate the vessels into morphologically characteristic segments, referred to as lymphangions, and prevent backflow of lymph, thereby also contributing to its proper propulsion (Figure 1) (Davis et al. 2011; Scallan et al. 2012). Interestingly, LECs within lymphatic valves were reported to show diverse morphologies, such as elongated or cuboidal structures, depending on the side they are located and the flow pattern they experience (Figure 2C) (Sabine et al. 2012; Tatin et al. 2013; Geng et al. 2016). Finally, lymph enters the largest lymphatic trunks (the thoracic duct and the right lymphatic duct), and drains into the blood vasculature via the subclavian veins, which are separated from the lymphatic trunks by specialized lymphovenous valves (Yang and Oliver 2014).

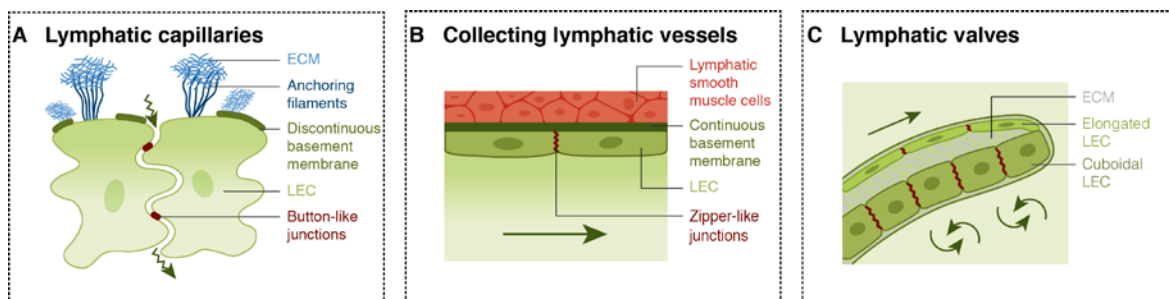


**Figure 2: Morphological differences of lymphatic vessel compartments.** (A) Lymphatic endothelial cells (LECs) of lymphatic capillaries are oak leaf-shaped and connected via button-like junctions, which allow uptake of interstitial fluid through intercellular spaces. Lymphatic capillaries are covered by only a discontinuous basement membrane and lack any mural cells. In addition, their LECs bind to the extracellular matrix (ECM) via anchoring filaments and integrins. (B) LECs of collecting lymphatic vessels are elongated and connected via zipper-like junctions, which prevent leakage of fluid during transport. Collecting lymphatic vessels are covered by a continuous basement membrane and are surrounded by lymphatic smooth muscle cells that contribute to lymph propulsion by phasic contractions. (C) LECs of lymphatic valves can be heterogeneous in morphology, as elongated and cuboidal LECs have been described to exist depending on the side of the valve and lymph flow pattern they are exposed to. Modified from (Urner et al. in press 2017).

### 3.1.2. Clinical relevance of the lymphatic vasculature

Lymphatic vascular dysfunctions are associated with a variety of pathological conditions. A direct consequence of non-functional lymphatic vasculature is a pathological accumulation of interstitial fluid, known as lymphedema. Lymphedema can have different causes, and therefore is distinguished in primary and secondary lymphedema. The first develops due to genetic defects that affect lymphatic vascular development, while secondary lymphedema is caused by acquired damage of the lymphatic vasculature. Specifically, surgical interventions, such as lymph node dissection or radiotherapy i.e. in the context of cancer treatment, but also inflammation or parasitic infections can cause

dysfunctions of the lymphatic vascular system leading to secondary lymphedema. As a consequence, fluid drainage and lymph transport is no longer efficiently working, and results in lymphatic stasis and tissue swelling (reviewed in (Mortimer and Rockson 2014)). Interestingly, recent work showed that lymphatic capillaries in the affected tissue are hyperplastic, thus show increased LEC proliferation, but are poorly functional (Rutkowski et al. 2006; Gousopoulos et al. 2016). Progressive lymphedema leads to inflammatory conditions, characterized by high immune cell infiltration and accumulation of inflammatory cytokines (Ly et al. 2017). Additionally, the ECM composition changes, as defined by degradation of elastic fibers, and simultaneous deposition of stiff and collagen-rich fibers (Gousopoulos et al. 2016). Consequently, non-functional lymphatic vasculature contributes to progressive fibrosis development (Rockson 2001; Saito et al. 2013).

Because of the high relevance of cardiovascular diseases, several groups during the last few years intensively studied the role of cardiac lymphatic vasculature in myocardial infarction (MI) (reviewed in (Vuorio et al. 2017)). Interestingly, the lymphatic vasculature in the heart has a complex, heterogeneous anatomy with differences in anterior, posterior and lateral regions, as well as in subepicardial, myocardial and subendocardial regions (Norman and Riley 2016; Tatin et al. 2017). This extensive lymphatic vascular network enables efficient cardiac lymph drainage, most likely in the directions from subendocardial towards subepicardial regions, and from the apex towards the base (Norman and Riley 2016). After MI however, the lymphatic vasculature in mouse, rat and human hearts was reported to undergo severe remodeling processes associated with hierarchical rearrangements, as well as dilation and hyperplasticity of lymphatic vessels (Ishikawa et al. 2007; Klotz et al. 2015; Henri et al. 2016; Tatin et al. 2017). Although these lymphatic vessels seem initially dysfunctional, and are associated with the formation of myocardial edema and cardiac fibrosis (Davis et al. 2000; Henri et al. 2016; Tatin et al. 2017), therapeutically induced lymphatic vascular growth after MI seems to improve fluid drainage, immune surveillance and cardiac function on the long-term (Klotz et al. 2015; Goichberg 2016; Henri et al. 2016). This new field of cardiovascular research demonstrates the essential role of cardiac lymphatic vasculature in pathophysiology.

Several other pathological conditions have been associated with the lymphatic vasculature, and include their role in obesity development, reverse cholesterol transport and atherosclerosis development, ocular hypertension and glaucoma, as well as cancer progression, underlining the clinical relevance of the lymphatic vascular system (Harvey et al. 2005; Lim et al. 2013; Martel et al. 2013; Karaman and Detmar 2014; Thomson et al. 2014; Vuorio et al. 2014; Dieterich and Detmar 2016; Escobedo et al. 2016).

### 3.1.3. Embryonic development of the lymphatic vasculature

More than 100 years ago, Florence Sabin was the first to analyze the development of the lymphatic vasculature in pig embryos (Sabin 1902). During the past decades, the lymphatic vasculature has been intensively studied using mouse embryos and adult mice. Indeed, the mouse (*Mus musculus*) has highly developed lymphatic valves, lymph nodes, and hierarchical vessel subtypes, and therefore represents an appropriate model system to study the complex mammalian lymphatic vasculature. The variety of different genetically modified mouse models, and analysis of immediate consequences of genetic deletion in mouse embryos enabled to uncover major mechanisms of the formation and morphogenesis of the developing lymphatic vasculature (Koltowska et al. 2013).

The mouse embryonic development of the circulatory system begins around embryonic day (E) 8.0 with the initiation of blood vascular development (Drake and Fleming 2000). This process is generally known as vasculogenesis, while further growth of blood vessels occurs via angiogenesis, which describes the formation of blood vessels out of pre-existing ones (Walls et al. 2008). As soon as a primitive blood vascular network is established, the development of the lymphatic vasculature is initiated. Interestingly, most analyses confirmed Sabin's original suggestion that the lymphatic vasculature primarily arises from the pre-existing venous blood vasculature (Wigle and Oliver 1999; Srinivasan et al. 2007). At around E9.0, a small population of vascular endothelial cells (VECs) within the anterior cardinal veins (CVs) and intersomitic vessels (ISVs) define LEC progenitor fate, characterized by high expression of COUP transcription factor 2 (COUP-TFII) and Sox18 (Srinivasan et al. 2007; Francois et al. 2008; Lin et al. 2010; Srinivasan et al. 2010; Yang et al. 2012). Both transcription factors are required to induce expression of Prox1 at around E9.5, thereby determining LEC specification (Figure 3A) (Francois et al. 2008; Lin et al. 2010; Srinivasan et al. 2010). Notably, Prox1 is not only critically required for initiation of LEC specification, but was also shown to be essential in LEC maintenance, since its loss results in dedifferentiation of LECs into VECs (Hong et al. 2002; Petrova et al. 2002; Wigle et al. 2002; Johnson et al. 2008). Another lymphatic-specific marker, Lyve1, is also expressed by LECs at around the same developmental stage, but its exact function remains unclear, since deletion of *Lyve1* results in the development of a functional lymphatic vasculature (Banerji et al. 1999; Oliver and Detmar 2002; Gale et al. 2007). From E10.5 onwards, LECs begin to migrate out of the venous system in a dorsolateral direction, most likely as streams of tightly interconnected cells (Figure 3B) (Yang et al. 2012). Migration of LECs correlates with the upregulated expression of podoplanin as well as the vascular endothelial growth factor receptor 3 (VEGFR3)

(Kaipainen et al. 1995; Schacht et al. 2003; Francois et al. 2012; Yang et al. 2012). Interestingly, VEGFR3 is expressed by VECs before the onset of lymphatic vascular development, and plays a critical role in blood vascular development, since its deletion results in early embryonic lethality (E9.5) due to cardiovascular failure (Dumont et al. 1998). As soon as LECs migrate, VEGFR3 expression is downregulated in VECs, and becomes mainly restricted to LECs during later embryonic development (Kaipainen et al. 1995). VEGFR3 together with its ligands vascular endothelial growth factor (VEGF)-C and -D, which are secreted by the surrounding mesenchyme, are strictly required for LEC migration and thus lymphatic vascular growth during embryonic development (Kukk et al. 1996; Jeltsch et al. 1997; Achen et al. 1998; Makinen et al. 2001a; Makinen et al. 2001b; Veikkola et al. 2001; Karkkainen et al. 2004). Additionally, collagen- and calcium-binding EGF domains 1 (CCBE1) has been shown to be required for reinforcing the effect of VEGF-C on VEGFR3 signaling during embryonic development (Bos et al. 2011). At around E11.5, the first lumenized lymphatic vascular structure is formed by migrating LECs, and is called jugular lymph sac (jls) or primordial thoracic duct (pTD) (Figure 3C) (reviewed in (Neufeld et al. 2014)).

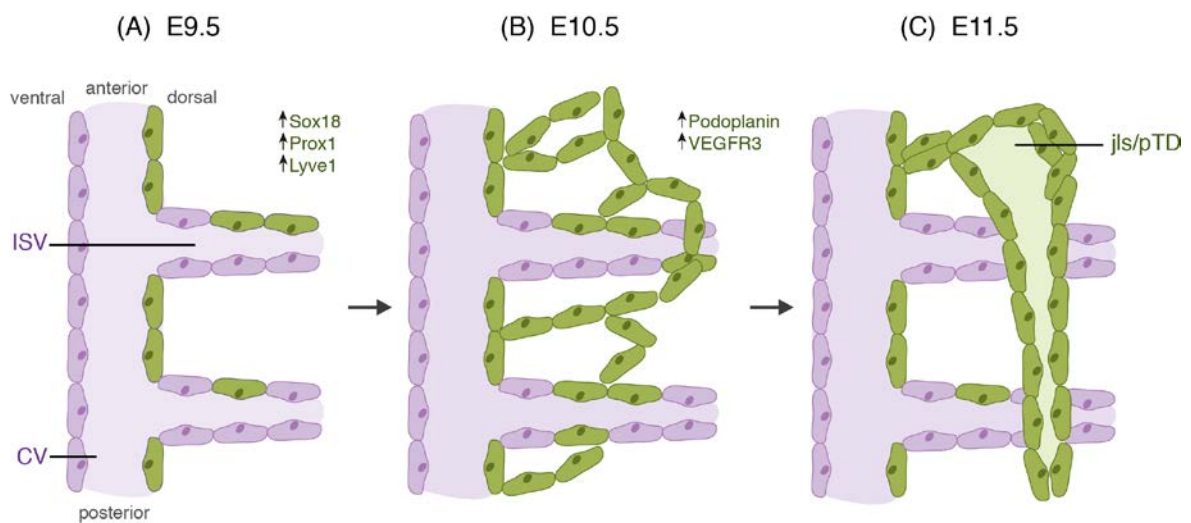


**Figure 3: Early lymphatic vascular development during mouse embryogenesis.** (A) At around E9.5 vascular endothelial cells (VECs, purple) within the anterior cardinal veins (CVs) and intersomitic vessels (ISVs) initiate expression of lymphatic-specific markers like Sox18 and Prox1, and thereby determine LEC (green) specification. (B) At around E10.5 LECs start to migrate out of the venous system in a dorsolateral direction, probably as streams of interconnected LECs. Simultaneously, podoplanin and VEGFR3 expression is upregulated. (C) At around E11.5 migrating LECs form the jugular lymph sac (jls) or primordial thoracic duct (pTD), which is the first lymphatic vascular structure giving rise to the majority of the whole embryonic lymphatic vascular network. Modified from (Neufeld et al. 2014).

The jls/pTD gives rise to the majority of the embryonic lymphatic vascular network (Yang et al. 2012; Hagerling et al. 2013). Interestingly, also non-venous sources have been described for the development of certain lymphatic vessels, including mesenteric, cardiac

and dermal lymphatic vessels (Mahadevan et al. 2014; Klotz et al. 2015; Martinez-Corral et al. 2015; Stanczuk et al. 2015). However, these studies might be seen critically, since only recently one of the used lineage tracing mouse lines (*Pdgfrb-Cre*) was shown to also label endothelial cells (Ulvmar et al. 2016). By around E15.5, the embryonic lymphatic drainage system starts to work, and almost simultaneously lymphatic valves develop, resulting in the formation of a primary hierarchical lymphatic vascular network consisting of lymphatic capillaries, pre-collecting and collecting lymphatic vessels (Oliver 2004; Sabine et al. 2012). Notably, also during further growth of lymphatic vessels, known as lymphangiogenesis, VEGFR3 signaling is essential for proper regulation.

### **3.2. Vascular endothelial growth factor receptor 3 (VEGFR3)**

#### **3.2.1. The vascular endothelial growth factor receptor (VEGFR) family**

VEGFR3, also known as fms-like tyrosine kinase 4 (Flt4), is one of three known mammalian members of the VEGFR family, and belongs to the receptor tyrosine kinases (RTKs). VEGFR1, or fms-like tyrosine kinase 1 (Flt1), is expressed in VECs, and mainly functions as a regulator of VEGFR2 activity (Fong et al. 1995; Hiratsuka et al. 1998). VEGFR2, or fetal liver kinase 1 (Flk1), is also expressed in VECs, where it is critically required for vasculogenesis and angiogenesis, but is also found in LECs (Terman et al. 1991; Terman et al. 1992; Shalaby et al. 1995; Feng et al. 2000; Nagy et al. 2002). In addition, both receptors are expressed in some non-endothelial cells, such as hematopoietic stem cells (Kato et al. 1995; Hattori et al. 2002). VEGFR3 expression is mainly restricted to LECs, while only a few VECs including fenestrated cells or tip cells during angiogenesis have been described to express VEGFR3 in the adult (Kaipainen et al. 1995; Partanen et al. 2000; Tammela et al. 2008). Additionally, also VEGFR3 is found in some non-endothelial cells, including neuronal progenitors, osteoblasts, and macrophages (Le Bras et al. 2006; Orlandini et al. 2006; Schmeisser et al. 2006). However, its main function is to control lymphatic vascular growth (Makinen et al. 2001b; Karkkainen et al. 2004).

All VEGFRs are similar in structure. They consist of an N-terminal extracellular part characterized by 7 immunoglobulin-like domains, a short transmembrane domain, as well as an intracellular part. The latter can be further subdivided into a short juxtamembrane domain, two tyrosine kinase domains that are separated by a kinase insert domain, and a C-terminal tail (Simons et al. 2016). In contrast to the other VEGFRs, a disulfide bridge replaces the fifth immunoglobulin-like domain in the extracellular part of VEGFR3 as a

consequence of proteolytic cleavage (Pajusola et al. 1992; Lee et al. 1996; Takahashi and Shibuya 2005). Classical signaling of RTKs is initiated by ligand binding to the extracellular part of the receptor (reviewed in (Lemmon and Schlessinger 2010)).

### 3.2.2. Ligand-induced VEGFR3 signaling

In general, five mammalian ligands are known that bind in an overlapping pattern to VEGFRs, including VEGF-A, -B, -C, -D and placental growth factor (PlGF) (Alvarez-Aznar et al. 2017). However, only VEGF-C and -D have been shown to bind to VEGFR3 with high affinity, and thereby inducing its signaling (Joukov et al. 1996; Achen et al. 1998). Particularly VEGF-C is of high importance, since its deletion results in failure of lymphatic vascular development, formation of edema, and early embryonic lethality (Karkkainen et al. 2004). In contrast, *Vegfd* deletion does not lead to any functional defects of the lymphatic vasculature, and is not embryonic lethal (Baldwin et al. 2005). However, VEGF-D addition can rescue the effect of *Vegfc*-deficiency on lymphatic vascular growth, demonstrating its VEGFR3 specificity (Karkkainen et al. 2004; Haiko et al. 2008). Both ligands were also shown to bind to VEGFR2 after proteolytic processing, but with lower affinity than to VEGFR3 (Joukov et al. 1996; Achen et al. 1998).

Ligand binding to VEGFR3 is immediately followed by receptor dimerization. Besides homodimerization, VEGFR3 can also form heterodimers with VEGFR2, which can also be detected in tip cells during angiogenesis (Dixelius et al. 2003; Alam et al. 2004; Nilsson et al. 2010). Furthermore, several other transmembrane receptors have been reported to act as co-receptors of VEGFR3, such as neuropilin-2 or ephrinB2, and are critically involved in lymphatic vascular growth (Yuan et al. 2002; Makinen et al. 2005; Favier et al. 2006; Wang et al. 2010; Xu et al. 2010). Following VEGFR3 homodimerization, at least five tyrosine (Tyr) residues are phosphorylated, including Tyr<sup>1230</sup>, Tyr<sup>1231</sup>, Tyr<sup>1265</sup>, Tyr<sup>1337</sup>, and Tyr<sup>1363</sup> (Dixelius et al. 2003). Interestingly, only three of them (Tyr<sup>1230</sup>, Tyr<sup>1231</sup>, and Tyr<sup>1265</sup>) seem to be phosphorylated upon VEGFR2 / VEGFR3 heterodimerization (Dixelius et al. 2003). The downstream signaling pathways of VEGFR3 likely involve Akt and Erk1/2, which might be activated in a phosphoinositide 3-kinase (PI3K)- as well as protein kinase C (PKC)-dependent manner, respectively (Makinen et al. 2001b; Salameh et al. 2005; Zhou et al. 2010; Coso et al. 2012; Alvarez-Aznar et al. 2017). In addition, full VEGFR3 signaling was shown to be coupled to its internalization after ligand binding, and might be functionally linked to co-receptors like ephrinB2 (Wang et al. 2010; Nakayama et al. 2013).

Most likely, endocytosis prolongs VEGFR3 tyrosine phosphorylation, as already demonstrated for VEGFR2 (Lampugnani et al. 2006).

Altogether, VEGFR3 activation by ligand binding results in the induction of LEC survival, migration and proliferation (Makinen et al. 2001b), thus leading to lymphatic vascular growth (Figure 4).

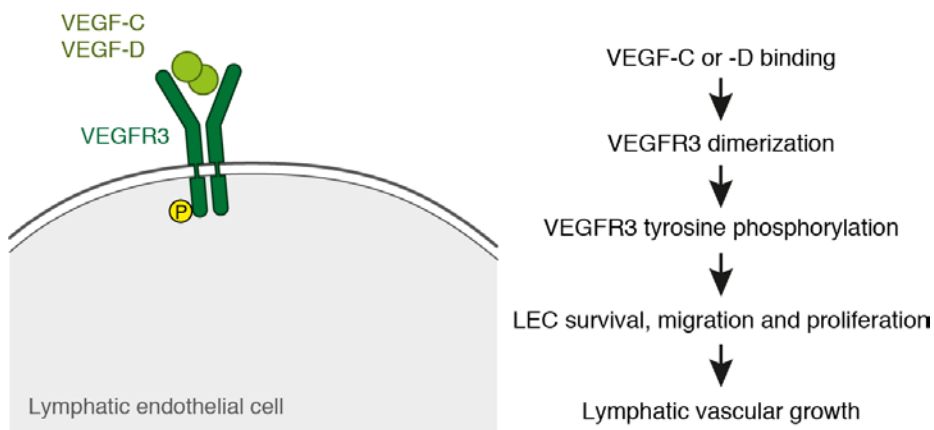


**Figure 4: Simplified schematic overview of ligand-induced VEGFR3 signaling in LECs.** Binding of VEGF-C or -D to the extracellular part of VEGFR3 results in immediate receptor dimerization, and induces autophosphorylation of tyrosine residues (P) on the intracellular part. This triggers downstream signaling resulting in LEC survival, migration and proliferation, therefore contributing to lymphatic vascular growth. Figure was drafted by Sofia Urner, and illustrated by Yousun Koh.

The relevance of ligand-induced VEGFR3 signaling in regulating lymphatic vascular growth is further demonstrated by *in vivo* experiments, in which the overexpression of the isoform VEGF-C156S, which binds specifically to VEGFR3, results in massive growth of lymphatic vessels, but not blood vessels in the skin of mice (Joukov et al. 1998; Veikkola et al. 2001). Further, mice with inactive *Flt4* kinase activity are characterized by dysfunctional lymphatic vessels, and develop edema (Karkkainen et al. 2001). Interestingly, also in humans, mutations in *FLT4* gene are highly associated with defective kinase activity, and result in primary lymphedema, also known as Milroy disease (Irrthum et al. 2000; Karkkainen et al. 2000; Ghalamkarpour et al. 2006).

### 3.2.3. Mechano-induced VEGFR3 signaling

Although the ligand-induced VEGFR3 signaling pathway is indispensable for proper lymphatic vascular development and growth, the combined deletion of *Vegfc* and *-d* does not phenocopy *Flt4*-deficiency, suggesting a ligand-independent VEGFR3 function (Haiko et al. 2008). Indeed, several studies from the last few years demonstrated that mechanical

forces play a critical role in lymphangiogenesis, and strongly suggest an additional mechano-induced VEGFR3 signaling pathway (reviewed in (Urner et al. in press 2017)).

The importance of mechanotransduction is illustrated by embryonic studies, where mechanical forces, such as stretch created by increased interstitial fluid pressure, or shear stress created by lymph flow, have been shown to be involved in lymphatic vascular development during embryogenesis (Planas-Paz and Lammert 2013; Planas-Paz and Lammert 2014). Interestingly, while the onset of lymph flow was mainly shown to correlate with lymphatic vascular remodeling, such as development of lymphatic valves, particularly changes in the interstitial fluid pressure have been linked to VEGFR3 activation, and induction of lymphatic vascular expansion during embryonic development (Planas-Paz et al. 2012; Sabine et al. 2012). Specifically, increased interstitial fluid in the developing mouse embryo leads to increased interstitial fluid pressure and swelling of the ECM. These forces affect the adhering LECs, and lead to their stretching (Planas-Paz et al. 2012). The mechanical stretch of LECs due to an increased interstitial fluid pressure highly correlates with increased VEGFR3 tyrosine phosphorylation and LEC proliferation, as also demonstrated by gain-of-fluid experiments (Planas-Paz et al. 2012). As a result, LECs increase in number, which leads to the expansion of the jls/pTD. In turn, the enlarged embryonic lymphatic vasculature leads to improved fluid drainage, and thus to normalization of the interstitial fluid pressure (Planas-Paz et al. 2012). This embryonic model of lymphatic vascular growth might also represent how lymphatic vessels in general adapt to changing demands of interstitial fluid uptake. Notably, *in vitro* experiments could show that stretch of human LECs results in increased VEGFR3 tyrosine phosphorylation and LEC proliferation, but does not change the expression of VEGF-C, indicative of ligand-independent VEGFR3 activation (Planas-Paz et al. 2012). Indeed, the response of VEGFR3 signaling to mechanical stretch upon increased interstitial fluid pressure critically depends on the transmembrane receptor  $\beta$ 1 integrin, and its endothelial cell-specific deletion results in strong reduction of VEGFR3 tyrosine phosphorylation, LEC proliferation, as well as LEC number, leading to edema formation and embryonic lethality (Planas-Paz et al. 2012).

$\beta$ 1 integrin (*Itgb1*) is a member of the integrin family, which consists of around 18  $\alpha$  and 8  $\beta$  subunits that can form up to 24 different heterodimers (Hynes 2002). All integrins consist of an extracellular, a transmembrane, and a short intracellular domain (Humphries et al. 2006). Integrins bind to different ECM components, such as fibronectin, laminin or collagen, depending on the exact integrin subunits, and thereby are critically required for cell adhesion (Humphries et al. 2006). Notably, although integrins lack any kinase activity,

they are also involved in mediating outside-in and inside-out signaling by interacting with intracellular signaling molecules (Schoenwaelder and Burridge 1999). In addition, integrins share signaling pathways with RTKs, and can either act synergistically with growth factors, or even activate RTK signaling in the absence of their ligands (Clark and Brugge 1995; Miyamoto et al. 1996; Sundberg and Rubin 1996; Moro et al. 1998; Aplin and Juliano 1999; Renshaw et al. 1999). Therefore, integrins are also involved in promoting cell survival, migration and proliferation. Interestingly, predominantly the group of  $\beta 1$  integrins has been reported to be required for lymphatic vascular development and growth (Huang et al. 2000; Okazaki et al. 2009; Garmy-Susini et al. 2010; Planas-Paz et al. 2012). Also, both *in vivo* and *in vitro* studies provide evidence that  $\beta 1$  integrin is required for full VEGFR3 signaling (Wang et al. 2001; Zhang et al. 2005; Galvagni et al. 2010; Planas-Paz et al. 2012).  $\beta 1$  integrin adhesion to the ECM usually leads to conformational changes in the extracellular domain, which is called  $\beta 1$  integrin activation, and shifts integrins from low- to high-affinity state for ECM binding (Luo et al. 2007; Su et al. 2016; Sun et al. 2016). Following  $\beta 1$  integrin activation, integrins cluster, and recruit several signaling molecules and F-actin bundles to the cytoplasmic integrin tails, resulting in the formation of adhesion complexes, such as focal adhesions (Choi et al. 2008; Iskratsch et al. 2013; Sun et al. 2016). Increased interstitial fluid pressure in the developing mouse embryo, as well as mechanical stretch of human LECs *in vitro* have been shown to activate  $\beta 1$  integrins (Planas-Paz et al. 2012). Further,  $\beta 1$  integrin stimulation by binding to ECM components, such as fibronectin, was also shown to result in its increased interaction with VEGFR3, correlating with increased VEGFR3 tyrosine phosphorylation, both in the presence or absence of VEGFR3 ligands (Wang et al. 2001; Zhang et al. 2005). The increase in VEGFR3 signaling thereby critically depends on  $\beta 1$  integrin (Wang et al. 2001; Zhang et al. 2005). Strikingly,  $\beta 1$  integrin-mediated VEGFR3 signaling was shown to result in the phosphorylation of tyrosine residues, which are mostly different from that induced by ligand binding, and involve Tyr<sup>830</sup>, Tyr<sup>833</sup>, Tyr<sup>853</sup>, Tyr<sup>1063</sup>, Tyr<sup>1333</sup> and Tyr<sup>1337</sup> (Galvagni et al. 2010). This phosphorylation likely depends on recruited kinases, such as the Src protein family kinase member c-Src, and might be independent of the intrinsic kinase activity of VEGFR3 (Galvagni et al. 2010). Further, downstream signaling pathways, such as PI3K-dependent Akt signaling, are induced (Zhang et al. 2005; Galvagni et al. 2010). Consequently,  $\beta 1$  integrin-mediated VEGFR3 activation leads to cell survival, migration, and proliferation, and thus also results in the induction of lymphatic vascular growth (Figure 5).

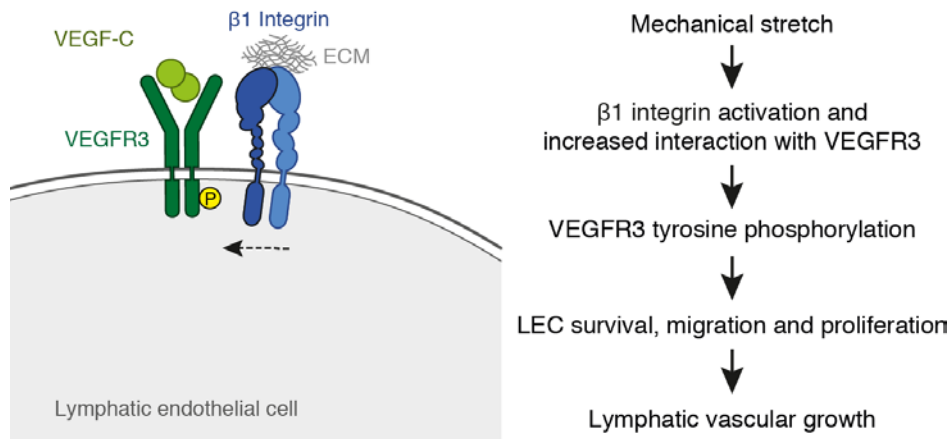


**Figure 5: Simplified schematic overview of mechano-induced VEGFR3 signaling in LECs.** Mechanical stretch, as i.e. created by increased interstitial fluid pressure and ECM swelling, leads to  $\beta 1$  integrin activation and its interaction with VEGFR3, in the presence or absence of VEGF-C. This induces VEGFR3 tyrosine phosphorylation (P), and triggers downstream signaling resulting in LEC survival, migration and proliferation, therefore contributing to lymphatic vascular growth. Figure was drafted by Sofia Urner, and illustrated by Yousun Koh.

An important part of integrin signaling is its linkage to the cytoskeleton, which enables outside-in and inside-out signal transduction. Several adaptor proteins have been discovered to be involved in connecting  $\beta 1$  integrin to F-actin filaments, and include particularly the integrin-linked kinase (ILK) (Hannigan et al. 1996; Schiller et al. 2011; Widmaier et al. 2012).

### 3.3. Integrin-linked kinase (ILK)

#### 3.3.1. Physiological function of ILK

The relevance of ILK in cytoskeletal organization is demonstrated by the fact that its global deletion results in early embryonic lethality due to failure of epiblast polarization, cell adhesion and actin accumulation (Sakai et al. 2003). Interestingly, *Ilk*-deficient mice die at the same developmental stage (between E5.5 and E6.5) as mice with global *Itgb1* deletion (Fassler and Meyer 1995; Stephens et al. 1995). When first identified, ILK was found to directly bind to  $\beta 1$  integrin tails via its C-terminal kinase-like domain (Hannigan et al. 1996). In addition, it was shown to interact with  $\beta 3$  integrin, though in contrast to  $\beta 1$  integrin, it is not clear whether ILK directly binds to  $\beta 3$  integrin tails (Pasquet et al. 2002). Originally, ILK was described to act as a serine / threonine kinase, and several studies followed identifying different potential targets that might be phosphorylated by ILK (reviewed in (Hannigan et al. 2011)). However, *in vivo* studies using mice with mutations in the proposed autophosphorylation site of the putative kinase domain develop normal

and are viable (Lange et al. 2009). Similar observations have been described in genetic studies using flies (*Drosophila melanogaster*) and worms (*Caenorhabditis elegans*), strongly suggesting that the putative kinase activity of ILK is not required for development and homeostasis (Zervas et al. 2001; Mackinnon et al. 2002). In addition, although ILK shows partial sequence homology to serine / threonine kinases, it lacks well-conserved motifs required for eukaryotic protein kinase activity (Hanks et al. 1988; Fukuda et al. 2009; Wickstrom et al. 2010b). Therefore, ILK is rather classified as a pseudokinase, which is catalytically inactive, but still involved in cellular processes by interacting with other proteins (Boudeau et al. 2006; Wickstrom et al. 2010b).

Indeed, many studies provide evidence for the critical role of ILK in microtubule organization, cell-matrix adhesions, focal adhesions, cell spreading, migration, and survival (reviewed in (Legate et al. 2006; Qin and Wu 2012; Widmaier et al. 2012)).

The role of ILK in microtubule organization refers to its function in connecting microtubule ends to the actin cortical network together with other interacting proteins (Wickstrom et al. 2010a). This ensures stabilization of microtubules, which has been shown to be critical for exocytotic processes. In this context, ILK was also reported to be required for the transport of caveolin-1 to the plasma membrane, and thus for the formation of functional caveolae (Wickstrom et al. 2010a). Caveolae are specialized membrane domains involved in endocytosis, control of lipid uptake, and regulation of different signaling pathways (reviewed in (Parton and Simons 2007)). Interestingly, VEGFR3 was shown to localize in caveolae, associated with inhibitory effects on its signaling, since silencing of *CAV1* results in upregulated VEGFR3 tyrosine phosphorylation *in vitro* (Galvagni et al. 2007). In addition, caveolae mislocalization caused by *Ilk*-deficiency was also shown to result in defective VEGFR2 signaling, suggesting a general regulatory function of caveolae in RTK signaling, while proper caveolae formation seems to depend on ILK (Wickstrom et al. 2010a; Malan et al. 2013).

In general, ILK is involved in the interaction with several different intracellular molecules, also referred to as ILK interactome (Dobрева et al. 2008; Wickstrom et al. 2010b; Qin and Wu 2012). Strikingly, most functions of ILK, such as its role in cell-matrix adhesions or focal adhesions, critically depend on the assembly of the ILK/PINCH/parvin (IPP) complex (Legate et al. 2006). While PINCH binds to the N-terminal domain of ILK, parvin interacts with the C-terminal kinase-like domain of ILK, and thereby connects the IPP complex to the actin cytoskeleton, since ILK is not able to directly bind to F-actin filaments (Li et al. 1999; Olski et al. 2001; Tu et al. 2001; Yamaji et al. 2001; Chiswell et al. 2008; Yang et al.

2009). All in all, every member of the IPP complex has several interaction partners, and therefore, its formation leads to the high involvement of the IPP complex in protein-protein and cell-matrix interactions (Legate et al. 2006).

### 3.3.2. The ILK/PINCH/parvin (IPP) complex

ILK is often described as the central component of the IPP complex that serves as a signaling platform, in which  $\beta$ 1 integrins interact with the actin cytoskeleton and other signaling molecules (Tu et al. 2001; Legate et al. 2006). The assembly of the IPP complex itself ensures stability of the individual components, and is required for proper cell-matrix adhesion (Zhang et al. 2002b; Fukuda et al. 2003). Interestingly, while only one isoform of ILK is expressed throughout all eukaryotic cells, two isoforms of PINCH, as well as three isoforms of parvin have been described to interact with ILK (Tu et al. 1999; Olski et al. 2001; Tu et al. 2001; Yamaji et al. 2001; Zhang et al. 2002a; Legate et al. 2006). Notably, ILK can only bind one isoform of each PINCH and parvin at the same time, and therefore distinct IPP complexes can be formed, which might result in distinct signaling outputs (Legate et al. 2006).

Both isoforms, PINCH-1 and PINCH-2, are widely expressed throughout different tissues, and binding of PINCH to ILK was mainly reported to be required for proper localization of ILK to focal adhesion sites (Li et al. 1999; Velyvis et al. 2001; Zhang et al. 2002a; Zhang et al. 2002b; Braun et al. 2003). Similar to *Ilk*-deficiency, loss of *Pinch1* also leads to defective epiblast polarization, and results in embryonic lethality between E6.5 and E7.5 (Li et al. 2005; Liang et al. 2005). In contrast, mice that lack *Pinch-2* are viable, and phenotypically normal, but also show upregulated expression of PINCH-1, suggesting that the functions of PINCH-1 and -2 might be overlapping (Stanchi et al. 2005).

Three mammalian isoforms of parvin ( $\alpha$ -,  $\beta$ -, and  $\gamma$ -parvin) have been reported to bind to ILK, and can either directly bind to F-actin filaments, or recruit other actin-binding proteins, thereby providing the connection of the IPP complex to the cytoskeleton (Nikolopoulos and Turner 2000; Olski et al. 2001; Yamaji et al. 2004). However, the expression pattern and relevance of different parvin members seem to be variable. While the expression of  $\gamma$ -parvin is mainly restricted to the hematopoietic system,  $\beta$ -parvin is expressed more ubiquitously, but highest in heart and skeletal muscle (Korenbaum et al. 2001; Yamaji et al. 2001). The probably most relevant member of the parvin family is  $\alpha$ -parvin (*Parva*), also known as actopaxin or CH-ILKBP, which is expressed in almost all tissue cells

(Korenbaum et al. 2001; Olski et al. 2001). In a SILAC (Stable isotope labeling by amino acids in cell culture) study,  $\alpha$ -parvin was shown to have the highest specific interaction with ILK compared to other ILK-binding proteins, such as PINCH-1 that showed a much lower binding specificity (Dobrev et al. 2008).  $\alpha$ -parvin connects the IPP complex to the cytoskeleton either by binding to F-actin filaments directly, or via its interaction with paxillin (Nikolopoulos and Turner 2000). Deletion of *Parva* results in embryonic lethality between E10.5 and E14.5 (Montanez et al. 2009). Interestingly, these embryos display severe cardiovascular abnormalities, such as blood vessel enlargement, impaired coverage by vascular SMCs, and formation of hemorrhages (Montanez et al. 2009). Further, they are characterized by the development of whole-body edema (Montanez et al. 2009). Also, endothelial cell-specific deletion of *Parva* results in embryonic lethality from E14.5 onwards, and is likewise associated with cardiovascular defects and formation of hemorrhages, pointing to the importance of  $\alpha$ -parvin in endothelial tissues (Fraccaroli et al. 2015).

In summary, particularly the IPP complex members ILK and parvin, such as  $\alpha$ -parvin, provide the connection between ECM-bound  $\beta 1$  integrin and the F-actin cytoskeleton, thus playing a critical role in integrin-mediated signaling (Figure 6).

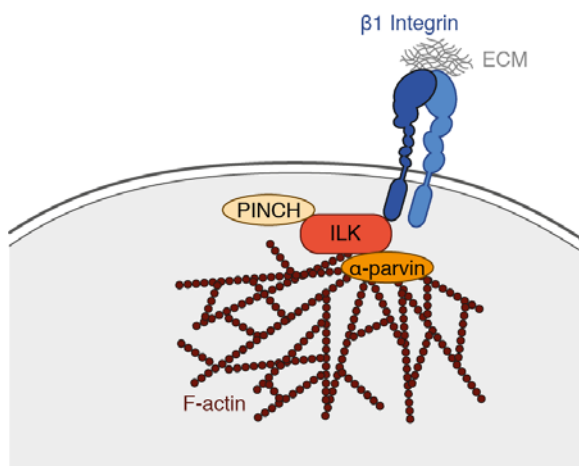


**Figure 6: Simplified schematic overview of the ILK/PINCH/parvin (IPP) complex in  $\beta 1$  integrin-mediated signaling.** While the extracellular domain of  $\beta 1$  integrin binds to certain components of the extracellular matrix (ECM), the intracellular tail of  $\beta 1$  integrin is connected to the F-actin cytoskeleton via the IPP complex members ILK (which interacts with  $\beta 1$  integrin) and  $\alpha$ -parvin (which interacts with F-actin filaments). Figure was drafted by Sofia Umer, and illustrated by Yousun Koh.

### 3.4. Aims of the study

Strikingly, in contrast to the established relevance of  $\beta 1$  integrin in VEGFR3 signaling and lymphatic vascular development, to our knowledge nothing has been reported about the function of its binding partner ILK in LECs yet. Therefore, the major aim of this thesis was to determine the role of ILK in VEGFR3 signaling and lymphatic vascular growth.

First, we used different genetically modified mouse embryos in order to prove the relevance of ILK in lymphatic vascular development, as well as to get insight into the underlying molecular mechanism. Therefore, we analyzed the effect of endothelial cell-specific deletion of *Ilk* on VEGFR3 tyrosine phosphorylation, LEC proliferation and lymphatic vascular expansion during embryonic development. Because of the reported importance of ILK in caveolae formation, and the described regulatory function of caveolae in VEGFR3 signaling *in vitro*, we further investigated whether *Cav1*-deficient embryos show a similar phenotype as *Ilk*-deficient ones in regard of VEGFR3 tyrosine phosphorylation and LEC proliferation *in vivo*. Next, we analyzed whether endothelial cell-specific deletion of *Ilk* changes interactions between VEGFR3 and  $\beta 1$  integrin in LECs during embryonic development. To explore whether this interaction is functional, we further analyzed VEGFR3 tyrosine phosphorylation, LEC proliferation and lymphatic vascular expansion in double knockout embryos with endothelial cell-specific deletion of *Ilk* as well as *Itgb1*. Finally, we also investigated whether the IPP complex member  $\alpha$ -parvin plays a role in VEGFR3 signaling, LEC proliferation and lymphatic vascular development by using embryos with endothelial cell-specific *Parva* deletion.

Further, we aimed to determine the relevance of ILK in the adult lymphatic vasculature. Therefore, we first established an *in vivo* knockdown of *Ilk* in the adult mouse cornea to analyze possible lymphatic vascular growth into the previously avascular tissue, and repeated these experiments in adult mice with tamoxifen-induced LEC-specific *Ilk* deletion. Next, we investigated mice with induced LEC-specific deletion of *Ilk* in regard of changes in VEGFR3 tyrosine phosphorylation, LEC proliferation and lymphatic vascular expansion in the completely established dermal lymphatic vasculature. In addition, we proved the relevance of ILK in lymphatic vascular growth during pathological conditions by analyzing mice with LEC-specific *Ilk*-deficiency after MI in regard of cardiac lymphatic vascular changes.

Finally, we used the *in vitro* system to reproduce our *in vivo* findings also in adult human LECs. Therefore, we analyzed VEGFR3 tyrosine phosphorylation, LEC proliferation as well as interactions between VEGFR3 and  $\beta 1$  integrin upon siRNA-mediated silencing of *ILK*. We further used human LECs to investigate the impact of mechanical stimulations, like stretch, on the interactions between ILK and  $\beta 1$  integrin.

With this study, we significantly contribute to the knowledge about regulatory processes of VEGFR3 signaling and lymphatic vascular growth during mouse embryonic development, but also in the adult, as demonstrated for physiological and pathological conditions in mice, as well as for human cells.

## 4. Experimental procedures

### 4.1. Mouse models

Different mouse models including adult mice and mouse embryos with different genetic backgrounds were used in this thesis. For mouse embryonic studies, the developmental stage was determined by the presence of a vaginal plague, and defined as E0.5. Detailed descriptions of mouse embryonic isolation procedures can be found in (Zeeb et al. 2012). C57Bl/6J (Janvier) mice were used for embryonic wild-type studies. For genetic deletion of *Ilk* in endothelial cells, previously described *Flk1-Cre* (Licht et al. 2004) and *Ilk-loxP* (Sakai et al. 2003) mice were used. For additional genetic deletion of *Itgb1* in endothelial cells, these mice were crossed with *Itgb1-loxP* (Potocnik et al. 2000) mice. Littermates, or embryos with a similar genetic background served as controls. For analysis of the relevance of caveolin-1 in lymphatic vascular growth, *Cav1<sup>-/-</sup>* (Jackson Laboratory) mice were used for embryonic analyses, and C57Bl/6J (Jackson Laboratory) mice served as controls. Embryos with endothelial cell-specific *Parva* deletion, as generated by crossings of *Tie2-Cre* (Kisanuki et al. 2001) and *Parva-loxP* (Montanez et al. 2009) mice, were provided by Dr. Eloi Montanez (Institute of Cardiovascular Physiology, Biomedical Center Munich), and were previously described (Fraccaroli et al. 2015). Adult male C57Bl/6J (Jackson Laboratory) mice at the age of 8-12 weeks were used for corneal angiogenesis assays with siRNA applications, and were performed in collaboration with Prof. Dr. Shayn Peirce-Cottler at the Department of Biomedical Engineering (University of Virginia) in Charlottesville, USA. Adult female *Prox1-CreER<sup>T2</sup>* (Bazigou et al. 2009) and *Ilk-loxP* mice at the age of 15-25 weeks (age-matched within each experiment) were further used to analyze the effect of genetic *Ilk* deletion in LECs. To induce Cre-mediated recombination, mice were given intraperitoneal tamoxifen injections (1 mg tamoxifen in 100 µl peanut oil) for six consecutive days. To analyze the consequences of LEC-specific deletion of *Ilk*, tissues were collected and analyzed either two days or two weeks after the last tamoxifen injection, as indicated in the results. These mice were also used for corneal angiogenesis assays and MI studies, as described in 4.2.2 and 4.2.3. All animal experiments performed at the Heinrich Heine University Düsseldorf were approved by the local Animal Ethics Committee of the Landesamt für Natur, Umwelt und Verbraucherschutz Nordrhein-Westfalen (LANUV North Rhine-Westphalia), and conducted according to the German Animal Protection Laws. Experiments performed at the University of Virginia in Charlottesville were approved by the Institutional Animal Care and Use Committee at the University of Virginia, and completed in accordance with the National Institutes of Health (NIH) Guide for the Care and Use of Laboratory Animals.

#### 4.1.1. Genotyping

For genotyping of mice, either tail tips or embryonic yolk sacs were lysed in 100  $\mu$ l lysis buffer containing 78  $\mu$ l dH<sub>2</sub>O, 20  $\mu$ l Flexi buffer (5x, Promega) and 2  $\mu$ l Proteinase K (20 mg/ml, Qiagen) at 56°C and 300rpm o/n. Polymerase chain reaction (PCR) was performed using following master mixes per tail or yolk sac:

Master mix components	<i>Flk1-Cre</i>	<i>Ilk-loxP</i>	<i>Itgb1-loxP</i>	<i>Cav1</i>	<i>Prox1-CreER<sup>T2</sup></i>
dH <sub>2</sub> O	12.8 $\mu$ l	12.8 $\mu$ l	12.8 $\mu$ l	11.9 $\mu$ l	13.44 $\mu$ l
Green Flexi buffer (5x, Promega)	4 $\mu$ l	4 $\mu$ l	4 $\mu$ l	4 $\mu$ l	4 $\mu$ l
MgCl <sub>2</sub> (25 mM, Promega)	1.2 $\mu$ l	1.2 $\mu$ l	1.2 $\mu$ l	1.2 $\mu$ l	1.2 $\mu$ l
dNTPs (10 mM, Sigma)	0.4 $\mu$ l	0.4 $\mu$ l	0.4 $\mu$ l	0.4 $\mu$ l	0.4 $\mu$ l
Primer forward (fwd) (100 pmol/ $\mu$ l, Eurofins)	0.2 $\mu$ l	0.2 $\mu$ l	0.2 $\mu$ l	0.1 $\mu$ l	0.13 $\mu$ l
Primer reverse (rev) (100 pmol/ $\mu$ l, Eurofins)	0.2 $\mu$ l	0.2 $\mu$ l	0.2 $\mu$ l	0.1 $\mu$ l	0.13 $\mu$ l
Primer common (com) (100 pmol/ $\mu$ l, Eurofins)	-	-	-	0.1 $\mu$ l	-
Taq Polymerase (5 U/ $\mu$ l, MPI-CGB)	0.2 $\mu$ l	0.2 $\mu$ l	0.2 $\mu$ l	0.2 $\mu$ l	0.2 $\mu$ l
Lysate	1 $\mu$ l	1 $\mu$ l	1 $\mu$ l	2 $\mu$ l	0.5 $\mu$ l

Following primer sequences were used:

Mouse lines	Primer sequences	Product size
<i>Flk1-Cre</i>	fwd: 5'- CCG GCA CAG TTC CGG GGT AGT -3' rev: 5'- GTG GCA GAT GGC GCG GCA ACA CCA TT -3'	1500 bp (Cre-positive)
<i>Ilk-loxP</i>	fwd: 5'- GTC TTG CAA ACC CGT CTC TGC G -3' rev: 5'- CAG AGG TGT CAG TGC TGG GAT G -3'	296 bp (wild-type) 370 bp (floxed)
<i>Itgb1-loxP (1)</i>	fwd: 5'- GGG TTG CCC TTC CCT CTA G -3' rev: 5'- GTG AAG TAG GTG AAA GGT AAC -3'	350 bp (wild-type) 450 bp (floxed)
<i>Itgb1-loxP (2)</i>	fwd: 5'- AGG TGC CCT TCC CTC TAG A -3' rev: 5'- GTG AAG TAG GTG AAA GGT AAC -3'	350 bp (wild-type) 450 bp (floxed)
<i>Cav1</i>	fwd: 5'- GCA CAC CAA GGA GAT TGA CC -3' rev: 5'- CTC CAG ACT GCC TTG GGA AAA -3' com: 5'- CTT GGC TGT CAC CAC ACA C -3'	661 bp (wild-type) 200 bp (mutant)
<i>Prox1-CreER<sup>T2</sup></i>	fwd: 5'- TGT CTG TGC CTC CAT CTC AG -3' rev: 5'- AGG CAA ATT TTG GTG TAC GG -3'	730 bp (Cre-positive)

For genotyping of *Itgb1-loxP* mice, the primer sequences as well as the PCR protocol was changed during this thesis due to increased frequency of non-working PCRs, and adapted from (Zong et al. 2009). In general, the following PCR protocols were used with a Professional Trio Thermocycler (Biometra):

<i>Flik1-Cre</i>	<i>Ilk-loxP</i>	<i>Itgb1-loxP (1)</i>
94°C, 5min	95°C, 5min	94°C, 3min
35x: 94°C, 1min	30x: 95°C, 30sec	10x: 94°C, 30sec
67°C, 1min	62°C, 30sec	63°C, 30sec
72°C, 1min	72°C, 30sec	72°C, 30sec
10°C, Pause	72°C, 7min	35x: 94°C, 30sec
	10°C, Pause	53°C, 30sec
		72°C, 30sec
		10°C, Pause

<i>Itgb1-loxP (2)</i>	<i>Cav1</i>	<i>Prox1-CreER<sup>T2</sup></i>
94°C, 2min	94°C, 2min	95°C, 5min
35x: 94°C, 1min	10x: 94°C, 20sec	30x: 95°C, 30sec
58°C, 1min	65°C, 15sec	55°C, 30sec
72°C, 1min	68°C, 10sec	72°C, 30sec
72°C, 10min	28x: 94°C, 15sec	72°C, 5min
10°C, Pause	60°C, 15sec	10°C, Pause
	72°C, 10sec	
	72°C, 2min	
	10°C, Pause	

Subsequently, PCR products were loaded on a 1% agarose (Bio-Budget Technologies, GmbH) gel containing 3% SYBR® Safe DNA Gel Stain (10.000x, Invitrogen), and gel electrophoresis was run for 20-35 minutes at 120 V with a Power PAC 1000 or 3000 System (Bio-Rad). Imaging of the gel was performed with the Chemidoc™ XRS Imaging System (Bio-Rad).

## 4.2. *Ex vivo* and *in vivo* methods

### 4.2.1. Magnetic-activated cell sorting (MACS)

To determine knockout efficiency of *Ilk* specifically in LECs of *Flik1-Cre;Ilk-loxP* embryos, these were used for magnetic-activated cell sorting (MACS). Specifically, immediately after isolation, embryos were dissociated using the gentleMACS™

Dissociator (Miltenyi Biotec), and LECs sorted as described in (Planas-Paz et al. 2012) as well as in the available customer protocol by Miltenyi Biotec (written by Dr. Lara Planas-Paz and Prof. Dr. Eckhard Lammert). Briefly, 600 U/ml Collagenase II (Worthington CLS-2) and 60 U/ml DNase I (AppliChem) were used in Hank's Balanced Salt Solution (HBSS) containing  $\text{Ca}^{2+}$  and  $\text{Mg}^{2+}$  (gibco® by Life Technologies™) for dissociation. Single-cell suspension was labeled with rat anti-mouse PECAM-1-FITC clone 390 (Millipore, CBL1337F) and rabbit anti-mouse Lyve1 (Abcam, ab14917) antibodies. Afterwards, the LECs were sorted using anti-FITC MultiSort microbeads (Miltenyi Biotec, 130-058-701) in a first step, followed by the use of goat anti-rabbit IgG microbeads (Miltenyi Biotec, 130-048-602) in a second step. Sorted LECs were finally resuspended in peqGold TriFast (Pepqlab), and used for RNA extraction and quantitative real-time PCR (see 4.4.1). MACS experiments as well as subsequent quantitative real-time PCR analyses were performed by Dr. Lara Planas-Paz.

#### 4.2.2. Corneal angiogenesis assays

Adult wild-type mice were used for siRNA-mediated knockdown of *Ilk* in the cornea. Therefore, siRNAs against mouse *Ilk* were applied into one eye, while non-targeting control siRNAs were applied into the contralateral eye of each mouse in same amounts and concentrations. siRNAs (Eurogentec) with following sequences were used:

ILK siRNA:	sense: 5'- CUG CGG UAU UGA CUU CAA A55 -3'
	antisense: 5'- UUU GAA GUC AAU ACC GGA G55 -3'
Control siRNA:	sense: 5'- AGU AUA AUC GUA UGA UCC A55 -3'
	antisense: 5'- UGG AUC AUA CGA UUA UAC U55 -3'

Immediately before use, siRNAs were thawed on ice, and diluted to a concentration of 1.5  $\mu\text{M}$  in ice-cold sterile 0.9% NaCl saline solution (Healthmark Services). For the topical application of siRNAs, mice were anesthetized with isoflurane (1.5-2.0 Vol.%, Butler Schein™ Animal Health), and siRNA solution was applied on the eyes in an amount of 10-15  $\mu\text{l}$ . Mice were kept anesthetized for 10 more minutes, so siRNAs would not be scratched off immediately. Heating pads were constantly used to keep body temperature of mice. In order to determine knockdown efficiency of *Ilk* in the cornea, siRNA applications were performed on 4 consecutive days, and mice were sacrificed on day 5 for the isolation of the cornea with subsequent use for RNA extractions and quantitative real-time PCR (see 4.4.1). For analysis of corneal lymphangiogenesis, siRNAs were applied on 10 consecutive days in total, and mice were sacrificed on day 11 for cornea isolation

with subsequent fixation and whole-mount stainings (see 4.6.1). These experiments were conducted at the University of Virginia in collaboration with Prof. Dr. Shayn Peirce-Cottler and Molly Kelly-Goss. In addition, corneas of adult *Prox1-CreER<sup>T2</sup>;Ilk-loxP* mice that were used for MI studies (see 4.2.3) were isolated after mice were sacrificed around 4 weeks after the last tamoxifen injections, and corneal lymphangiogenesis was analyzed by whole-mount stainings (see 4.6.1).

### 4.2.3. Myocardial infarction

To study the role of ILK in cardiac lymphatic vascular growth after MI, mice were subjected to temporary left anterior descending coronary artery (LAD) ligation for the induction of ischemia, followed by reperfusion. For the surgical procedures a closed-chest model was chosen in order to reduce inflammatory reactions that are due to the surgical trauma itself (Nossuli et al. 2000). Therefore, *Prox1-CreER<sup>T2</sup>* and *Prox1-CreER<sup>T2</sup>;Ilk-loxP* mice were used around one week after the last tamoxifen injections for surgical interventions, in which the chest was opened, and the suture placed underneath the LAD, closely following the detailed protocol described in (Merx et al. 2014). Mice were anesthetized by intraperitoneal injections of ketamine (100 mg/kg bodyweight, KetanestS®, Pfizer Pharma GmbH) and xylazine (10 mg/kg bodyweight, Rompun™, Bayer Healthcare). As soon as anesthesia was sufficient, mice were intubated and respirated with isoflurane (2.0 Vol.%, Piramal Healthcare) via an Uno Microventilator at a rate of 140 strokes per minute, and a tidal volume of 200 µl. Mice were placed on a warming plate to ensure a constant body temperature of 37°C, and electrocardiography (ECG) (Hugo Sachs Apparatus) was monitored. Heart was accessed between the third and fourth rib on the left side with subsequent dissection of the pericardium. A 7-0 surgical suture (Ethicon, Johnson and Johnson) was carefully passed underneath the LAD at a position around 1 mm from the tip of the left auricle. The suture was cut, and both ends were threaded through a 1 mm section of PE-10 tubing, thereby surrounding the LAD. The ends of the suture were knotted, and the loop was placed in the subcutaneous tissue. Afterwards, the chest was closed using a 5-0 suture (Ethicon, Johnson and Johnson).

Around one week later, mice were re-anesthetized by inhalation of isoflurane (2.0 Vol.%), while being placed on a warming plate under an infrared heating lamp. ECG was monitored to document ST-segment elevation. The skin was carefully re-opened and the suture loop was dissected. Both ends of the suture were fixed to metal picks, and ischemia was induced by gently pulling the metal picks apart until ST-elevation was detectable on the ECG. After 60 minutes of ischemia, metal picks were pushed against

each other, resulting in reperfusion, which was confirmed by resolution of ST-elevation. Finally, the skin was closed and anesthesia was turned off. Mice were post-operative observed for 2 or 5 days and treated with temgesic (0.05-0.1 mg/kg bodyweight, subcutaneous injections, Essex-Pharma GmbH) every 6 to 8 hours for analgesia. Myocardial infarction studies were performed by Carina Henning at the Division of Cardiology, Pulmonology, and Vascular Medicine, Medical Faculty, University Düsseldorf. Mouse hearts were isolated and analyzed around 4 weeks after MI by Sofia Urner.

### 4.3. *In vitro* methods

#### 4.3.1. Cell culture and transfections

*In vitro* studies were performed with adult human dermal microvascular LECs (HMVEC-dLyAd, Lonza, CC-2810 or HDLEC-c adult, PromoCell, C-12217). LECs were kept in culture in endothelial cell growth medium MV2 (EGM-2 MV, PromoCell or Lonza) at 37°C (5% CO<sub>2</sub> atmosphere and humidified), and used at passages ≤ P6 with a confluence of 70-90%. For all transfections, the Nucleofector™ 2b Device or the 4D-Nucleofector™ System (Lonza) was used.

To achieve a knockdown of *ILK*, LECs were transfected with three different stealth siRNAs against *ILK* (Invitrogen), respectively:

ILK siRNA-1:	5'- GCCUGUGGCUGGACAACACGGAGAA -3'
ILK siRNA-2:	5'- CAGCCAGUCAUGGACACCGUGAUAU -3'
ILK siRNA-3:	5'- GCAUUGACUUCAAACAGCUUAACUU -3'

In addition, a non-targeting siRNA with a similar GC content (Invitrogen) was used as control. Stealth siRNAs were transfected in a concentration of 500 nM, while around 500.000 LECs were used. Subsequently, transfected cells were collected in fresh EGM-2 MV medium, and distributed into cell culture dishes that were previously coated with fibronectin in a concentration of 2.5 µg/cm<sup>2</sup> (Human Plasma Fibronectin Purified Protein, Millipore). For stainings, cells were plated on coverslips (VWR), while for quantitative real-time PCR or Western Blotting cells were cultured on tissue culture plates (SARSTEDT or VWR). After an incubation of 72 hours, LECs were used for further analyses (see 4.3.2, 4.4.1, 4.5.2, 4.5.3, 4.6.3).

For mechanical stretch experiments, human LECs were also transfected with a plasmid encoding the expression of C-terminally Human influenza hemagglutinin (HA)-tagged  $\beta 1$  integrin (Sino Biological, HG10587-CY). Before using the plasmid for *in vitro* experiments, it was transformed into DH5 $\alpha$  competent cells (Invitrogen), and amplified using a QIAGEN Plasmid Midi Kit according to the manufacturer's protocol. Afterwards, 1  $\mu$ g plasmid was used for transfection of 500.000 human LECs. Cells were subsequently distributed into fibronectin-coated STREX stretch chambers (BioCat, ST-CH-04-BR), and used for mechanical stretch experiments 48 hours after transfection. As soon as mechanical stretch was carefully induced, cells were kept in culture for 30 minutes. This was the general procedure for experiments with transfected, but also non-transfected cells. Afterwards, the chambers were put on ice in stretched conditions, and immediately used for co-immunoprecipitation experiments or proximity ligation assays (see 4.5.1 and 4.6.3).

### 4.3.2. *In vitro* proliferation assays

*In vitro* proliferation was determined by performing 5-bromo-2'-deoxyuridine (BrdU) incorporation assays with LECs after ILK siRNA transfections. Therefore, EGM-2 MV medium was removed, and LECs were incubated with 10  $\mu$ M BrdU (Sigma) and 100 ng/ml VEGF-C156S (R&D Systems, 752-VC-025) in endothelial basal medium (EBM-2, PromoCell or Lonza) for 1 hour. LECs were fixed with ethanol fixative, consisting of 70% absolute ethanol (Honeywell Riedel-de Haen) and 30% glycine (50 nM, AppliChem), for 20 minutes on ice. For cell denaturation, LECs were incubated with 2M HCl (Sigma-Aldrich) for 20 minutes at room temperature (RT), followed by a neutralization step with 1M sodium tetraborate (pH 8.5, Aldrich Chemistry) for 2 minutes at RT. In between, cells were washed with buffer containing 0.5% bovine serum albumin (BSA, AppliChem) and 0.02% NaN<sub>3</sub> (Sigma-Aldrich) in PBS (gibco® by Life Technologies™), which was further used for antibody dilutions. Following primary and secondary antibodies were used:

Primary antibodies	Dilution	Secondary antibodies	Dilution
mouse anti-BrdU (BD Bioscience, 555627)	1/500	donkey anti-mouse AF488-conjugated (Molecular probes) DAPI (Sigma)	1/500  1/1000

Cells were incubated with primary antibody for 1 hour at RT, under agitation. The secondary antibody was incubated for 30 minutes at RT, under agitation. In addition, DAPI was used to counterstain cell nuclei. Coverslips were mounted with Fluoroshield™ (Sigma), and analyzed via Fluorescence microscopy (Nikon Eclipse Ti-S) and the

ImageJ/Fiji software. Proliferation rates were determined by the number of BrdU-positive cells divided by the total number of LECs.

### 4.4. Molecular biological methods

#### 4.4.1. Quantitative real-time PCR

To determine knockdown efficiencies, such as after siRNA application within the cornea angiogenesis assays, fresh corneas were immediately homogenized in 700  $\mu$ l ice-cold peqGold TriFast (Peqlab) after isolation, and lysates were incubated on ice for 3-4 hours. For analysis of knockdown efficiencies *in vitro*, human LECs were briefly washed with PBS (gibco® by Life Technologies™) 72 hours after transfection, and lysed in 300  $\mu$ l ice-cold peqGold TriFast (Peqlab). In general, lysates were either used directly for RNA extractions, or stored at  $-80^{\circ}\text{C}$ . RNA extractions were performed either using the PureLink™ RNA Micro Scale Kit (Invitrogen by Thermo Fisher Scientific) according to the manufacturer's protocol, or using the single-step acid guanidinium thiocyanate-phenol-chloroform extraction method (Chomczynski and Sacchi 1987). Subsequently, RNA quality and concentrations were measured using a NanoDrop 2000C or BioMate™ 3 (Thermo Fisher Scientific). 0.5-1  $\mu$ g RNA was used for DNase I treatment (Thermo Scientific), and subsequent cDNA synthesis, which was performed using SuperScript™ II Reverse Transcriptase (Invitrogen by Thermo Fisher Scientific) according to the manufacturer's protocol. Following master-mix was used for quantitative real-time PCR per sample:

- 5  $\mu$ l Mix1 (FastStart Essential DNA Green Master, Roche)
- 2  $\mu$ l Primer-Mix (fwd and rev, pre-diluted to 3 $\mu$ M, see below)
- 2  $\mu$ l dH<sub>2</sub>O (Mix2, FastStart Essential DNA Green Master, Roche)
- 1  $\mu$ l cDNA

Primers with following sequences were used:

Primer	Primer sequences
Mouse <i>Ilk</i> (Eurofins) (MACS experiments)	fwd: 5'- GTG GCT GGA CAA CAC AGA GA -3' rev: 5'- ATC CCC ACG ATT CAT CAC AT -3'
Mouse <i>beta-2-microglobulin (b2m)</i> (Eurofins) (MACS experiments)	fwd: 5'- GAG CCC AAG ACC GTC TAC TG -3' rev: 5'- GCT ATT TCT TTC TGC GTG CAT -3'
Mouse <i>Ilk</i> (Eurogentec) (Cornea experiments)	fwd: 5'- GTG GCT GGA CAA CAC AGA GA -3' rev: 5'- ATC CCC ACG ATT CAT CAC AT -3'
Mouse <i>peptidylprolyl isomerase A (PPIA)</i> Eurogentec) (cornea experiments)	fwd: 5'- AAT GCT GGA CCA AAC ACA AA-3' rev: 5'- TTC CAC AAT GTT CAT GCC TT-3'
Human <i>ILK</i> (Eurofins) ( <i>In vitro</i> experiments)	fwd: 5'- AAG GTG CTG AAG GTT CGA GA -3' rev: 5'- ATA CGG CAT CCA GTG TGT GA-3'
Human <i>B2M</i> (Eurofins) ( <i>In vitro</i> experiments)	fwd: 5'- TTT CAT CCA TCC GAC ATT GA -3' rev: 5'- CCT CCA TGA TGC TGC TTA CA-3'

Quantitative real-time PCR was run on the CFX96 Detection System (Bio-Rad) or the LightCycler Nano Device (Roche) with following protocols:

Cornea experiments	MACS and <i>in vitro</i> experiments
95°C, 10min	95°C, 10min
40x: 95°C, 10sec	40x: 95°C, 20sec
60°C, 60sec	60°C, 20sec
	72°C, 20sec
	60°C, 20sec
	95°C, 20sec

All experiments were performed in duplicates or triplicates. For analysis of knockdown efficiencies in MACS-sorted LECs from mouse embryos, *Ilk* mRNA levels were normalized to the housekeeping gene *beta-2-microglobulin (b2m)*. Same housekeeping gene was used for *in vitro* studies with human LECs. For analysis of knockdown efficiencies in mouse corneas, *Ilk* mRNA levels were normalized to *peptidylprolyl isomerase A (PPIA)* as housekeeping gene (Ren et al. 2010). For all analyses, the comparative  $C_T$  method was used, in which  $2^{-\Delta C_T}$  is presented (with  $\Delta C_T$  defined as  $C_T$  gene of interest -  $C_T$  housekeeping gene), as previously described (Livak and Schmittgen 2001; Schmittgen and Livak 2008).

## 4.5. Biochemical methods

### 4.5.1. Co-immunoprecipitation (Co-IP)

Co-immunoprecipitation (Co-IP) assays were performed with LECs that were previously transfected with HA-tagged  $\beta 1$  integrin plasmids, and stretched for 30 minutes. Afterwards, stretched chambers were kept on ice for a brief washing with PBS (gibco® by Life Technologies™), and immediately lysed in following lysis buffer (300  $\mu$ l / chamber) for 20 minutes on ice:

50 mM HEPES pH 7.0 (Fisher Scientific)  
150 mM NaCl (Fisher Chemical)  
10% glycerol (Roth)  
1% Triton X-100 (AppliChem)  
1 mM  $\text{Na}_3\text{VO}_4$  (Aldrich)  
1x cocktail of protease inhibitors (25x, Roche)  
1x cocktail of phosphatase inhibitors (10x, Roche or 100x, Sigma)  
in  $\text{dH}_2\text{O}$

Cells were scraped off the chambers using cell scraper (SARSTEDT), and lysates were centrifuged for 10 minutes at 13.000rpm at 4°C. The supernatants were collected, and protein concentrations were determined using the Pierce™ BCA Protein Assay (Thermo Fisher Scientific). Equal amounts of protein (300  $\mu$ g) were taken for a pre-clearing step with 30  $\mu$ l Protein G Plus/Protein A Agarose Suspension (Millipore, IP05-1.5ml) for 1 hour at 4°C under rotation. After centrifugation for 10 minutes at 5.000g at 4°C, supernatants were incubated with 3  $\mu$ l rabbit anti-HA tag antibody (Cell Signaling, 3724) at 4°C o/n under rotation. On the next day, 15  $\mu$ l Protein G Plus/Protein A Agarose Suspension were added to the lysates, and incubated for 3 more hours at 4°C under rotation. Afterwards, supernatants were removed, and beads were washed three times using the lysis buffer with short centrifugation steps (1 minute at 5.000g, 4°C) in between, in which the supernatants were discarded. For Western Blotting, beads were finally collected in 2x Laemmli buffer following the protocol described in 4.5.2.

### 4.5.2. Western Blotting

For protein analyses, Western Blotting was performed to determine knockdown efficiencies after siRNA transfections, as well as for Co-IP assays. LECs, which were

previously transfected with siRNAs, were briefly washed with PBS (gibco® by Life Technologies™), and directly collected with 1x Laemmli buffer with following composition:

- 10 mM NaF (Sigma-Aldrich)
- 1 mM Na<sub>3</sub>VO<sub>4</sub> (Aldrich)
- 1x cocktail of protease inhibitors (25x, Roche)
- 1x cocktail of phosphatase inhibitors (10x, Roche or 100x, Sigma)
- 1x Laemmli Sample Buffer (4x, Bio-Rad)
- 1% 2-Mercaptoethanol (Roth)
- in dH<sub>2</sub>O

Co-IP samples were lysed in same buffer containing 2x Laemmli Sample Buffer instead of 1x (50-60 µl buffer were used per IP). Lysates were immediately heated at 95°C for 5 minutes, and Western Blotting was either started directly, or lysates were stored at -80°C, and heated up again before starting the Western Blot. For protein separation Invitrogen novex Mini-Cell Device (Thermo Fisher Scientific) was used with 1x MOPS buffer (novex by Life Technologies). Depending on the exact gels that were used (NuPAGE™ 4-12% Bis-Tris Gel, Invitrogen by Thermo Fisher Scientific), 20-25 µl lysate were loaded, and protein separation was run for around 90 minutes at 180 V. Afterwards, gels were briefly incubated in 2x Transfer buffer (novex by Life Technologies) containing 10% methanol, and subsequently used for Western Blotting with Trans-Blot® Turbo™ Transfer membranes (Bio-Rad) and the Trans-Blot Turbo Transfer System (Bio-Rad), which was run 2x 13 minutes (high molecular weight program). Membranes were blocked with PBS (Ca<sup>2+</sup>, Mg<sup>2+</sup>) containing 5% BSA (AppliChem) and 0.5% Tween-20 (AppliChem) for 1 hour at RT under agitation, and blocking buffer was used for the dilution of following primary and secondary antibodies:

Primary antibodies	Dilution	Secondary antibodies	Dilution
rabbit anti-HA tag (Cell Signaling, 3724)	1/500	donkey anti-rabbit HRP-conjugated (dianova, Jackson ImmunoResearch)	1/500
mouse anti-ILK (BD Biosciences, 611803)	1/500	donkey anti-mouse HRP-conjugated (dianova, Jackson ImmunoResearch)	1/500
rabbit anti-ILK (Cell Signaling, 3862)	1/500 or 1/1000		
rabbit anti-GAPDH (Abcam, ab9485)	1/5000		

Primary antibodies were incubated o/n at 4°C under agitation. Horse Radish Peroxidase (HRP)-conjugated secondary antibodies were incubated for 1 hour at RT under agitation

on the next day. For detection, Clarity™ Western ECL Substrate solution (Bio-Rad) was used, and after an incubation of 1 minute Western Blots were detected using a Chemidoc™ XRS Imaging System (Bio-Rad). Since Co-IP assays often showed high variability in the amount of HA-tagged  $\beta$ 1 integrin protein although protein amounts were normalized before, Western Blots were repeated with adjusted loading amounts, so virtually equal amounts of HA-tagged  $\beta$ 1 integrin were present within one Western Blot. The amount of detected ILK protein levels was normalized to the amount of HA-tagged  $\beta$ 1 integrin protein within each sample. For determination of knockdown efficiencies, ILK protein levels were normalized to the detected GAPDH levels within each sample. Analysis of protein bands was performed with ImageJ/Fiji software using the gel analysis tool.

### 4.5.3. ELISA

To determine VEGFR3 tyrosine phosphorylation levels in mouse skin lysates, ears were collected after mice were sacrificed, and tissue layers were quickly separated in ice-cold PBS (gibco® by Life Technologies™). The inner ear skin layer was immediately homogenized using following ice-cold lysis buffer:

- 50 mM HEPES pH 7.0 (Fisher Scientific)
- 150 mM NaCl (Fisher Chemical)
- 10% glycerol (Roth)
- 1% Triton X-100 (AppliChem)
- 1 mM Na<sub>3</sub>VO<sub>4</sub> (Aldrich)
- 1x cocktail of protease inhibitors (25x, Roche)
- 1x cocktail of phosphatase inhibitors (10x, Roche or 100x, Sigma)
- in dH<sub>2</sub>O

The same buffer was used for lysis of human LECs in order to determine VEGFR3 tyrosine phosphorylation. In this context, LECs were starved o/n in EBM-2 (0.5% Fetal Bovine Serum, FBS, gibco® by Life Technologies™), washed with PBS (gibco® by Life Technologies™), and stimulated with 100 ng/ml VEGF-C156S (R&D Systems, 752-VC-025) diluted in EBM-2 only (PromoCell or Lonza). After 5 minutes of incubation, cells were put on ice, immediately washed with ice-cold PBS (gibco® by Life Technologies™), and incubated with lysis buffer for 20 minutes on ice. Lysates were afterwards scratched off, centrifuged for 10 minutes at 13.000rpm at 4°C, and supernatants were collected. Protein concentrations were determined using the Pierce™ BCA Protein Assay (Thermo Fisher

Scientific). Within each experiment, equal amounts of protein were loaded on the ELISA plates. In general, following ELISAs were used according to the manufacturer's protocol:

DuoSet IC human phospho-VEGFR3 ELISA (R&D Systems, DYC2724-5)

DuoSet IC human total VEGFR3 ELISA (R&D Systems, DYC3491-5)

ELISA results were determined by using a NanoQuant Infinite M200 Reader (TECAN). For quantifications of VEGFR3 tyrosine phosphorylation in mouse skin lysates, the values of the phospho-VEGFR3 ELISA were normalized to the values of the total VEGFR3 ELISA, since the lysates did not represent a pure LEC population. In contrast, no such normalization was performed for *in vitro* studies with human LECs because of prior normalization to protein amounts.

#### 4.6. Histochemical methods

##### 4.6.1. Whole-mount stainings

For whole-mount stainings (WMS), mouse corneas were collected in 1.5ml eppendorf tubes after isolation, briefly washed in PBS ( $\text{Ca}^{2+}$ ,  $\text{Mg}^{2+}$ ), and immediately fixed in acetone (VWR) for 20 minutes at RT. Afterwards, corneas were washed again, before they were blocked in PBS ( $\text{Ca}^{2+}$ ,  $\text{Mg}^{2+}$ ) containing 5% Normal Donkey Serum (NDS, Jackson ImmunoResearch), 5% BSA (AppliChem) and 0.2% Saponin (Sigma) for 1 h at RT under agitation. Blocking buffer was used for the dilution of following primary and secondary antibodies:

Primary antibodies	Dilution	Secondary antibodies	Dilution
goat anti-mouse Lyve1 (R&D Systems, AF2125)	1/200	donkey anti-goat AF488-conjugated (Molecular probes)	1/500
rat biotin anti-mouse CD31 (BioLegend, 102504)	1/400	donkey anti-rat AF555- / Cy3-conjugated (Molecular probes / Jackson ImmunoResearch)	1/500
		DAPI (Sigma)	1/1000

Primary antibodies were incubated o/n at 4°C under agitation. Secondary antibodies were incubated for 1 hour at RT under agitation on the next day. In addition, DAPI was used to counterstain cell nuclei. Corneas were mounted on slides with Fluoroshield™ (Sigma) in a way that the outer cornea layer could be used for imaging and analysis (see 4.6.4).

For WMS of the adult mouse ear skin, ears were collected after mice were sacrificed, and tissue layers were gently separated. The inner ear skin layer was fixed in freshly prepared 4% paraformaldehyde (PFA, Chemsolute, Th. Geyer) o/n at 4°C under agitation. On the next day, the skins were washed in PBS (Ca<sup>2+</sup>, Mg<sup>2+</sup>), before they were blocked in PBS (Ca<sup>2+</sup>, Mg<sup>2+</sup>) containing 5% NDS (Jackson ImmunoResearch), 1% BSA (AppliChem) and 0.5% Triton X-100 (AppliChem) for 1 h at RT shaking at 300rpm. Blocking buffer was used for the dilution of following primary and secondary antibodies:

Primary antibodies	Dilution	Secondary antibodies	Dilution
goat anti-mouse VEGFR3 (R&D Systems, AF743)	1/50	donkey anti-goat AF488-conjugated (Molecular probes)	1/500
rat anti-mouse CD31/Pecam-1 (BD Bioscience, 553370)	1/50	donkey anti-rat Cy5-conjugated (Jackson ImmunoResearch)	1/500
rabbit anti-phospho-Histone H3 (Millipore, 06-570)	1/100	donkey anti-rabbit AF555- / Cy3- conjugated (Molecular probes or Jackson ImmunoResearch)	1/500
		DAPI (Sigma)	1/1000

Primary antibodies were incubated for 3 hours at 31°C shaking at 300rpm. Secondary antibodies were incubated for 1 hour at 33°C shaking at 300rpm. In addition, DAPI was used to counterstain cell nuclei. Ear skins were mounted on slides with Fluoroshield™ (Sigma) in a way that the internal-facing side could be used for imaging and analysis (see 4.6.4).

#### 4.6.2. Immunohistochemistry

Adult mouse hearts as well as whole mouse embryos were further used for immunohistochemistry. Therefore, hearts or embryos were collected and fixed in freshly prepared 4% PFA (Chemsolute, Th. Geyer) o/n at 4°C under rotation. On the next day, tissues were washed in PBS (Ca<sup>2+</sup>, Mg<sup>2+</sup>), and slowly cryopreserved in 15% and 30% sucrose (Sigma) o/n at 4°C under rotation, respectively. Afterwards, hearts as well as embryos were embedded transversally into embedding molds (Peel-A-Way®, Polyscience Inc.) filled with Tissue Tek OCT embedding media (Thermo Fisher Scientific), and stored at -80°C. During cryo-sectioning, tissues were separated into 12 µm cryo-sections using a cryostat microtome HM 560 (Thermo Fisher Scientific), and immediately used for stainings or stored at -20°C. Slides were washed in PBS (Ca<sup>2+</sup>, Mg<sup>2+</sup>) before blocking in PBS (Ca<sup>2+</sup>, Mg<sup>2+</sup>) containing 5% NDS (Jackson ImmunoResearch), 1% BSA (AppliChem) and 0.2%

Triton X-100 (AppliChem) for 1 h at RT, using humidified chambers. Blocking buffer was used for the dilution of following primary and secondary antibodies:

Primary antibodies	Dilution	Secondary antibodies	Dilution
rabbit anti-mouse Lyve1 (Abcam, ab14917)	1/100	donkey anti-rabbit AF488-conjugated (Molecular probes)	1/500
goat anti-mouse Lyve1 (R&D Systems, AF2125)	1/100	donkey anti-rabbit AF555- / Cy3- conjugated (Molecular probes or Jackson ImmunoResearch)	1/500
rat anti-mouse CD31/Pecam-1 (BD Bioscience, 553370)	1/50	donkey anti-goat AF488-conjugated (Molecular probes)	1/500
goat anti-CD31 (R&D Systems, AF3628)	1/20	donkey anti-goat AF555- / Cy3- conjugated (Molecular probes or Jackson ImmunoResearch)	1/500
rabbit anti-phospho-Histone H3 (Millipore, 06-570)	1/100	donkey anti-goat Cy5-conjugated (Jackson ImmunoResearch)	1/500
rat anti-activated $\beta 1$ integrin clone 9EG7 (BD Bioscience, 553715)	1/100	donkey anti-rat AF555- / Cy3-conjugated (Molecular probes or Jackson ImmunoResearch)	1/500
		donkey anti-rat Cy5-conjugated (Jackson ImmunoResearch)	1/500
		DAPI (Sigma)	1/1000

Primary antibodies were incubated either 1 hour at RT or o/n at 4°C. Secondary antibodies were incubated for 1 hour at RT under agitation. In addition, DAPI was used to counterstain cell nuclei. For imaging and analysis, slides were mounted with Fluoroshield™ (Sigma) and stored at 4°C until imaging and analysis (see 4.6.4).

#### 4.6.3. Proximity ligation assays (PLA)

Proximity ligation assays (PLA) were used to detect VEGFR3 tyrosine phosphorylation as well as interactions between VEGFR3 and  $\beta 1$  integrin, both *in vivo* and *in vitro*. PLAs were performed using the Duolink In situ reagents (Olink Bioscience) according to the manufacturer's protocol. PBS ( $\text{Ca}^{2+}$ ,  $\text{Mg}^{2+}$ ) was used for washing steps. Mouse embryonic sections, stretch chambers or cell culture dishes with human LECs were blocked in PBS ( $\text{Ca}^{2+}$ ,  $\text{Mg}^{2+}$ ) containing 5% NDS (Jackson ImmunoResearch), 1% BSA (AppliChem) and 0.2% Triton X-100 (AppliChem) for 1 h at RT using humidified

chambers. Blocking buffer was used for the dilution of following primary and secondary antibodies:

Primary antibodies	Dilution	Secondary antibodies	Dilution
goat anti-mouse VEGFR3 (R&D Systems, AF743)	1/50	donkey anti-rabbit AF488-conjugated (Molecular probes)	1/500
mouse anti-phospho-Tyrosine 4G10 Platinum (Millipore, 05-1050)	1/100	AF488-conjugated phalloidin (Invitrogen by Thermo Fisher Scientific, A12379)	1/200
anti-mouse $\beta$ 1 integrin clone MB1.2 (Millipore, MAB1997)	1/50	DAPI (Sigma)	1/1000
goat anti-human VEGFR3 (R&D Systems, AF349)	1/100		
mouse anti-human $\beta$ 1 integrin (Millipore, MAB19887)	1/100		
rabbit anti-mouse Lyve1 (Abcam, ab14917)	1/100		

Antibodies against Lyve1 and Phalloidin were used for co-stainings. Primary antibodies were incubated either 1 hour at RT or o/n at 4°C. In addition, DAPI was used to counterstain cell nuclei. After stainings, the stretch chambers were cut, and only the thin part containing the cell layer was mounted on slides using Fluoroshield™ (Sigma). All slides were stored at -20°C until imaging and analysis (see 4.6.4).

#### 4.6.4. Imaging and image analysis

Images were acquired using Laser Scan Microscopy (LSM 710, Zeiss), and analyzed using the ImageJ/Fiji Software. For whole-mount stainings of the cornea and the ear skin, tile scans and z-stacks were performed in order to image the tissue as a whole. PLAs were also imaged as z-stacks. Maximum intensity projections were performed for all z-stacks before analysis. Lymph vessel densities were determined by adjusting a threshold on VEGFR3 or Lyve1 staining, measure the area limited to threshold, and normalize to the total analyzed tissue area. Cell numbers on embryonic cross-sections were quantified manually, while an automated cell counting tool in ImageJ/Fiji was used to determine cell numbers in *in vitro* studies. PLA sites were analyzed by using standardized macros for all images within one experiment, or quantified manually if the macros did not fit. The number of PLA dots was normalized either to the Lyve1-positive area or to the number of cells in the analyzed image.

### 4.7. Statistics

Statistical significance was determined by using Prism software (GraphPad Inc.). For comparisons of two groups, unpaired two-tailed Student's *t*-test was performed in most cases, with the exception of siRNA-based cornea angiogenesis assays (see 4.2.2), in which comparisons concentrated on the differences between the corneas per mouse. Therefore, a paired two-tailed Student's *t*-test was performed. For multiple comparisons, one-way ANOVA followed by Dunnett's post hoc-test was used. Statistical differences were considered significant with a *P* value less than 0.05. All quantified data are presented as mean  $\pm$  standard error of the mean (SEM). Significant outliers were detected by the extreme studentized deviate method (Grubbs' test) and excluded from the statistical analysis.

### 4.8. Personal contributions

Sofia Urner performed most of the experiments and was supervised by Prof. Dr. Eckhard Lammert; funded by the DFG, IRTG1902.

Dr. Lara Planas-Paz started the project, and performed first experiments on the embryonic phenotype of *Ilk*-deficient embryos, as well as on first *in vitro* studies; funded by the DFG, LA-1216/5-1.

Molly Kelly-Goss and Sofia Urner performed *in vivo* corneal angiogenesis assays in adult mice at the Department of Biomedical Engineering with supervision by Prof. Dr. Shayn Peirce-Cottler (University of Virginia, Charlottesville, USA). Sofia Urner performed immunostainings, imaging and analysis.

Carina Henning performed myocardial infarction surgeries in adult mice. Sofia Urner performed tamoxifen injections, and experimental procedures including harvesting, cryo-sectioning of hearts, and immunostainings, as well as imaging and analysis.

Laura Sophie Hilger was co-supervised by Sofia Urner during her Master Thesis in 2016-2017, and contributed to some *in vitro* results.

Sofia Urner further co-supervised Dominik Gebel during his Bachelor Thesis in 2015, as well as Theresa Ohly during an internship of 3 months in 2015/2016, who worked on related topics to this thesis.

Within collaborations, *Prox1-CreER<sup>T2</sup>* mice and respective tamoxifen injection protocol were provided by Dr. Lukas Stanczuk and Prof. Dr. Taija Mäkinen (Department of Immunology, Genetics and Pathology, Uppsala, Sweden), while *Tie2-Cre;Parva-loxP* embryos and respective controls were provided by Dr. Bettina Pitter and Dr. Eloi Montanez (Institute of Cardiovascular Physiology, Biomedical Center Munich, Germany).

## 5. Results

### 5.1. Role of ILK in lymphatic vascular growth during mouse embryonic development

In order to determine whether ILK plays a role in lymphatic vascular development, mouse embryos with endothelial cell-specific *Ilk* deletion were analyzed. Specifically, *Flk1-Cre;Ilk<sup>+/-</sup>* embryos with heterozygous deletion of *Ilk* were used as control embryos (referred to as ‘control’), and compared to *Flk1-Cre;Ilk<sup>Δ/Δ</sup>* embryos with homozygous deletion of *Ilk* (referred to as ‘ILK K.O.’). These embryos showed about 75% reduction of *Ilk* mRNA expression levels in LECs compared to control embryos (Figure 7A). Deletion of *Ilk* further resulted in formation of edema in dorsolateral regions, as well as formation of hemorrhages in the head regions (Figure 7B-D). In addition, ILK K.O. embryos showed increased lethality from E14.5 onwards, as only around 36% of analyzed ILK K.O. embryos were alive at this embryonic stage (Figure 7D).

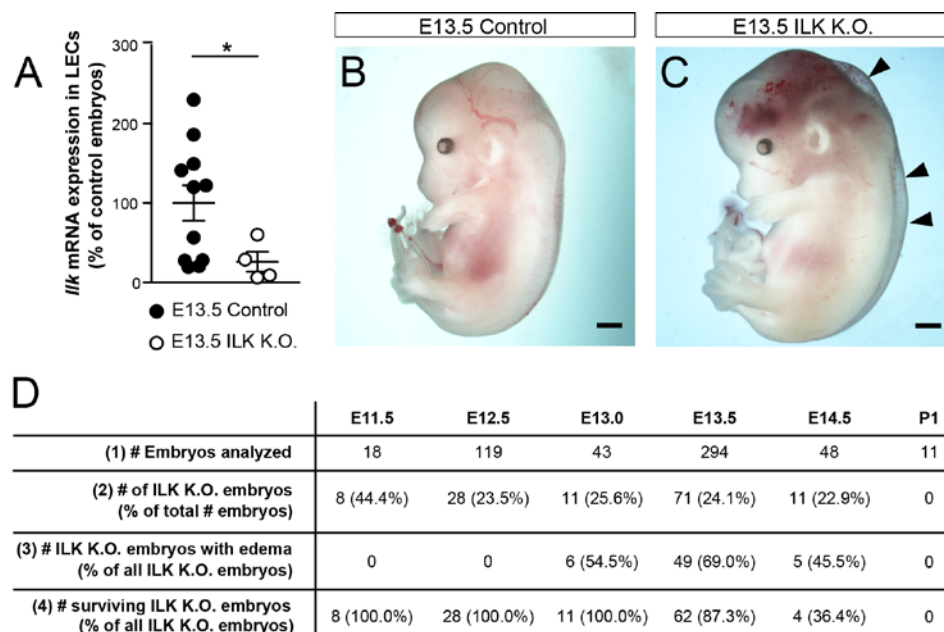


**Figure 7: *Ilk* is efficiently deleted in LECs using *Flk1-Cre*, and results in edema formation and embryonic lethality.** (A) Quantifications of *Ilk* mRNA expression levels in LECs of control (*Flk1-Cre;Ilk<sup>+/-</sup>*) and ILK K.O. (*Flk1-Cre;Ilk<sup>Δ/Δ</sup>*) embryos, shown as percentage of control embryos. All values are shown as means ± SEM with  $n \geq 4$  embryos per genotype; statistical significance was determined by unpaired two-tailed Student’s t-test (\* $P < 0.05$ ). (B, C) Representative bright-field images of an E13.5 control (B) and ILK K.O. (C) embryo with arrowheads pointing to the edema in the dorsolateral part. Scale bars, 500  $\mu\text{m}$ . (D) Overview table of the number of (1) total analyzed embryos including (2) ILK K.O. embryos, (3) ILK K.O. embryos with edema, and (4) surviving ILK K.O. embryos. Dr. Lara Planas-Paz performed the presented experiments.

### 5.1.1. ILK controls lymphatic vascular expansion and LEC proliferation during mouse embryonic development

The jls/pTD is the first lymphatic vascular structure, which forms pairwise in the developing mouse embryo from E11.5 onwards, and gives rise to the majority of the lymphatic vascular network (Srinivasan et al. 2007; Yang et al. 2012; Hagerling et al. 2013). Therefore, ILK K.O. embryos were investigated at different embryonic stages between E11.5 and E13.5 by analyzing the size of the jls/pTD in embryonic cross-sections. Thereby, ILK K.O. embryos showed a strongly enlarged jls/pTD from E13.0 onwards (Figure 8A-H). Further, the total LEC number within the jls/pTD region of ILK K.O. embryos was significantly increased at E13.5 (Figure 8I), indicating that ILK controls lymphatic vascular expansion during embryonic development.

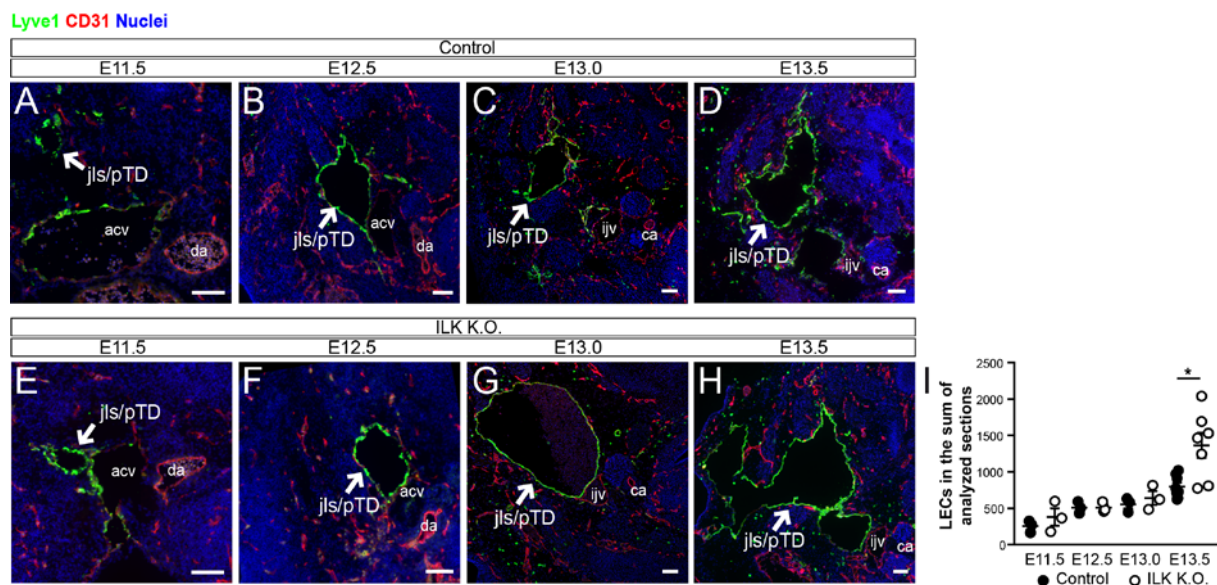


**Figure 8: Endothelial cell-specific deletion of *Ilk* results in enlarged jls/pTD and increased LEC number during embryonic development. (A-H)** Representative LSM images of cross-sections through the jugular lymph sac (jls) / primordial thoracic duct (pTD) of control (*Flk1-Cre;Ilk<sup>+/-</sup>*) embryos at E11.5-E13.5 (A-D), and ILK K.O. (*Flk1-Cre;Ilk<sup>Δ/Δ</sup>*) embryos at E11.5-E13.5 (E-H). Arrows point to the jls/pTD, identified by the expression of the lymphatic endothelial cell marker Lyve1 (green). Co-stainings for the endothelial cell marker CD31 (red) and nuclei (blue) are also shown. Scale bars, 100  $\mu$ m. Anterior cardinal vein (acv), dorsal aorta (da), internal jugular vein (ijv) and carotid artery (ca) are also indicated. **(I)** Quantifications of the LEC number in the sum of analyzed sections of control and ILK K.O. embryos at the embryonic stages E11.5-E13.5. All values are shown as means  $\pm$  SEM with  $n \geq 3$  embryos per genotype and stage; statistical significance was determined by unpaired two-tailed Student's t-test (\* $P < 0.05$ ). Dr. Lara Planas-Paz performed the presented experiments.

In order to determine the reason for the increased LEC number in ILK K.O. embryos, the proliferation of LECs within the jls/pTD was investigated by phospho-Histone H3 (pH3) stainings of embryonic cross-sections (Figure 9A-D). ILK K.O. embryos showed significantly more proliferating LECs within the jls/pTD region at E13.0 and E13.5, while earlier embryonic

stages showed no difference between the genotypes (Figure 9E). These results indicate that ILK inhibits LEC proliferation, and thereby controls LEC number and lymphatic vascular expansion during embryonic development.

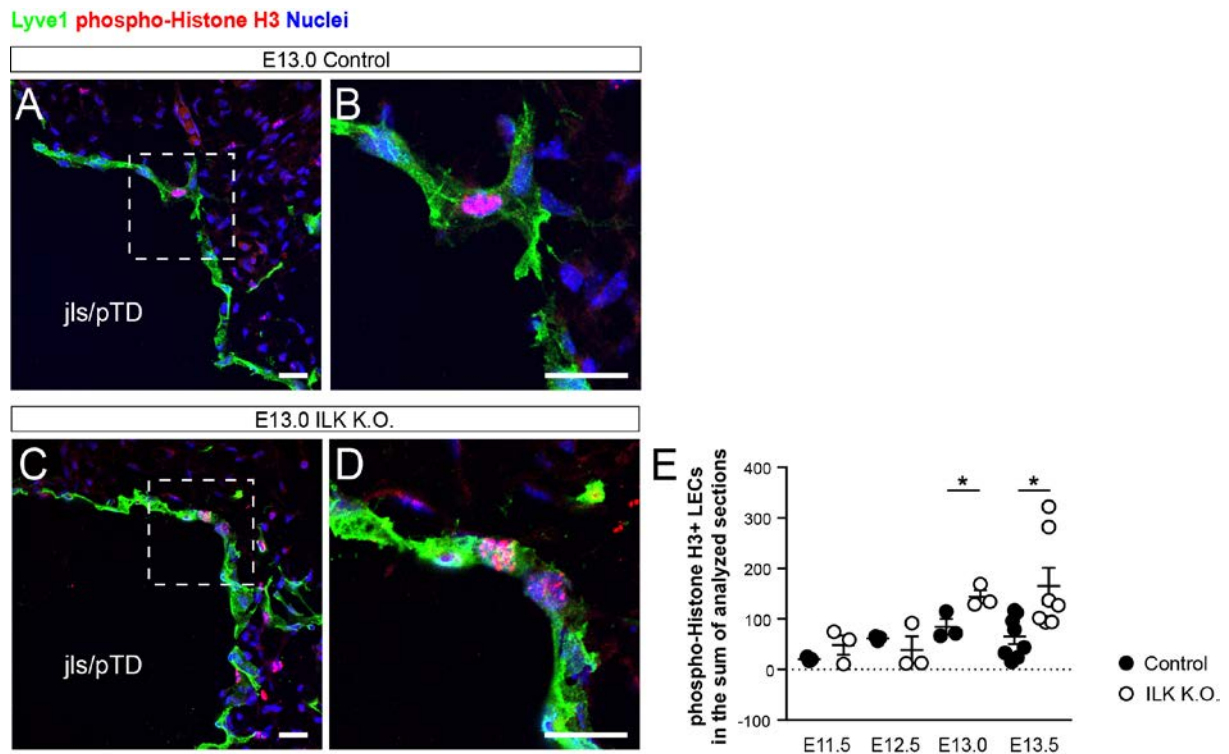


**Figure 9: Endothelial cell-specific deletion of *Ilk* results in increased LEC proliferation during embryonic development.** (A-D) Representative LSM images of cross-sections through the jugular lymph sac (jls) / primordial thoracic duct (pTD) of an E13.0 control (*Flk1-Cre;Ilk<sup>+Δ</sup>*) embryo (A, B) and ILK K.O. (*Flk1-Cre;Ilk<sup>ΔΔ</sup>*) embryo (C, D) stained for Lyve1 (green), the cell proliferation marker phospho-Histone H3 (red) and nuclei (blue). Scale bars, 20  $\mu$ m. (E) Quantifications of phospho-Histone H3-positive LECs in the sum of analyzed sections of control and ILK K.O. embryos at the embryonic stages E11.5-E13.5. All values are shown as means  $\pm$  SEM with  $n \geq 3$  embryos per genotype and stage; statistical significance was determined by unpaired two-tailed Student's t-test (\* $P < 0.05$ ). Dr. Lara Planas-Paz performed the presented experiments.

### 5.1.2. ILK controls VEGFR3 rather than VEGFR2 signaling in LECs during mouse embryonic development

VEGFR3 is highly expressed by LECs from E10.5 onwards, and regulates cell survival, migration and proliferation (Kaipainen et al. 1995; Makinen et al. 2001b). Therefore, we analyzed VEGFR3 activity in ILK K.O. embryos at E13.5, since this embryonic stage showed both significantly more proliferating LECs and significantly higher LEC numbers (Figure 8 and 9). *In vivo* VEGFR3 tyrosine phosphorylation was determined by proximity ligation assays (PLAs), in which antibodies against VEGFR3 and phospho-Tyrosine (p-Tyr) were used on embryonic cross-sections (Figure 10A-D). ILK K.O. embryos showed significantly

more VEGFR3/p-Tyr PLA sites per LEC (Figure 10E), strongly indicating that ILK inhibits VEGFR3 phosphorylation and thus its signaling.

Lyve1 VEGFR3/p-Tyr Nuclei

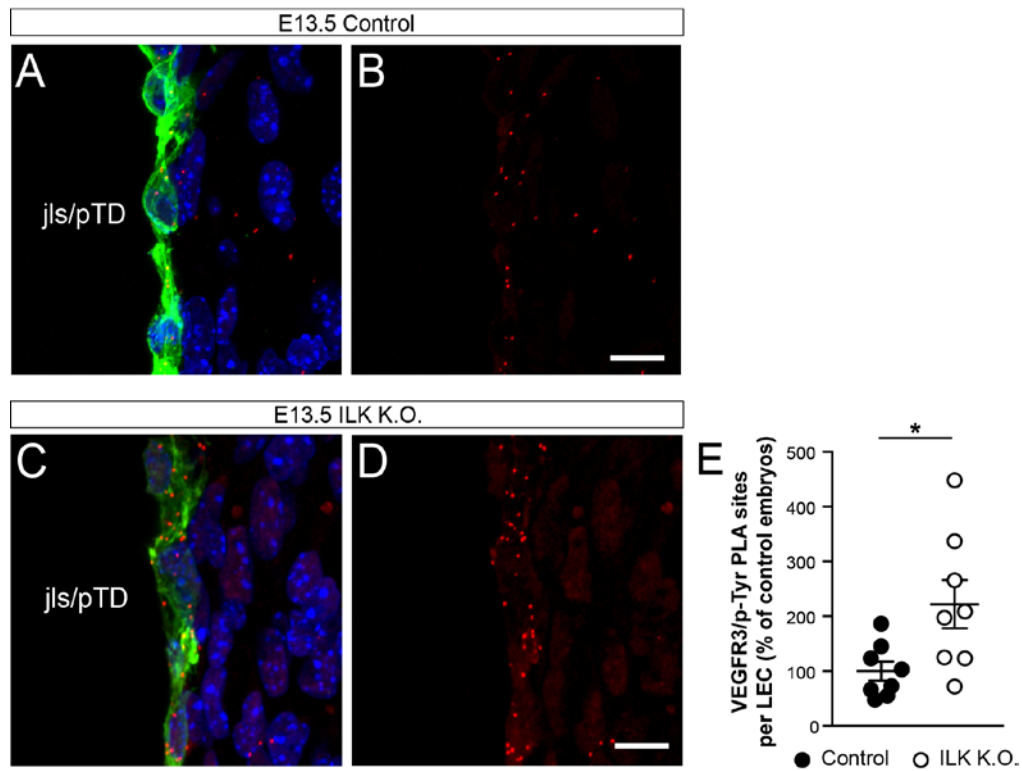


**Figure 10: Endothelial cell-specific deletion of *Ilk* results in increased VEGFR3 tyrosine phosphorylation in LECs during embryonic development.** (A-D) Representative LSM images of cross-sections through the jugular lymph sac (jls) / primordial thoracic duct (pTD) of an E13.5 control (*Flk1-Cre;Ilk<sup>+Δ</sup>*) embryo (A, B) and ILK K.O. (*Flk1-Cre;Ilk<sup>Δ/Δ</sup>*) embryo (C, D) showing VEGFR3/phospho-Tyrosine (p-Tyr) proximity ligation assay (PLA) sites (red). A co-staining for Lyve1 (green) and nuclei (blue) is also shown (A, C). Scale bars, 10  $\mu$ m. (E) Quantifications of VEGFR3/p-Tyr PLA sites per LEC in control and ILK K.O. embryos, shown as percentage of control embryos. All values are shown as means  $\pm$  SEM with  $n = 8$  embryos per genotype; statistical significance was determined by unpaired two-tailed Student's t-test (\* $P < 0.05$ ). Sofia Urner and Dr. Lara Planas-Paz both performed the presented experiments.

LECs also express VEGFR2 in addition to high VEGFR3 expression levels, and both receptors can form heterodimers in LECs (Dixelius et al. 2003). Therefore, VEGFR2 signaling in LECs was also analyzed in ILK K.O. embryos by performing PLAs with antibodies against VEGFR2 and p-Tyr (Figure 11A-D). In contrast to VEGFR3 however, the phosphorylation of VEGFR2 was unchanged between control and ILK K.O. embryos, as indicated by similar numbers of VEGFR2/p-Tyr PLA sites per LEC (Figure 11E). These results suggest that ILK specifically controls VEGFR3 rather than VEGFR2 signaling.

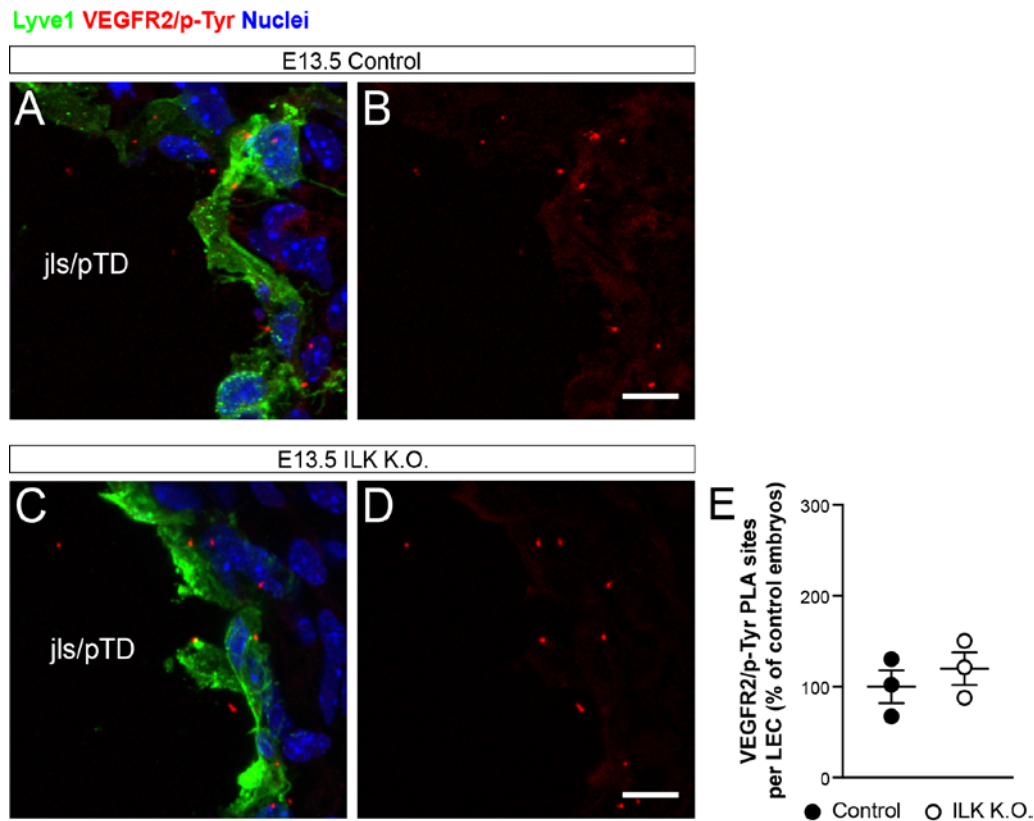


**Figure 11: Endothelial cell-specific deletion of *Ilk* results in unchanged VEGFR2 tyrosine phosphorylation in LECs during embryonic development.** (A-D) Representative LSM images of cross-sections through the jugular lymph sac (jls) / primordial thoracic duct (pTD) of an E13.5 control (*Flk1-Cre;Ilk<sup>+Δ</sup>*) embryo (A, B) and ILK K.O. (*Flk1-Cre;Ilk<sup>ΔΔ</sup>*) embryo (C, D) showing VEGFR2/phospho-Tyrosine (p-Tyr) proximity ligation assay (PLA) sites (red). A co-staining for Lyve1 (green) and nuclei (blue) is also shown (A, C). Scale bars, 10  $\mu$ m. (E) Quantifications of VEGFR2/p-Tyr PLA sites per LEC in control and ILK K.O. embryos, shown as percentage of control embryos. All values are shown as means  $\pm$  SEM with n = 3 embryos per genotype; unpaired two-tailed Student's t-test was performed to analyze statistical significance. Dr. Lara Planas-Paz performed the presented experiments.

Interestingly, previously performed analyses (by Dr. Lara Planas-Paz) of *Ilk* mRNA expression levels in LECs of wild-type embryos indicate an inverse correlation between *Ilk* expression and VEGFR3 tyrosine phosphorylation as well as LEC proliferation at different embryonic stages. Strikingly, no such correlation was observed with VEGFR2 phosphorylation, supporting that ILK specifically regulates VEGFR3 signaling.

All in all, the described results strongly indicate that ILK critically controls VEGFR3 signaling, LEC proliferation, and thus lymphatic vascular expansion during embryonic development.

## 5.2. Role of caveolin-1 in lymphatic vascular growth during mouse embryonic development

On the one hand, ILK was reported to be required for proper localization of caveolin-1 at the plasma membrane, and loss of *Ilk* results in diminished caveolae formation (Wickstrom et al. 2010a; Malan et al. 2013). On the other hand, caveolin-1, as a major component of caveolae, was previously reported to interact with VEGFR3 *in vitro*, and thereby most likely to inhibit its phosphorylation (Galvagni et al. 2007). Therefore, we aimed to investigate whether caveolin-1 might be part of the underlying mechanism of how ILK regulates VEGFR3 signaling. Thus, we used embryos with global *Cav1* deletion to find out whether loss of *Cav1* might show a phenocopy of *Ilk*-deficient embryos in regard of VEGFR3 phosphorylation and LEC proliferation. Specifically, we analyzed *Cav1*<sup>-/-</sup> embryos with global homozygous deletion of *Cav1* (referred to as 'Cav1 K.O.'), which were also reported as *Cav1* null mutants (Razani et al. 2001), and compared them to wild-type embryos (*Cav1*<sup>+/+</sup>, referred to as 'control'). In general, E13.5 *Cav1* K.O. embryos were viable, which is consistent with previous reports showing that *Cav1*-deficiency does not result in embryonic lethality (Razani et al. 2001). Also, none of the analyzed embryos was indicative of edema (Figure 12A-C).

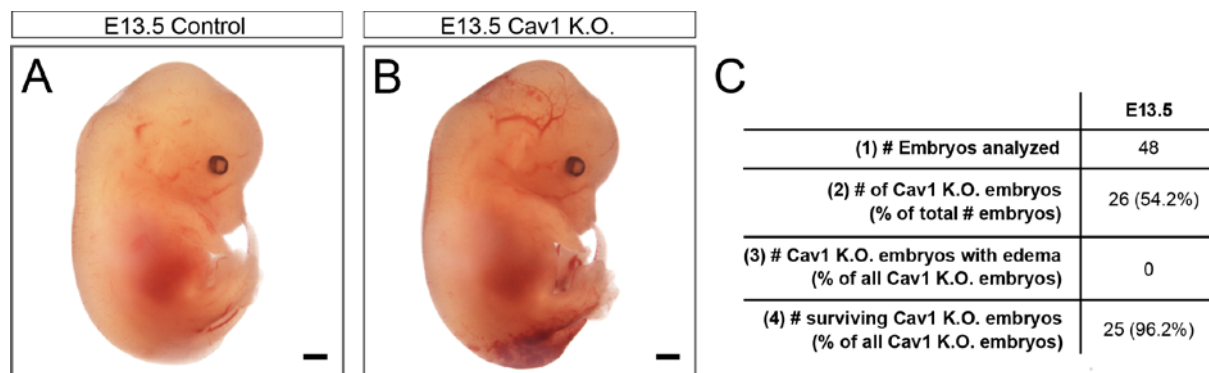


**Figure 12: *Cav1*-deficient embryos are phenotypically normal and viable.** (A, B) Representative bright-field images of an E13.5 control (*Cav1*<sup>+/+</sup>) (A) and *Cav1* K.O. (*Cav1*<sup>ΔΔ</sup>) (B) embryo. Scale bars, 500 μm. (C) Overview table of the number of (1) total analyzed embryos including (2) *Cav1* K.O. embryos, (3) *Cav1* K.O. embryos with edema, and (4) surviving *Cav1* K.O. embryos. Sofia Urner performed the presented experiments.

### 5.2.1. Caveolin-1 is not required to control lymphatic vascular expansion, LEC proliferation and VEGFR3 signaling during mouse embryonic development

We analyzed the jls/pTD in cross-sections of *Cav1* K.O. embryos at E13.5, since at this embryonic stage we observed most striking differences in ILK K.O. embryos (Figure 8-10). Interestingly, the size of the jls/pTD in *Cav1* K.O. embryos was not apparently changed when compared to control embryos (Figure 13A, B). Also, the number of pH3-positive LECs per

jls/pTD section was not significantly different, and by tendency Cav1 K.O. embryos showed rather a reduction in LEC proliferation, as indicated by around 23% less pH3-positive LECs (Figure 13C-E). Thus, *Cav1*-deficiency does not show similar effects as *Ilk*-deficiency regarding LEC proliferation. Instead, our results indicate that caveolin-1 is not required to control LEC proliferation and lymphatic vascular expansion during embryonic development.

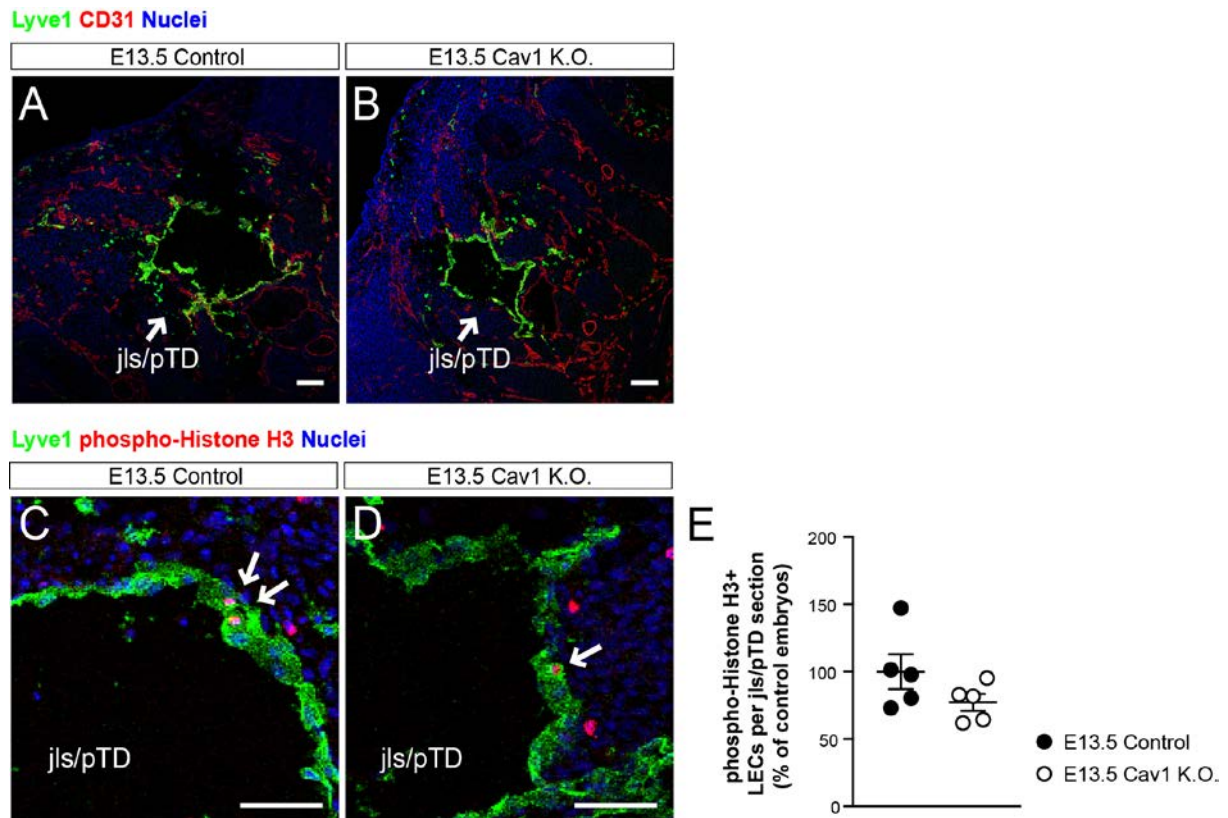


**Figure 13: *Cav1*-deficiency results in unchanged jls/pTD size and LEC proliferation during embryonic development.** (A, B) Representative LSM images of cross-sections through the jugular lymph sac (jls) / primordial thoracic duct (pTD) of an E13.5 control (*Cav1*<sup>+/+</sup>) embryo (A) and *Cav1* K.O. (*Cav1*<sup>Δ/Δ</sup>) embryo (B) stained for Lyve1 (green), CD31 (red) and nuclei (blue). Scale bars, 100 μm. (C, D) Representative LSM images of cross-sections through the jls/pTD of an E13.5 control embryo (C) and *Cav1* K.O. embryo (D) stained for Lyve1 (green), phospho-Histone H3 (red) and nuclei (blue). Scale bars, 50 μm. (E) Quantifications of phospho-Histone H3-positive LECs per analyzed jls/pTD section of control and *Cav1* K.O. embryos at E13.5, shown as percentage of control embryos. All values are shown as means ± SEM with n = 5 embryos per genotype; unpaired two-tailed Student's t-test was performed to analyze statistical significance. Sofia Urner performed the presented experiments.

Originally, we hypothesized that deletion of *Cav1* might result in increased VEGFR3 phosphorylation *in vivo*, as already described by *in vitro* studies (Galvagni et al. 2007). Therefore, we analyzed VEGFR3 signaling in LECs of E13.5 *Cav1* K.O. embryos by performing PLAs on cross-sections. However, consistent with the results of unchanged LEC proliferation in *Cav1* K.O. embryos, we observed no significant changes in the number of VEGFR3/p-Tyr PLA sites normalized to the Lyve1-positive area (Figure 14A-E), strongly

suggesting that caveolin-1 is not required to control VEGFR3 signaling in LECs during embryonic development.

Lyve1 VEGFR3/p-Tyr Nuclei

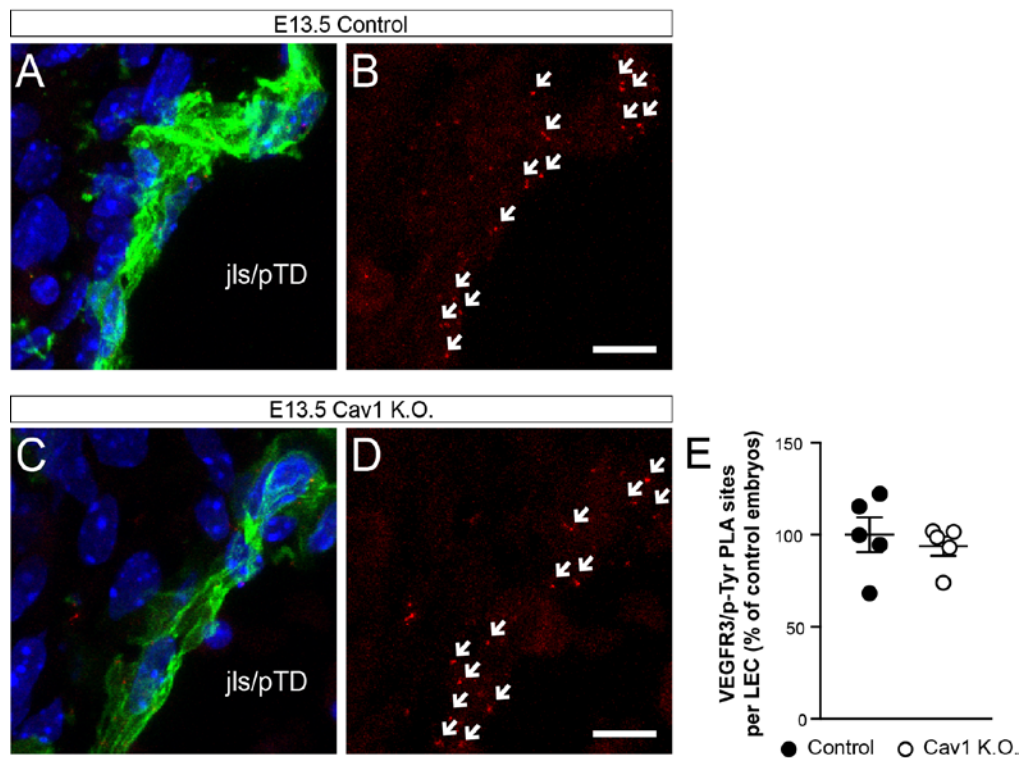


**Figure 14: Cav1-deficiency results in unchanged VEGFR3 tyrosine phosphorylation in LECs during embryonic development.** (A-D) Representative LSM images of cross-sections through the jugular lymph sac (jls) / primordial thoracic duct (pTD) of an E13.5 control (*Cav1*<sup>+/+</sup>) embryo (A, B) and Cav1 K.O. (*Cav1*<sup>ΔΔ</sup>) embryo (C, D) showing VEGFR3/phospho-Tyrosine (p-Tyr) proximity ligation assay (PLA) sites (red). A co-staining for Lyve1 (green) and nuclei (blue) is also shown (A, C). Scale bars, 10 μm. (E) Quantifications of VEGFR3/p-Tyr PLA sites normalized to Lyve1-positive area of control and Cav1 K.O. embryos at E13.5, shown as percentage of control embryos. All values are shown as means ± SEM with n = 5 embryos per genotype; unpaired two-tailed Student's t-test was performed to analyze statistical significance. Sofia Uner performed the presented experiments.

Previous studies that showed interdependence between ILK and caveolin-1 (Wickstrom et al. 2010a; Malan et al. 2013) raised the idea that their loss might result in similar phenotypes. However, based on our results, we excluded that caveolin-1 plays an essential role in the underlying mechanism of how ILK regulates VEGFR3 signaling and LEC proliferation, since its deletion had no effect on lymphatic vascular growth during embryonic development.

### 5.3. Role of $\beta$ 1 integrin in ILK-regulated lymphatic vascular growth during mouse embryonic development

ILK was previously reported to interact with  $\beta$ 1 and  $\beta$ 3 integrin (Hannigan et al. 1996; Pasquet et al. 2002). Several studies showed that particularly  $\beta$ 1 integrin plays a highly relevant role in VEGFR3 activity and lymphatic vascular development (Huang et al. 2000; Wang et al. 2001; Zhang et al. 2005; Okazaki et al. 2009; Galvagni et al. 2010; Garmy-Susini et al. 2010; Planas-Paz et al. 2012). Therefore, we focused on analyzing whether  $\beta$ 1 integrin plays a role in the effect of *Ilk* deletion on VEGFR3 signaling as well as lymphatic vascular growth during embryonic development.

#### 5.3.1. ILK controls interactions between VEGFR3 and $\beta$ 1 integrin in LECs during mouse embryonic development

Full VEGFR3 signaling depends on  $\beta$ 1 integrin (Planas-Paz et al. 2012). Further,  $\beta$ 1 integrin-mediated VEGFR3 phosphorylation was shown to involve physical interaction between VEGFR3 and  $\beta$ 1 integrin (Wang et al. 2001; Zhang et al. 2005). Therefore, we wanted to know whether the increased VEGFR3 phosphorylation that we observed upon *Ilk* deficiency at E13.5 (Figure 10), might be due to altered interactions between VEGFR3 and  $\beta$ 1 integrin. In this context, we performed PLAs, which is a suitable method to detect close proximity between two proteins (Soderberg et al. 2006), and analyzed interactions between VEGFR3 and  $\beta$ 1 integrin by using antibodies against both proteins on cross-sections of ILK K.O. and control embryos (Figure 15A-D). We quantified the number of VEGFR3/ $\beta$ 1 integrin PLA sites normalized to the Lyve1-positive area, and found these to be strongly upregulated in *Ilk*-deficient embryos, as indicated by a significant increase of around 100% (Figure 15E). These results implicate that ILK prevents interactions between VEGFR3 and  $\beta$ 1 integrin in LECs during embryonic development.

In addition, previously performed experiments (by Dr. Lara Planas-Paz) showed that *Ilk* deletion does not change  $\beta$ 1 integrin activation, which is associated with conformational changes of the extracellular domain of  $\beta$ 1 integrin upon ECM binding (Luo et al. 2007; Su et al. 2016; Sun et al. 2016). This suggests that ILK is not required to control  $\beta$ 1 integrin activation in LECs, but rather controls its physical interaction with VEGFR3.

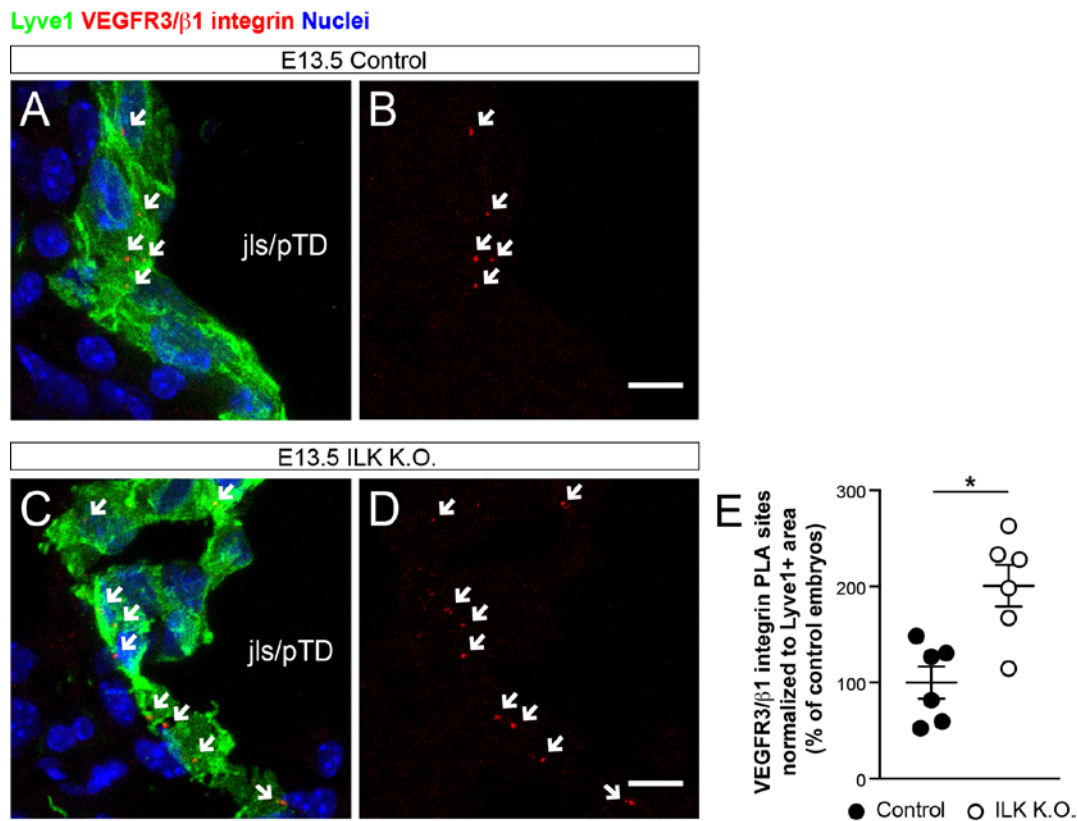


**Figure 15: Endothelial cell-specific deletion of *Ilk* results in increased interactions between VEGFR3 and  $\beta$ 1 integrin in LECs during embryonic development. (A-D)** Representative LSM images of cross-sections through the jugular lymph sac (jls) / primordial thoracic duct (pTD) of an E13.5 control (*Flik1-Cre;Ilk<sup>+Δ</sup>*) embryo (A, B) and ILK K.O. (*Flik1-Cre;Ilk<sup>Δ/Δ</sup>*) embryo (C, D) showing VEGFR3/ $\beta$ 1 integrin proximity ligation assay (PLA) sites (red). A co-staining for Lyve1 (green) and nuclei (blue) is also shown (A, C). Scale bars, 10  $\mu$ m. **(E)** Quantifications of VEGFR3/ $\beta$ 1 integrin PLA sites normalized to Lyve1-positive area in control and ILK K.O. embryos, shown as percentage of control embryos. All values are shown as means  $\pm$  SEM with n = 6 embryos per genotype; statistical significance was determined by unpaired two-tailed Student's t-test (\*P < 0.05). Sofia Urner performed the presented experiments.

### 5.3.2. The effect of *Ilk* deletion on lymphatic vascular expansion during mouse embryonic development depends on $\beta$ 1 integrin

Previous studies showed that endothelial cell-specific deletion of *Itgb1* results in diminished VEGFR3 phosphorylation, reduced LEC proliferation and impaired lymphatic vascular growth during embryonic development (Planas-Paz et al. 2012). Surprisingly, ILK K.O. embryos show the exact opposite phenotype in regard of these criteria. Since our observations further indicate that *Ilk* deletion results in increased VEGFR3/ $\beta$ 1 integrin interactions (Figure 15), we aimed to investigate whether reduction of *Itgb1* expression additional to *Ilk* deletion might rescue the effect of *Ilk*-deficiency on VEGFR3 signaling and LEC proliferation. Therefore, we created double knockout embryos, in which both *Ilk* and *Itgb1* were deleted in endothelial cells. We used E13.5 *Flik1-Cre;Ilk<sup>+Δ</sup>;Itgb1<sup>+Δ</sup>* embryos with

heterozygous deletion of both *Ilk* and *Itgb1* as control embryos (referred to as ‘control’), and focused on analyzing E13.5 *Flk1-Cre;Ilk<sup>ΔΔ</sup>;Itgb1<sup>+Δ</sup>* embryos with homozygous deletion of *Ilk* and heterozygous deletion of *Itgb1* (referred to as ‘ILK & β1 integrin K.O.’) (Figure 16A, B). Strikingly, most *Flk1-Cre;Ilk<sup>ΔΔ</sup>;Itgb1<sup>ΔΔ</sup>* embryos with homozygous deletion of both genes (referred to as ‘full ILK & β1 integrin K.O.’) were not alive at E13.5, but seemed to die during earlier embryonic stages even before the onset of lymphatic vascular development (Figure 16C, D). Interestingly, around 23% of analyzed ILK & β1 integrin K.O. embryos also showed edema in the dorsolateral regions (Figure 16D) as observed in ILK K.O. embryos with higher frequency (69%, Figure 7). Further, around 30% of ILK & β1 integrin K.O. embryos died before E13.5, indicating that they are also embryonic lethal (Figure 16D).

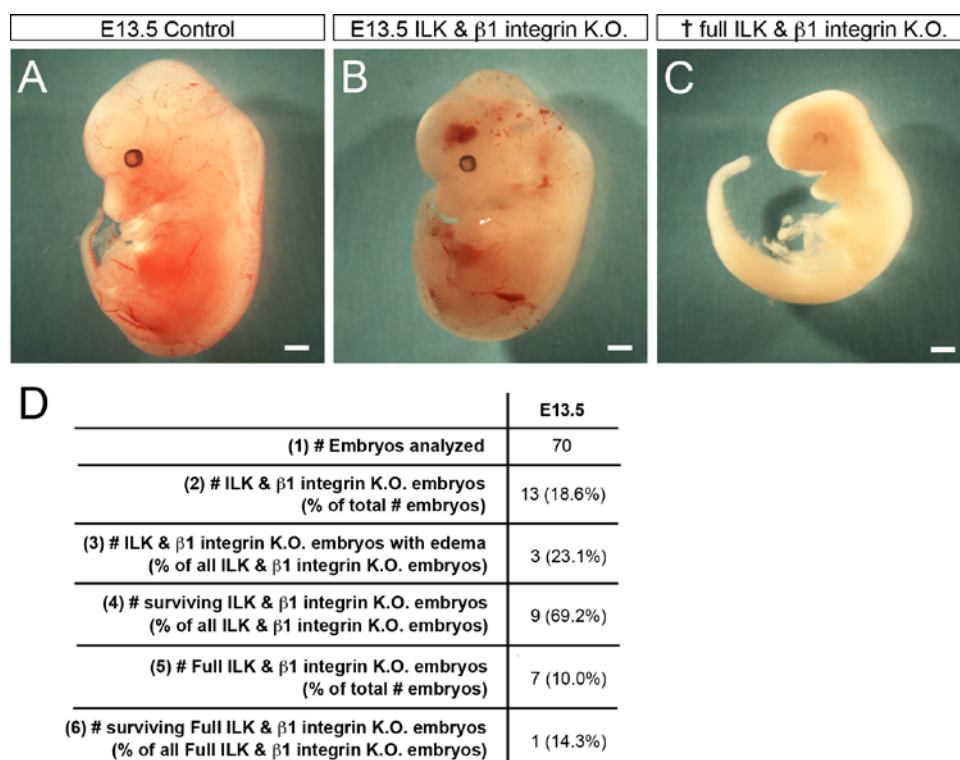


**Figure 16: Endothelial cell-specific deletion of *Ilk* and *Itgb1* results in embryonic lethality.** (A-C) Representative bright-field images of an E13.5 control (*Flk1-Cre;Ilk<sup>+Δ</sup>;Itgb1<sup>+Δ</sup>*) embryo (A), an E13.5 ILK & β1 integrin K.O. (*Flk1-Cre;Ilk<sup>ΔΔ</sup>;Itgb1<sup>+Δ</sup>*) embryo (B), and a dead full ILK & β1 integrin K.O. (*Flk1-Cre;Ilk<sup>ΔΔ</sup>;Itgb1<sup>ΔΔ</sup>*) embryo (C) isolated on E13.5. Scale bars, 500 μm. (D) Overview table of the number of (1) total analyzed embryos including (2) ILK & β1 integrin K.O. embryos, (3) ILK & β1 integrin K.O. embryos with edema, (4) surviving ILK & β1 integrin K.O. embryos, (5) full ILK & β1 integrin K.O. embryos, and (6) surviving full ILK & β1 integrin K.O. embryos. Sofia Urner performed the presented experiments.

When analyzing cross-sections through the jls/pTD region, ILK & β1 integrin K.O. embryos showed only a slightly enlarged jls/pTD compared to control embryos (Figure 17A, B). Further, the quantifications of the total LEC number per jls/pTD section revealed no difference between control and ILK & β1 integrin K.O. embryos (Figure 17C).

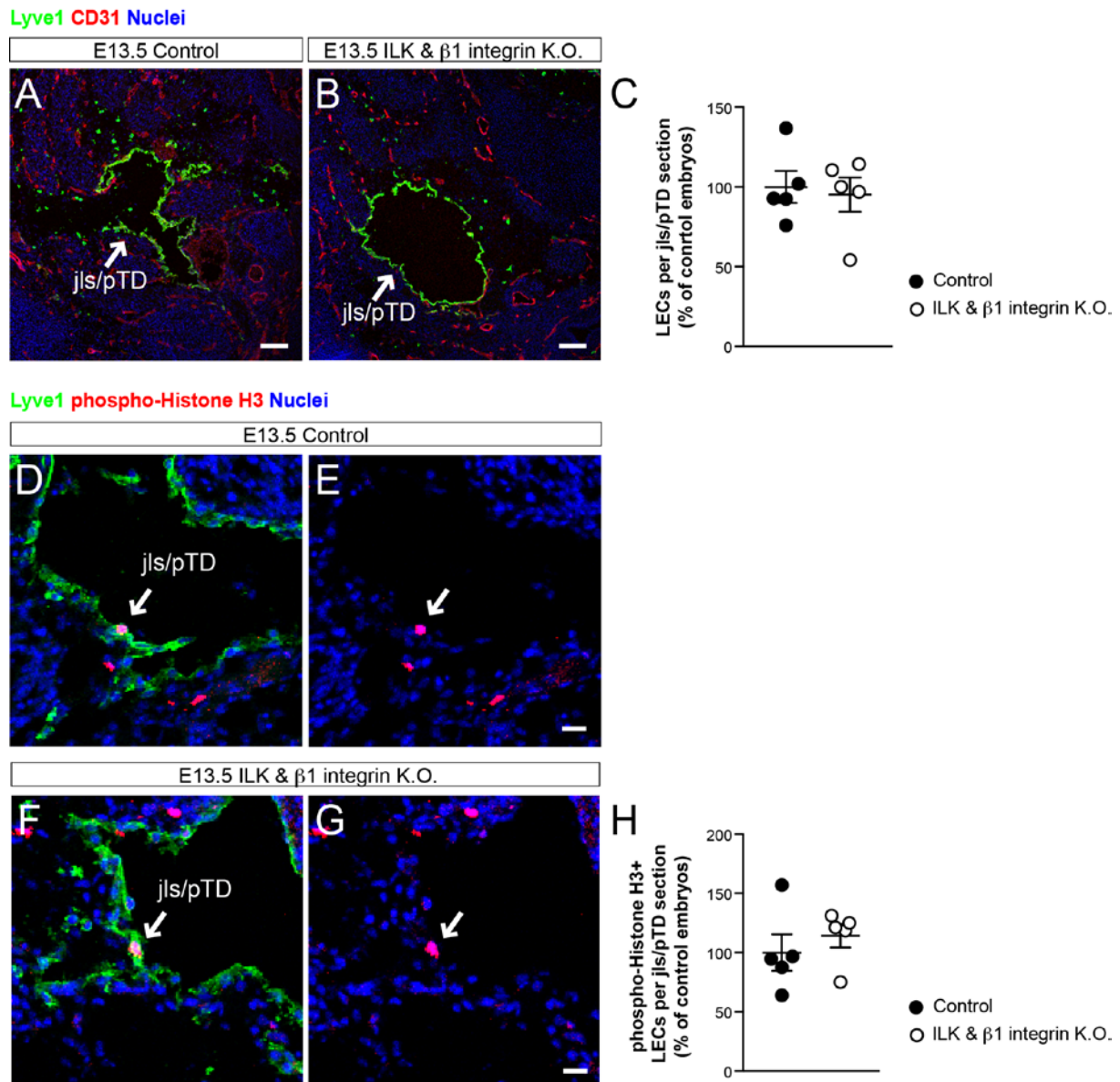


**Figure 17: The effect of homozygous *Ilk* deletion on LEC proliferation and total LEC number during embryonic development can be genetically rescued by additional heterozygous deletion of *Itgb1*.** (A, B) Representative LSM images of cross-sections through the jugular lymph sac (jls) / primordial thoracic duct (pTD) of an E13.5 control (*Flk1-Cre;Ilk<sup>+/-</sup>;Itgb1<sup>+/-</sup>*) embryo (A) and an ILK &  $\beta$ 1 integrin K.O. (*Flk1-Cre;Ilk<sup>-/-</sup>;Itgb1<sup>+/-</sup>*) embryo (B). Arrows point to the jls/pTD identified by the expression of Lyve1 (green). Co-stainings for CD31 (red) and nuclei (blue) are also shown. Scale bars, 100  $\mu$ m. (C) Quantifications of the LEC number per analyzed jls/pTD section of control and ILK &  $\beta$ 1 integrin K.O. embryos at E13.5, shown as percentage of control embryos. (D-G) Representative LSM images of cross-sections through the jls/pTD of an E13.5 control embryo (D, E) and ILK &  $\beta$ 1 integrin K.O. embryo (F, G) stained for Lyve1 (green), phospho-Histone H3 (red) and nuclei (blue). Scale bars, 20  $\mu$ m. (H) Quantifications of phospho-Histone H3-positive LECs per analyzed jls/pTD section of control and ILK &  $\beta$ 1 integrin K.O. embryos at E13.5, shown as percentage of control embryos. (C, H) All values are shown as means  $\pm$  SEM with n = 5 embryos per genotype; unpaired two-tailed Student's t-test was performed to analyze statistical significance. Sofia Urner performed the presented experiments.

In addition, we performed pH3 stainings in order to quantify the number of proliferating LECs within the jls/pTD region of these embryos (Figure 17D-H). Consistent with the analyses of

the total LEC number, ILK &  $\beta 1$  integrin K.O. embryos showed also no significant difference in the number of pH3-positive LECs per jls/pTD section (Figure 17H). This strongly indicates that, in regard of LEC proliferation and lymphatic vascular expansion during embryonic development, additional reduction of *Itgb1* expression rescues the effect of *Ilk*-deficiency only.

Finally, we also investigated the effect of reduced *Itgb1* expression in addition to *Ilk* deletion on VEGFR3 activity in LECs, since ILK K.O. embryos showed strongly upregulated VEGFR3 phosphorylation at E13.5 (Figure 10). We performed PLAs on embryonic cross-sections to investigate VEGFR3 tyrosine phosphorylation *in vivo* (Figure 18A-D). Consistently, also the number of VEGFR3/p-Tyr PLA sites per LEC was not significantly different in ILK &  $\beta 1$  integrin K.O. embryos compared to control embryos (Figure 18E), indicating that the effect of ILK deletion on VEGFR3 signaling depends on  $\beta 1$  integrin.

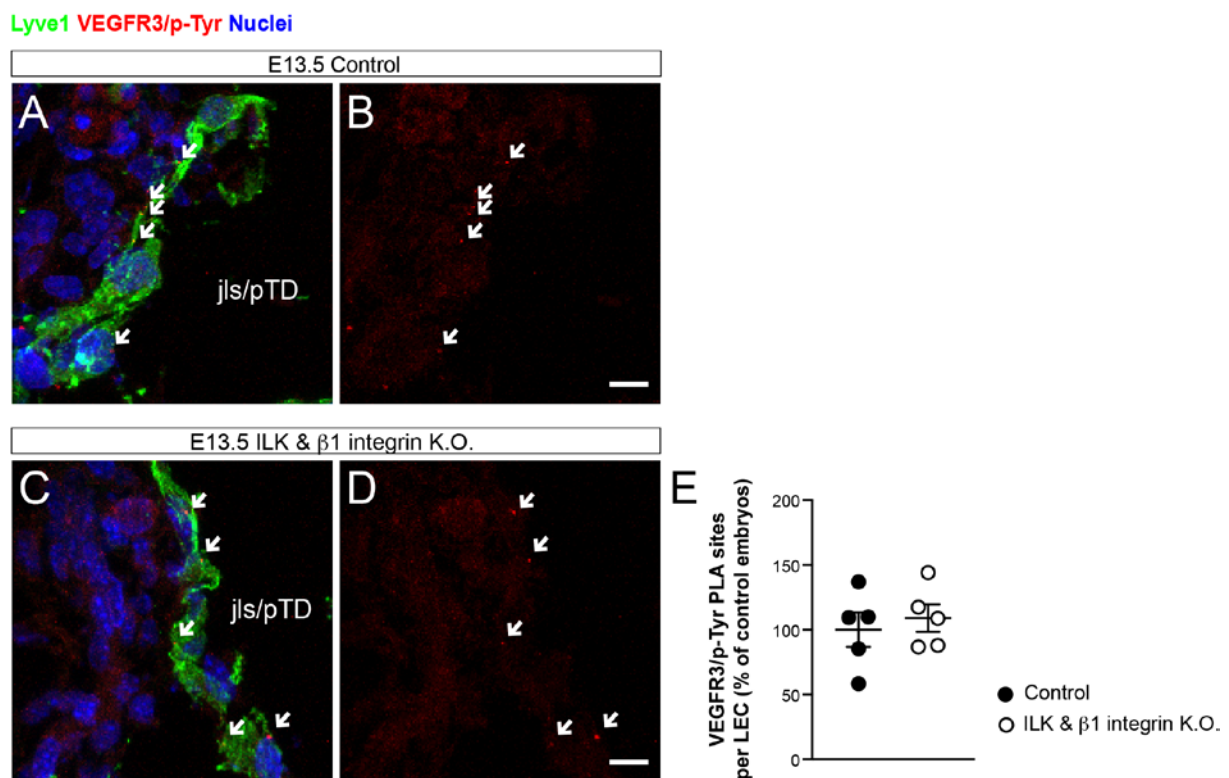


**Figure 18: The effect of homozygous *Ilk* deletion on VEGFR3 tyrosine phosphorylation in LECs during embryonic development can be genetically rescued by additional heterozygous deletion of *Itgb1*.** (A-D) Representative LSM images of cross-sections through the jugular lymph sac (jls) / primordial thoracic duct (pTD) of an E13.5 control (*Flk1-Cre;Ilk<sup>+/-</sup>;Itgb1<sup>+/-</sup>*) embryo (A, B) and an ILK &  $\beta 1$  integrin K.O. (*Flk1-Cre;Ilk<sup>-/-</sup>;Itgb1<sup>+/-</sup>*) embryo (C, D) showing VEGFR3/phospho-Tyrosine (p-Tyr) proximity ligation assay (PLA) sites (red). A co-staining for Lyve1 (green) and nuclei (blue) is also shown (A, C). Scale bars, 10  $\mu$ m. (E) Quantifications of VEGFR3/p-Tyr PLA sites per LEC in control and ILK &  $\beta 1$  integrin K.O. embryos, shown as percentage of control embryos at E13.5. All values are shown as means  $\pm$  SEM with  $n = 5$  embryos per genotype; unpaired two-tailed Student's t-test was performed to analyze statistical significance. Sofia Urner performed the presented experiments.

Interestingly, one of all analyzed *Flk1-Cre;Ilk<sup>ΔΔ</sup>;Itgb1<sup>ΔΔ</sup>* embryos with homozygous deletion of both *Ilk* and *Itgb1* was still alive when isolated at E13.5 (Figure 16D). We also analyzed this embryo, and found the jls/pTD in this embryo to be strongly reduced in size when compared to control embryos. In addition, LEC proliferation was reduced by almost 60% in this embryo compared to controls, and VEGFR3 tyrosine phosphorylation showed a reduction of around 35% (performed by Sofia Urner). Though we could not perform any statistical analyses with only one embryo, these observations indicate that the effect of *Itgb1* deletion, as described in (Planas-Paz et al. 2012), might be more dominant over the effect of *Ilk* deletion, suggesting that ILK acts upstream of  $\beta 1$  integrin in regard of regulating VEGFR3 signaling and lymphatic vascular growth.

In summary, our results show that deletion of only one *Itgb1* allele in addition to the deletion of both *Ilk* alleles is sufficient to rescue the effect of *Ilk*-deficiency only, in which strongly upregulated VEGFR3 phosphorylation, increased LEC proliferation and lymphatic vascular overgrowth could be observed (Figure 8-10). Consequently, these genetic rescue experiments implicate that ILK controls  $\beta 1$  integrin-mediated VEGFR3 signaling, LEC proliferation and thus lymphatic vascular growth during embryonic development.

#### **5.4. Role of $\alpha$ -parvin in lymphatic vascular growth during mouse embryonic development**

Since ILK is often described as the central component of the IPP complex, we aimed to find out whether other IPP complex members might be involved in the regulatory effect of ILK on lymphatic vascular development. We focused on analyzing the role of  $\alpha$ -parvin, since parvin proteins together with ILK provide the connection between ECM-bound  $\beta 1$  integrin and the F-actin cytoskeleton, and therefore might be also relevant in  $\beta 1$  integrin-mediated signaling. In addition, particularly  $\alpha$ -parvin has been previously shown to be relevant in blood vascular development (Montanez et al. 2009; Fraccaroli et al. 2015). However, its role in lymphatic vascular development to our knowledge has not been investigated, yet. We analyzed E13.5 *Tie2-Cre;Parva<sup>ΔΔ</sup>* embryos with homozygous endothelial cell-specific deletion of *Parva* (referred to as ' $\alpha$ -parvin K.O.') in regard of VEGFR3 signaling and LEC proliferation to see whether they might show a similar phenotype as *Ilk*-deficient embryos. We compared these embryos with only floxed embryos without *Cre* (*Parva<sup>fl/fl</sup>*, referred to as 'control'). Interestingly, the analyzed  $\alpha$ -parvin K.O. embryos displayed no edema at E13.5 (Figure 19A, B), while global *Parva*-deficient embryos were reported to develop whole-body

edema from E12.5 onwards (Montanez et al. 2009). Further,  $\alpha$ -parvin K.O. embryos are embryonic lethal from around E14.5 onwards (Fraccaroli et al. 2015).

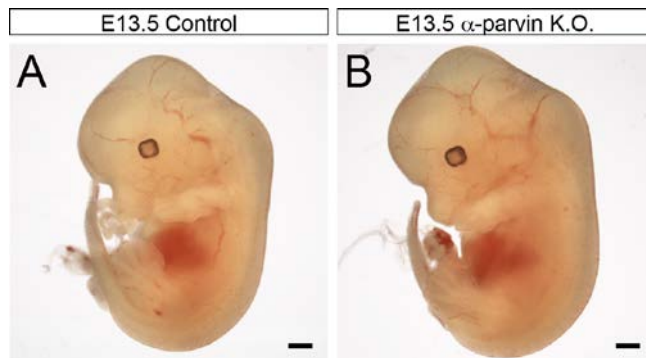


**Figure 19: Embryos with endothelial cell-specific deletion of *Parva* display no edema at E13.5. (A, B)** Representative bright-field images of an E13.5 control (*Parva<sup>fl/fl</sup>*) embryo (A) and an  $\alpha$ -parvin K.O. (*Tie2-Cre; Parva <sup>$\Delta/\Delta$</sup>* ) embryo (B). Scale bars, 500  $\mu$ m. Embryos were isolated and provided by Dr. Bettina Pitter and Dr. Eloi Montanez.

#### 5.4.1. $\alpha$ -parvin is involved in controlling lymphatic vascular expansion and LEC proliferation during mouse embryonic development

We analyzed  $\alpha$ -parvin K.O. embryos for the size of the jls/pTD on embryonic cross-sections, and recognized that it was slightly enlarged when compared to control embryos (Figure 20A, B). However, the effect was not as dramatic as observed upon *Ilk*-deficiency (Figure 8D, H). Quantifications of the total LEC number supported our observations, and showed an increase of around 42% (Figure 20C). In addition, pH3 stainings revealed significantly increased LEC proliferation in  $\alpha$ -parvin K.O. embryos, indicated by around 30% more pH3-positive LECs per jls/pTD section (Figure 20D-H). These results suggest that  $\alpha$ -parvin inhibits LEC proliferation and lymphatic vascular expansion during embryonic development.

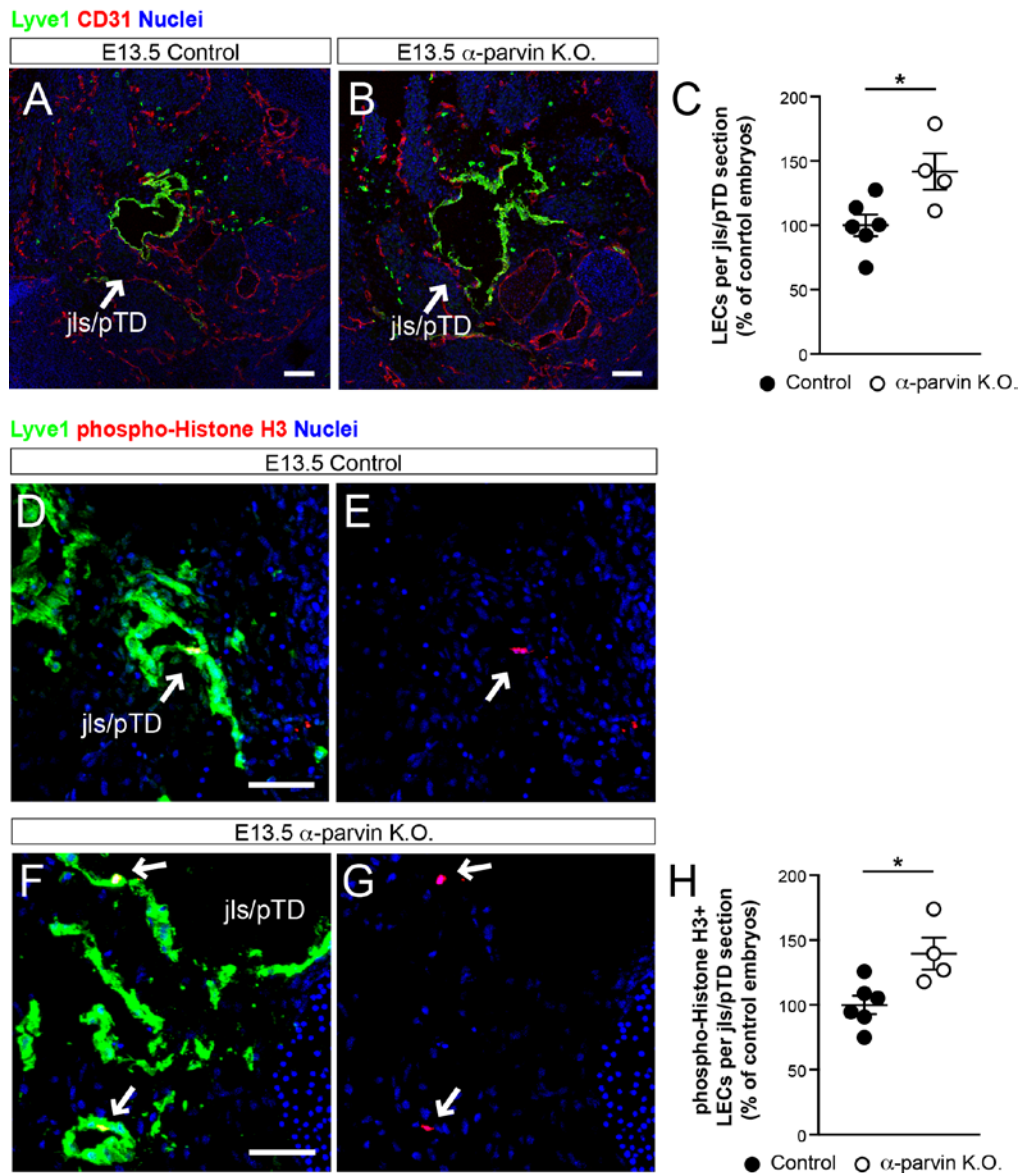


**Figure 20: Endothelial cell-specific deletion of *Parva* results in increased LEC number and LEC proliferation during embryonic development.** (A, B) Representative LSM images of cross-sections through the jugular lymph sac (jls) / primordial thoracic duct (pTD) of an E13.5 control (*Parva<sup>fl/m</sup>*) embryo (A) and an  $\alpha$ -parvin K.O. (*Tie2-Cre;Parva<sup>ΔA</sup>*) embryo (B). Arrows point to the jls/pTD identified by the expression of Lyve1 (green). Co-stainings for CD31 (red) and nuclei (blue) are also shown. Scale bars, 100  $\mu$ m. (C) Quantifications of the LEC number per analyzed jls/pTD section of control and  $\alpha$ -parvin K.O. embryos at E13.5, shown as percentage of control embryos. (D-G) Representative LSM images of cross-sections through the jls/pTD of an E13.5 control embryo (D, E) and  $\alpha$ -parvin K.O. embryo (F, G) stained for Lyve1 (green), phospho-Histone H3 (red) and nuclei (blue). Scale bars, 50  $\mu$ m. (H) Quantifications of phospho-Histone H3-positive LECs per analyzed jls/pTD section of control and  $\alpha$ -parvin K.O. embryos at E13.5, shown as percentage of control embryos. (C, H) All values are shown as means  $\pm$  SEM with  $n \geq 4$  embryos per genotype; statistical significance was determined by unpaired two-tailed Student's t-test ( $*P < 0.05$ ). Sofia Urner performed the presented experiments.

Further, we analyzed VEGFR3 signaling in  $\alpha$ -parvin K.O. embryos by PLAs. Quantifications of VEGFR3/p-Tyr PLA sites per LEC revealed a non-significant increase of around 44% in  $\alpha$ -parvin K.O. embryos compared to control embryos (Figure 21A-E). Thus, E13.5  $\alpha$ -parvin K.O.

embryos only by trend show a similar effect on VEGFR3 signaling as ILK K.O. embryos (Figure 10).

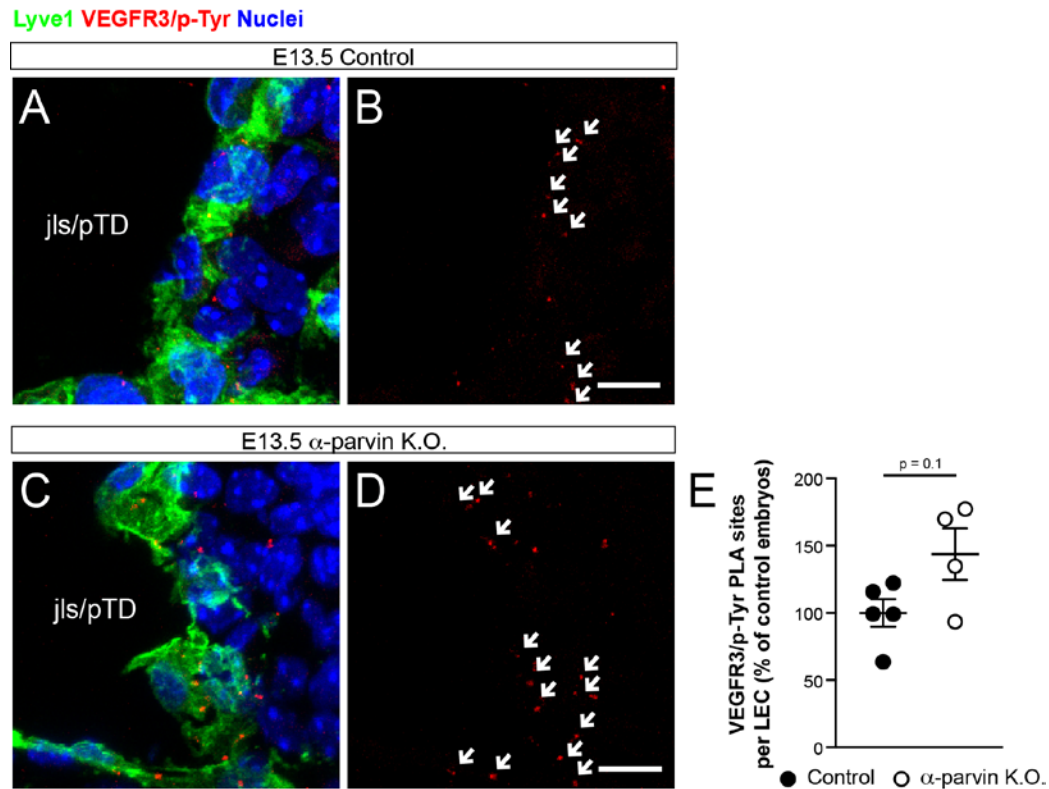


**Figure 21: Endothelial cell-specific deletion of *Parva* results in non-significant increase of VEGFR3 tyrosine phosphorylation in LECs during embryonic development.** (A-D) Representative LSM images of cross-sections through the jugular lymph sac (jls) / primordial thoracic duct (pTD) of an E13.5 control (*Parva<sup>fl/fl</sup>*) embryo (A, B) and an  $\alpha$ -parvin K.O. (*Tie2-Cre;Parva <sup>$\Delta/\Delta$</sup>* ) embryo (C, D) showing VEGFR3/phospho-Tyrosine (p-Tyr) proximity ligation assay (PLA) sites (red). A co-staining for Lyve1 (green) and nuclei (blue) is also shown (A, C). Scale bars, 10  $\mu$ m. (E) Quantifications of VEGFR3/p-Tyr PLA sites per LEC in control and  $\alpha$ -parvin K.O. embryos, shown as percentage of control embryos at E13.5. All values are shown as means  $\pm$  SEM with  $n \geq 4$  embryos per genotype; unpaired two-tailed Student's t-test was performed to analyze statistical significance. Sofia Urner performed the presented experiments.

Based on the described observations, we conclude that  $\alpha$ -parvin is involved in controlling LEC proliferation and lymphatic vascular growth during embryonic development. However, our results also indicate that ILK as the central component of the IPP complex might be more relevant than  $\alpha$ -parvin, since the effects of *Parva* deletion on VEGFR3 signaling, LEC proliferation and LEC number were weaker than the effects of *Ilk* deletion.

## 5.5. Role of ILK in the adult mouse lymphatic vasculature

By using mouse embryos we could show that ILK critically controls VEGFR3 signaling and LEC proliferation during lymphatic vascular development. However, we still lacked the knowledge about its function in the adult lymphatic vasculature. In the adult, physiologically intact lymphatic vasculature is rather quiescent, and LECs barely proliferate. Upon pathological conditions like lymphedema or myocardial infarction however, lymphatic vascular growth is strongly initiated (Klotz et al. 2015; Gousopoulos et al. 2016). We aimed to determine whether ILK plays a role in the adult lymphatic vasculature, and therefore might be a general regulator of VEGFR3 signaling and LEC proliferation, beyond its developmental function.

### 5.5.1. ILK controls lymphatic vascular expansion in the avascular adult mouse cornea

The lymphatic vasculature is found all over the body in almost all tissues. However, there also exist a few tissues, such as the cornea, that are free of blood and lymphatic vessels. The cornea is the most outer layer of the eye, and proper vision depends on its avascularity (Regenfuss et al. 2012). Therefore, the cornea is a suitable tissue to study neo-lymphangiogenesis, particularly because it is easily accessible and susceptible to manipulations (Cao et al. 2011). In collaboration with Prof. Dr. Shayn Peirce-Cottler and Molly Kelly-Goss (Department of Biomedical Engineering, University of Virginia, USA) we used the cornea to analyze the effect of *Ilk* silencing on potential lymphatic vascular growth into the avascular tissue. Therefore, we established an *in vivo* knockdown of *Ilk* by daily applications of ILK siRNAs into the eyes of adult wild-type mice. Importantly, we applied ILK siRNA into one eye, and used the contralateral eye for control siRNA treatment in same concentration and volume (Figure 22A). We determined the best knockdown efficiency in the corneas after 4 days of consecutive siRNA treatment (Figure 22A), as indicated by significant reduction in *Ilk* mRNA expression by around 35% (Figure 22B). Next, we continued consecutive siRNA treatment for a total time of 10 days to allow possible lymphatic vascular growth into the cornea (Figure 22A). Subsequently, we analyzed corneal vasculature by performing whole-mount-stainings (WMS) for blood and lymphatic vessels (Figure 22C, D). We found that ILK siRNA treatment resulted in frequent ingrowth of lymphatic vessels from the surrounding corneal limbus region into the cornea (Figure 22D). Although statistically not significant, our quantifications revealed the strongest difference in the average length of lymphatic vessels within the cornea, which was upregulated by around 43% (Figure 22E). Strikingly, we did not observe any blood vascular growth into the cornea upon ILK siRNA treatment (Figure 22C, D).

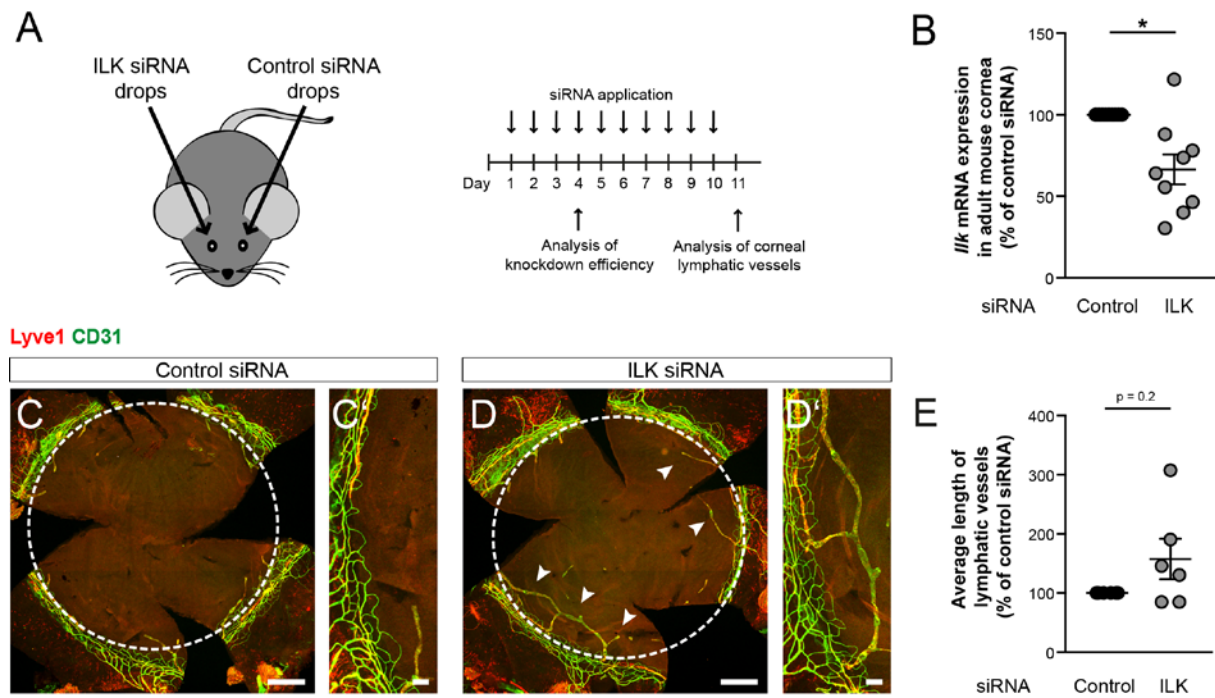


**Figure 22: *Ilk* is significantly downregulated in the adult mouse cornea by using ILK siRNAs, and results in lymphatic vascular ingrowth into the adult cornea by trend. (A)** Schematic overview of the experimental set-up, including the application of ILK siRNA drops into one eye and control siRNA drops into the contralateral eye of adult wild-type mice. **(B)** Quantifications of *Ilk* mRNA expression levels in the corneas treated with ILK siRNA and normalized to the expression in the contralateral cornea treated with control siRNA; shown as percentage of control siRNA. **(C, C', D, D')** Representative LSM images of a cornea treated with control siRNA (C, C') and ILK siRNA (D, D') stained for Lyve1 (red) and CD31 (green). Scale bars, 500  $\mu$ m (C, D) and 100  $\mu$ m (C', D'). **(E)** Quantifications of the average length of lymphatic vessels in the corneas treated with ILK siRNA and normalized to the average length of the contralateral cornea treated with control siRNA; shown as percentage of control siRNA. **(B, E)** All values are shown as means  $\pm$  SEM with  $n \geq 6$  corneas per siRNA; statistical significance was determined by a paired two-tailed Student's t-test (\* $P < 0.05$ ). Sofia Urner and Molly Kelly-Goss performed the presented experiments.

These results suggest that ILK could be relevant in inhibiting lymphatic vascular growth in the adult. However, due to high variability in the effect of siRNA-mediated silencing on the knockdown efficiency of *Ilk* (Figure 22B) as well as on the average length of corneal lymphatic vessels (Figure 22E), we decided to repeat these analyses in adult mice with tamoxifen-induced genetic deletion of *Ilk* in LECs. In addition, while knockdown of *Ilk* in the corneas was not LEC-specific, using *Prox1-CreER<sup>T2</sup>;Ilk<sup>fl/fl</sup>* mice (referred to as 'adult ILK K.O.') allowed targeted depletion of *Ilk* specifically in LECs upon tamoxifen injections (Bazigou et al. 2011). We injected these mice together with *Prox1-CreER<sup>T2</sup>* control mice (referred to as 'adult control') with tamoxifen for 6 consecutive days. Since these mice also were used for myocardial infarction analyses (see 3.5.3), we isolated and analyzed the corneas around 6 weeks after the last tamoxifen injection. Strikingly, we observed a significantly higher number of lymphatic vessel sprouts in the corneas of adult ILK K.O. mice compared to control mice, increased by around 45% (Figure 23A-C). These results indicate

that deletion of *Ilk* in LECs results in induced lymphatic vascular growth into the previously barely vascularized tissue, suggesting that ILK critically controls lymphatic vascular expansion in the adult cornea.

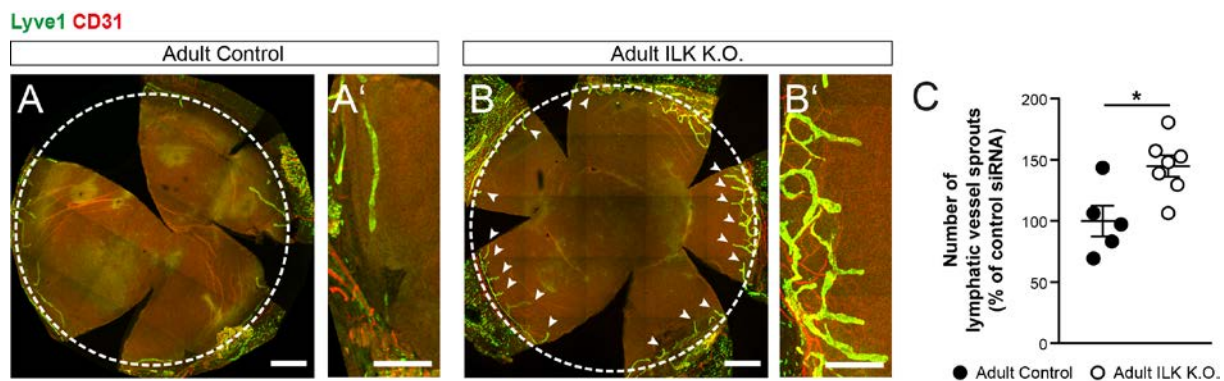


**Figure 23: Tamoxifen-Induced LEC-specific deletion of *Ilk* results in lymphatic vascular ingrowth into the adult cornea.** (A, A', B, B') Representative LSM images of the cornea of an adult control (*Prox1-CreERT<sup>2</sup>*) mouse (A, A') and an adult ILK K.O. (*Prox1-CreERT<sup>2</sup>;Ilk<sup>fl/fl</sup>*) mouse (B, B') isolated around 6 weeks after the last tamoxifen injection, and stained for Lyve1 (green) and CD31 (red). Scale bars, 500  $\mu$ m (A, B) and 100  $\mu$ m (A', B'). (C) Quantifications of the number of lymphatic vessel sprouts in the cornea of adult control and adult ILK K.O. mice, shown as percentage of control mice. All values are shown as means  $\pm$  SEM with  $n \geq 5$  corneas per genotype; statistical significance was determined by an unpaired two-tailed Student's t-test (\* $P < 0.05$ ). Sofia Urner performed the presented experiments.

### 5.5.2. ILK controls lymphatic vascular expansion, LEC proliferation and VEGFR3 signaling in the adult mouse skin

We further wanted to determine whether *Ilk*-deficiency also has an effect on the completely established network of lymphatic vasculature in the adult. For these analyses, we used the mouse ear skin, which allows studying the dermal lymphatic vasculature as a whole network of different hierarchical lymphatic vessels (reviewed in (Breslin 2014)). We isolated the ear skin of adult ILK K.O. mice and control mice around 2 weeks after the last tamoxifen injection to analyze the lymphatic vasculature by WMS (Figure 24A). Strikingly, we found a significantly increased lymph vessel density (around 28%) in adult ILK K.O. mice, as determined by VEGFR3-positive area normalized to the total analyzed ear skin area (Figure 24B-D), showing that tamoxifen-induced deletion of *Ilk* in LECs is sufficient to induce lymphatic vascular growth in the adult.

In order to find out whether the increased amount of dermal lymphatic vessels was due to upregulated LEC proliferation and VEGFR3 signaling, we chose a sooner time point (2 days) after the last tamoxifen injection to analyze possible changes on the molecular level (Figure 24A). We analyzed LEC proliferation by pH3 co-stainings of the whole ear skin, and quantifications of pH3-positive LECs normalized to the analyzed lymph vessel area revealed

a significant upregulation in LEC proliferation by around 66% (Figure 24E-G). In addition, we lysed the whole ear skin to perform an ELISA for tyrosine phosphorylated VEGFR3. In line with the proliferation analyses, we observed a strong increase in VEGFR3 signaling by trend ( $p$ -value = 0.06) in adult ILK K.O. mice, as indicated by around 95% more VEGFR3 phosphorylation (Figure 24H).

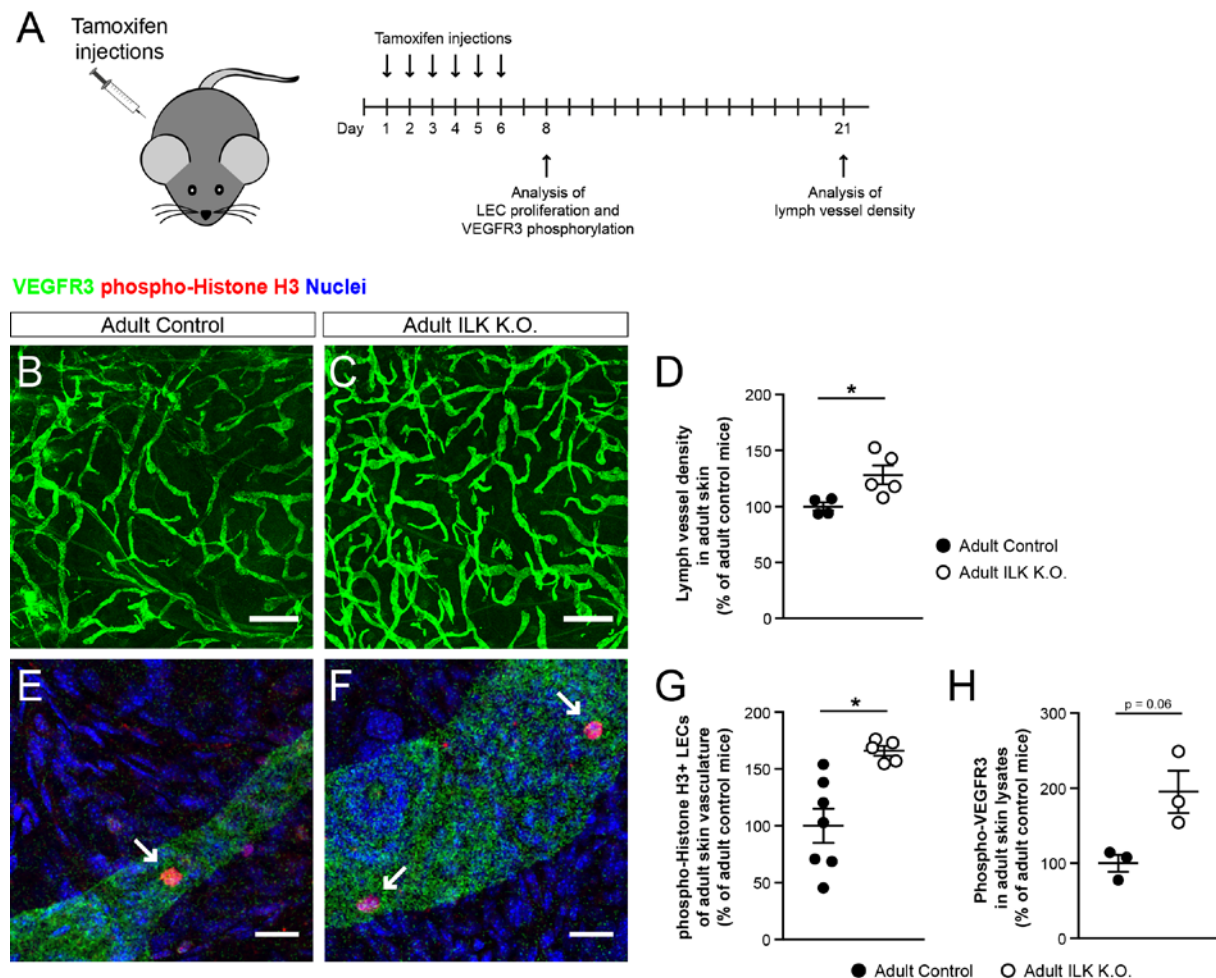


**Figure 24: Tamoxifen-induced LEC-specific deletion of *Ilk* results in increased lymph vessel density, LEC proliferation and VEGFR3 tyrosine phosphorylation in the adult skin. (A)** Schematic overview of the experimental set-up. **(B, C)** Representative LSM images of the ear skin of an adult control (*Prox1-CreER<sup>T2</sup>*) mouse (B) and an adult ILK K.O. (*Prox1-CreER<sup>T2</sup>; Ilk<sup>fl/fl</sup>*) mouse (C) whole-mount stained for VEGFR3 (green). Scale bars, 500  $\mu$ m. **(D)** Quantifications of the dermal lymph vessel density of adult control and adult ILK K.O. mice as determined by VEGFR3-positive area normalized to the total analyzed ear skin area, shown as percentage of control mice. **(E, F)** Representative LSM images of the ear skin of an adult control (E) and an adult ILK K.O. (F) mouse whole-mount stained for VEGFR3 (green), phospho-Histone H3 (red) and nuclei (blue). Scale bars, 20  $\mu$ m. **(G)** Quantifications of phospho-Histone H3-positive LECs normalized to the analyzed lymph vessel area detected by VEGFR3 staining, shown as percentage of control mice. **(H)** Quantifications of phosphorylated VEGFR3 in whole skin lysates, as determined by ELISA, shown as percentage of control mice. **(D, G, H)** All values are shown as means  $\pm$  SEM with  $n \geq 3$  mice per genotype; statistical significance was determined by an unpaired two-tailed Student's t-test (\* $P < 0.05$ ). Sofia Urner performed the presented experiments.

---

All in all, these results strongly indicate that ILK is a general inhibitor of VEGFR3 signaling, LEC proliferation and lymphatic vascular growth in the adult mouse, in addition to its regulatory functions in embryonic development of the lymphatic vasculature.

### **5.5.3. ILK controls lymphatic vascular expansion after myocardial infarction (MI) in the adult mouse heart**

Recently, several publications showed that cardiac lymphatic vessels play a highly relevant role in the heart after MI (reviewed in (Vuorio et al. 2017)). In most studies, MI was shown to induce growth and remodeling of cardiac lymphatic vessels, which in turn also affects cardiac function (Ishikawa et al. 2007; Klotz et al. 2015; Henri et al. 2016; Tatin et al. 2017). Because of this high relevance, we decided to investigate the role of ILK in the cardiac lymphatic vasculature. First, we investigated the hearts of adult ILK K.O. mice and control mice around 2 weeks after the last tamoxifen injection by cross-sectioning and subsequent stainings for blood and lymphatic vessels (Figure 25A, B). Interestingly, we found very heterogeneous effects of *Ilk* deletion on the cardiac lymphatic vasculature depending on the heart region. While we observed significant increase in the lymph vessel density within lateral regions of the heart ventricles, we observed only a non-significant trend towards increased cardiac lymph vessel density in total heart sections (Figure 25C). These results suggest that ILK controls lymphatic vascular growth also in the adult myocardium, but that its role depends on the pre-existing lymphatic vascular network, which was previously described to be inhomogeneous in the adult heart (Norman and Riley 2016; Tatin et al. 2017).

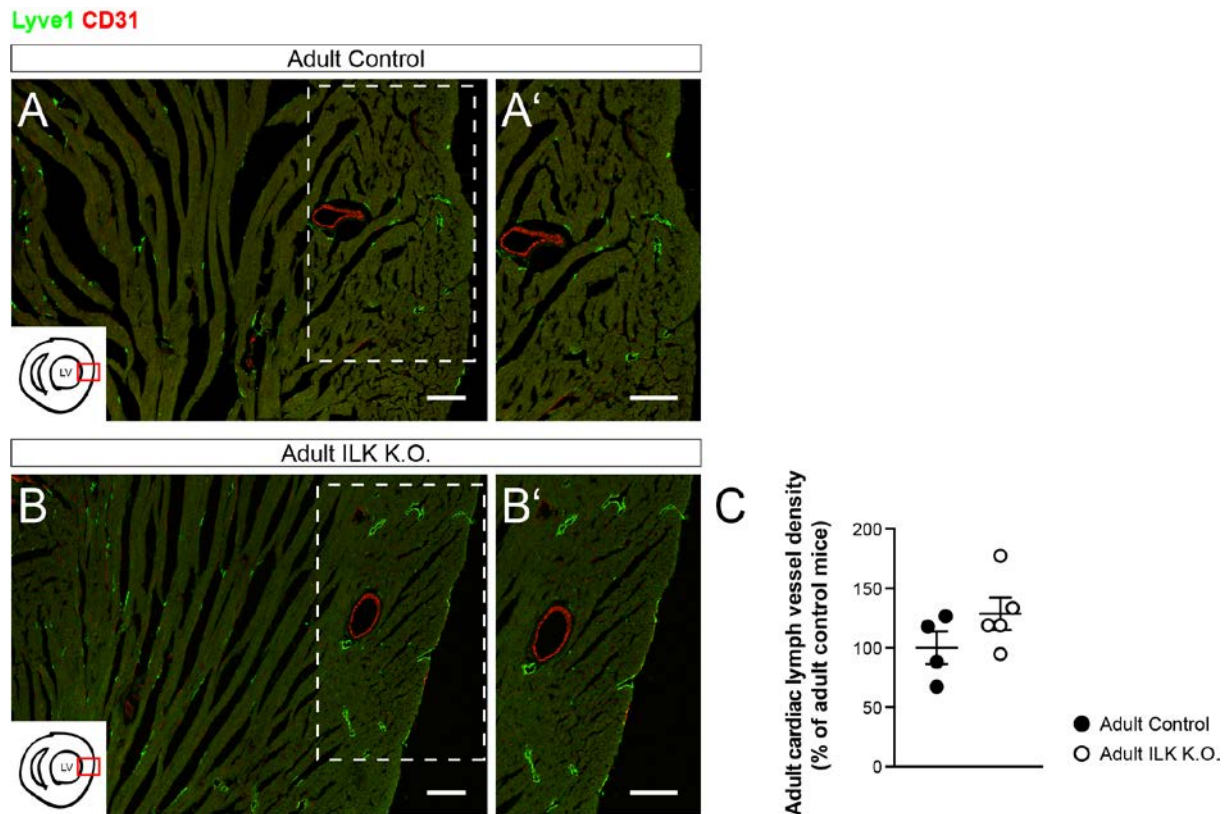


**Figure 25: Tamoxifen-induced LEC-specific deletion of *Ilk* results in non-significantly increased lymph vessel density in the adult heart. (A, A', B, B')** Representative LSM images of cross-sections through the heart of an adult control (*Prox1-CreERT<sup>2</sup>*) mouse (A, A') and an adult ILK K.O. (*Prox1-CreERT<sup>2</sup>; Ilk<sup>fl/fl</sup>*) mouse (B, B'), showing the lateral region of the left ventricle stained for Lyve1 (green) and CD31 (red). Scale bars, 100  $\mu$ m. **(C)** Quantifications of the cardiac lymph vessel density of adult control and adult ILK K.O. mice as determined by Lyve1-positive area normalized to the total analyzed myocardium area; shown as percentage of control mice. All values are shown as means  $\pm$  SEM with  $n \geq 4$  mice per genotype; unpaired two-tailed Student's t-test was performed to analyze statistical significance. Sofia Urner performed the presented experiments.

Next, we investigated the role of ILK in cardiac lymphatic vessels after MI. Therefore, adult ILK K.O. mice and control mice first were subjected to a surgical intervention, in which the thorax was opened, and a suture was placed below the left anterior descending coronary artery (LAD) (performed by Carina Henning). This procedure was done around one week after the last tamoxifen injection, and mice were given another week of rest to reduce the impact of possible immunological influence by the surgery itself before inducing MI (Nossuli et al. 2000). Consequently, around 2 weeks after the last tamoxifen injection, when we also observed significant differences in the dermal lymph vessel density (Figure 24), myocardial ischemia was induced in a closed-chest model by occlusion of the LAD for 60 minutes with subsequent reperfusion (performed by Carina Henning) (Nossuli et al. 2000; Merx et al. 2014). We analyzed cardiac lymphatic vasculature of these mice around 4 weeks after MI by cross-sectioning and subsequent stainings for blood and lymphatic vessels (Figure 26A, B). Strikingly, our quantifications revealed that adult ILK K.O. mice after MI showed higher cardiac lymph vessel density ( $p$ -value = 0.05) compared to adult control mice after MI (Figure

26C). These observations indicate that ILK also controls lymphatic vascular expansion in the adult mouse heart after myocardial ischemia.

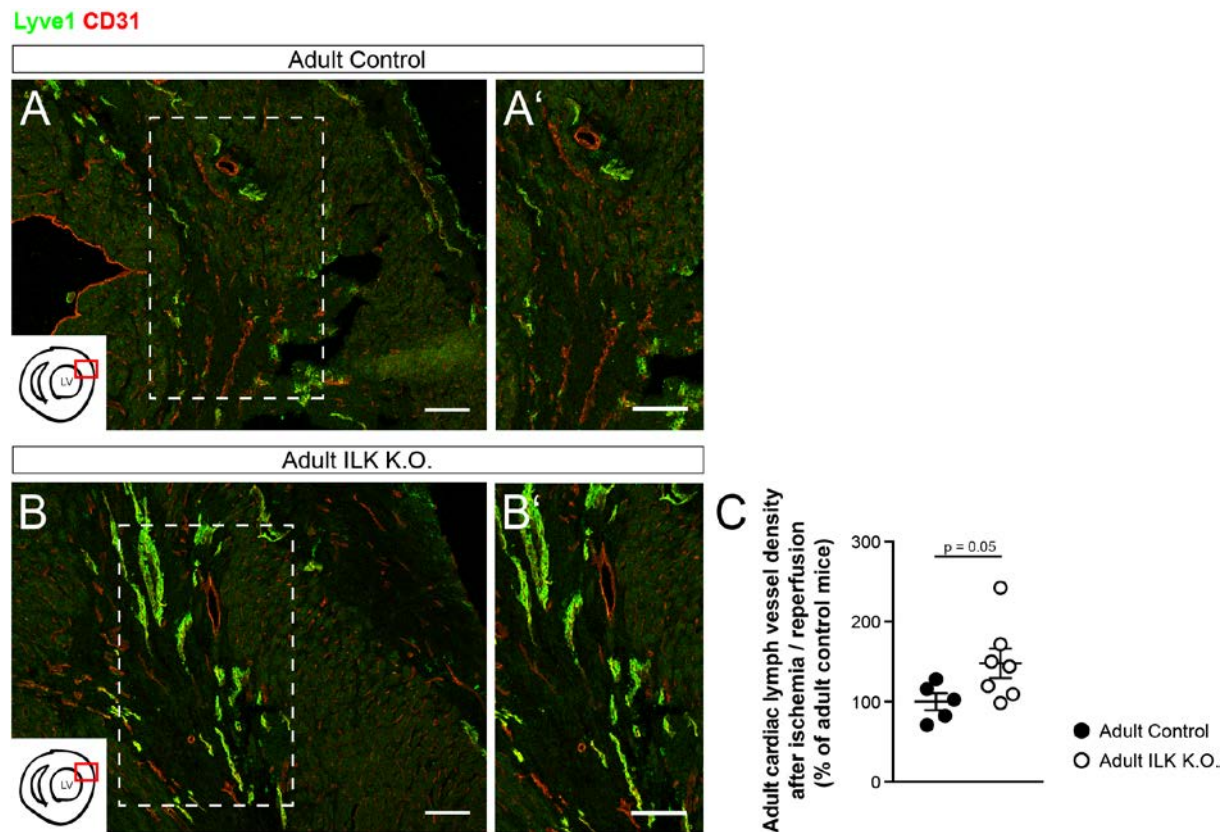


**Figure 26: Tamoxifen-induced LEC-specific deletion of *Ilk* results in increased lymph vessel density in the adult heart after myocardial infarction. (A, A', B, B')** Representative LSM images of cross-sections through the heart of an adult control (*Prox1-CreER<sup>T2</sup>*) mouse (A, A') and an adult ILK K.O. (*Prox1-CreER<sup>T2</sup>; Ilk<sup>fl/fl</sup>*) mouse (B, B') after myocardial ischemia and reperfusion, showing the lateral region of the left ventricle stained for Lyve1 (green) and CD31 (red). Scale bars, 100  $\mu$ m. **(C)** Quantifications of the cardiac lymph vessel density of adult control and adult ILK K.O. mice after myocardial ischemia and reperfusion as determined by Lyve1-positive area normalized to the total analyzed myocardium area, shown as percentage of control mice. All values are shown as means  $\pm$  SEM with  $n \geq 5$  mice per genotype; unpaired two-tailed Student's t-test was performed to analyze statistical significance. Carina Henning performed the surgical interventions, and Sofia Urner performed the presented experiments.

## 5.6. Role of ILK in adult human LECs

Finally, after demonstrating the relevance of ILK in regulating lymphatic vascular expansion during mouse embryonic development as well as in the adult mouse, we aimed to reproduce our observations also in human LECs. We therefore used primary adult human LECs, predominantly with dermal origin, which we transfected with siRNAs against human *ILK*. To increase specificity and precision, we used three different ILK siRNAs (referred to as 'ILK-1, ILK-2 and ILK-3') in addition to a non-targeting control siRNA (referred to as 'control').

We could significantly reduce *ILK* mRNA expression by each of the transfected ILK siRNA (Figure 27A). Consistently, we also observed significant downregulation of ILK protein expression by around 69-83%, as determined by Western Blotting (Figure 27B, C).

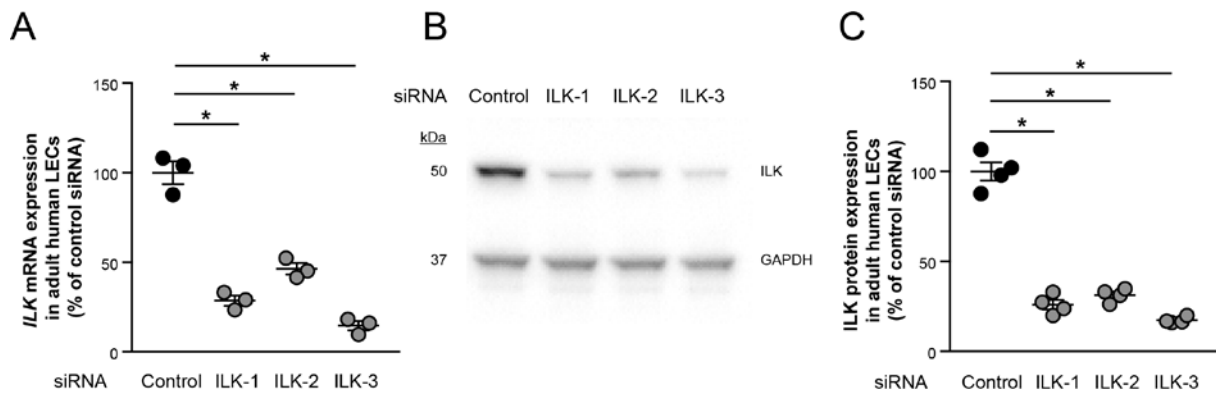


**Figure 27: *ILK* is efficiently silenced in adult human LECs by using ILK siRNAs.** (A) Quantifications of *ILK* mRNA expression levels in human LECs 72 hours after transfection of control siRNA (Control) or one of three different siRNAs against ILK (ILK-1, ILK-2, ILK-3), shown as percentage of control siRNA. (B) Representative Western Blot image of human LEC lysates 72 hours after transfection of control, ILK-1, -2 or -3 siRNA showing protein bands of ILK and GAPDH serving as loading control. (C) Quantifications of ILK protein expression levels in human LECs 72 hours after transfection of control, ILK-1, -2 or -3 siRNA, shown as percentage of control siRNA. All values are shown as means  $\pm$  SEM with  $n \geq 3$  independent transfections per siRNA; statistical significance was determined by one-way ANOVA and Dunnett's multiple comparisons test (\* $P < 0.05$ ). Sofia Urner and Laura Sophie Hilger performed the presented experiments, while Dr. Lara Planas-Paz established the transfection protocol.

### 5.6.1. ILK controls LEC proliferation and VEGFR3 signaling in adult human LECs

In order to determine whether ILK has a similar function in adult human LECs as observed in mouse embryonic and mouse adult LECs, we performed BrdU incorporation assays to determine the effect of *ILK* silencing on human LEC proliferation (Figure 28). Therefore, BrdU was given to the cells in addition to VEGF-C156S as a stimulus for proliferation, and LECs were analyzed after one hour of incubation. Our results showed significantly increased LEC proliferation as determined by the number of BrdU-positive LECs normalized to the total cell number (Figure 28A-C). Specifically, LEC proliferation was upregulated by around 58-130%, depending on the ILK siRNA (Figure 28C), strongly indicating that ILK is required to control proliferation of human LECs. Further, we performed an ELISA for tyrosine phosphorylated VEGFR3 with LEC lysates, and found VEGFR3 signaling to be significantly upregulated upon *ILK* knockdown by around 73-121% (Figure 28D), showing that ILK also controls VEGFR3 signaling in human LECs. Importantly, we also stimulated LECs with VEGF-C156S for 5 minutes before cell lysis to be able to detect

VEGFR3 phosphorylation in control cells. Thus, *ILK* silencing further upregulated LEC proliferation as well as VEGFR3 phosphorylation in addition to the presence of VEGF-C165S.

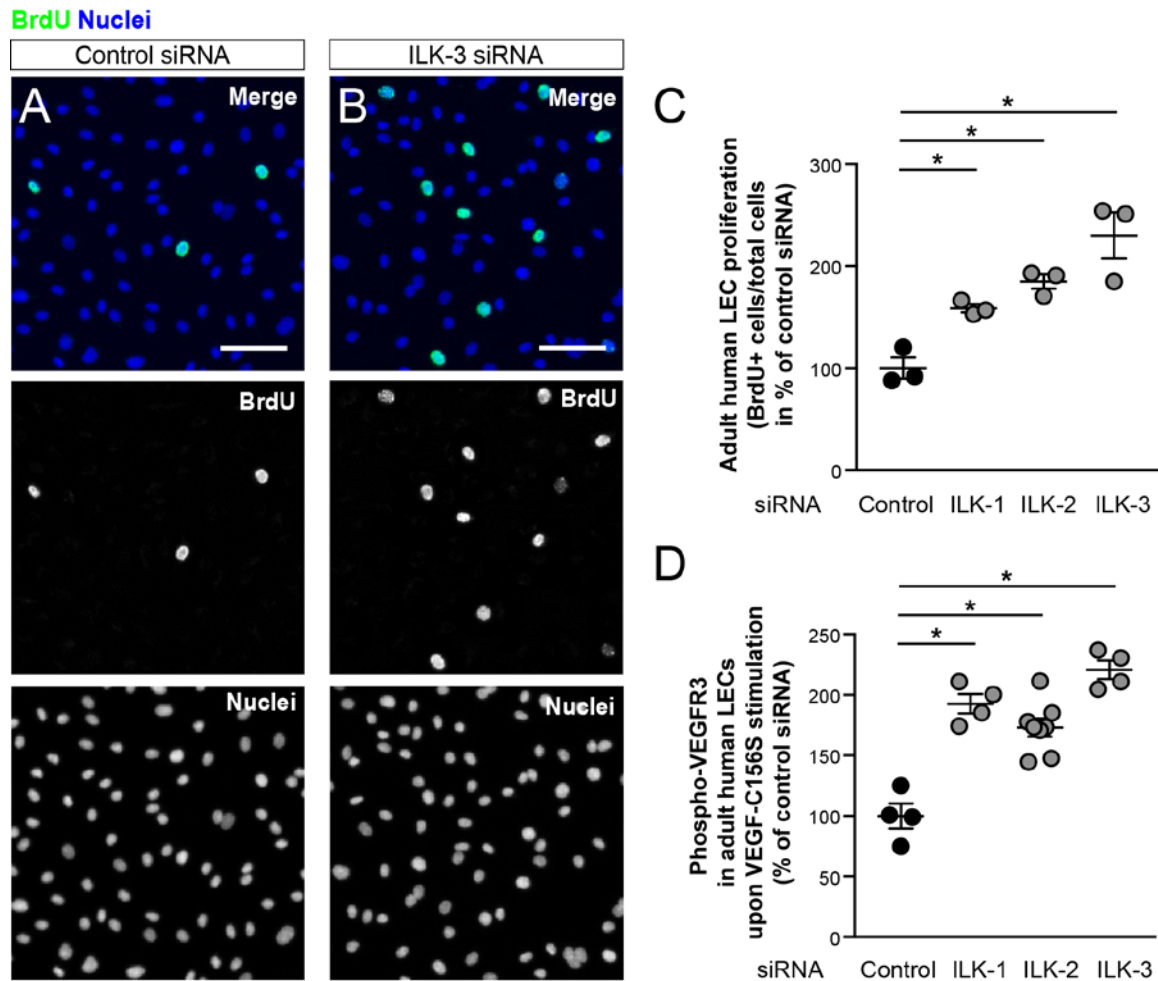


**Figure 28: Silencing of *ILK* in adult human LECs results in increased LEC proliferation and VEGFR3 tyrosine phosphorylation.** (A, B) Representative images of human LECs transfected with control siRNA (Control) (A) or ILK siRNA (ILK-3) (B), and incubated with VEGF-C156S and the proliferation marker BrdU for 1 hour. Staining shows BrdU (green) and nuclei (blue). Scale bars, 50  $\mu$ m. (C) Quantifications of BrdU-positive LECs normalized to total cells that were transfected with control siRNA or one of three different siRNAs against ILK (ILK-1, ILK-2, ILK-3), shown as percentage of control siRNA. (D) Quantifications of phosphorylated VEGFR3 in lysates of LECs that were transfected with control, ILK-1, -2 or -3 siRNA and stimulated with VEGF-C156S for 5 minutes, shown as percentage of control siRNA. (C, D) All values are shown as means  $\pm$  SEM with  $n \geq 3$  independent transfections per siRNA; statistical significance was determined by one-way ANOVA and Dunnett's multiple comparisons test (\* $P < 0.05$ ). Sofia Urner and Dr. Lara Planas-Paz performed the presented experiments.

### 5.6.2. ILK controls interactions between VEGFR3 and $\beta 1$ integrin in adult human LECs

Our mouse embryonic data strongly suggest that ILK prevents interactions between VEGFR3 and  $\beta 1$  integrin, which likely result in increased VEGFR3 phosphorylation and thus induced LEC proliferation. Therefore, we also investigated the interaction between VEGFR3

and  $\beta 1$  integrin in adult human LECs (Figure 29). Similar to the *in vivo* experiments, we performed PLAs using antibodies against human VEGFR3 and human  $\beta 1$  integrin. Our analysis revealed significantly more VEGFR3/ $\beta 1$  integrin PLA sites per LEC in cells that were previously transfected with ILK-2 and ILK-3 siRNA, while transfection with ILK-1 siRNA resulted in a non-significant trend towards an increase (Figure 29A-C). Interestingly, similar to the proliferation and VEGFR3 phosphorylation results, we observed strongest increase (by around 82%) in VEGFR3/ $\beta 1$  integrin PLA sites in LECs transfected with ILK-3 siRNA, which is consistent with the highest *ILK* knockdown efficiency upon ILK-3 siRNA (Figure 27). Thus, we conclude that ILK is required to prevent interaction between VEGFR3 and  $\beta 1$  integrin in adult human LECs.

### VEGFR3/ $\beta 1$ integrin Nuclei

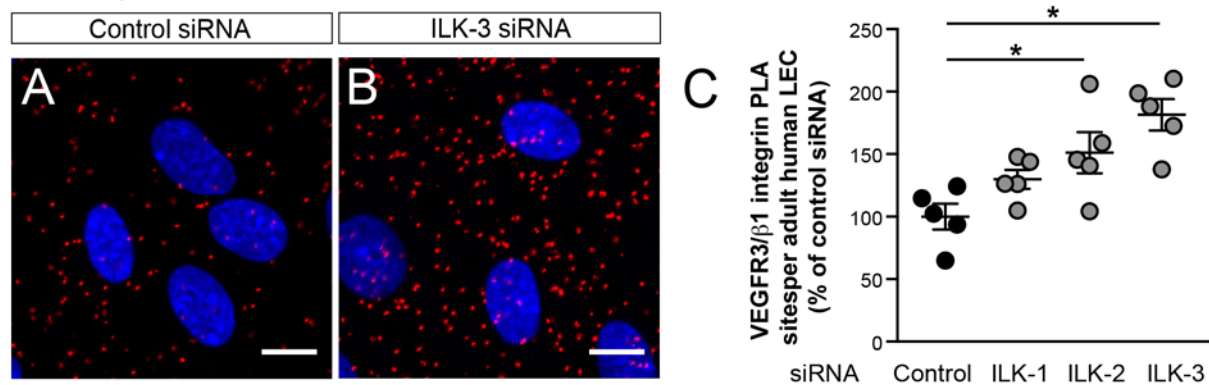


**Figure 29: Silencing of *ILK* in adult human LECs results in increased interactions between VEGFR3 and  $\beta 1$  integrin.** (A, B) Representative LSM images of human LECs transfected with control siRNA (Control) (A) or ILK siRNA (ILK-3) (B) showing VEGFR3/ $\beta 1$  integrin proximity ligation assay (PLA) sites (red) and nuclei (blue). Scale bars, 10  $\mu$ m. (C) Quantifications of VEGFR3/ $\beta 1$  integrin PLA sites per LEC; cells were transfected with control siRNA or one of three different siRNAs against ILK (ILK-1, ILK-2, ILK-3); shown as percentage of control siRNA. All values are shown as means  $\pm$  SEM with  $n = 5$  independent transfections per siRNA; statistical significance was determined by one-way ANOVA and Dunnett's multiple comparisons test (\* $P < 0.05$ ). Sofia Urner performed the presented experiments.

### 5.6.3. ILK dissociates from $\beta 1$ integrin upon mechanical stimulations of adult human LECs

As a next step, we aimed to find out how the effect of experimental *ILK* deletion might be put into a physiological context. Since we found  $\beta 1$  integrin to be involved in ILK-regulated VEGFR3 signaling and LEC proliferation, as demonstrated by *in vitro* and *in vivo* data, we focused on the relevance of mechano-induced VEGFR3 signaling. Previous work in our lab demonstrated that increased interstitial fluid pressure results in increased stretching of LECs, and thereby triggers  $\beta 1$  integrin-induced VEGFR3 phosphorylation (Planas-Paz et al. 2012). Therefore, we cultured adult human LECs on *in vitro* stretch chambers, and mechanically

stimulated them by stretch for 30 minutes. Subsequently, we performed PLAs with antibodies against human VEGFR3 and human  $\beta$ 1 integrin to determine their interaction (Figure 30), which was previously suggested to increase upon stretch (Planas-Paz et al. 2012). Our analysis revealed that mechanically stretched LECs show significantly more VEGFR3/ $\beta$ 1 integrin PLA sites per LEC (Figure 30A-E), similar to what we observed upon knockdown of *ILK* (Figure 29).

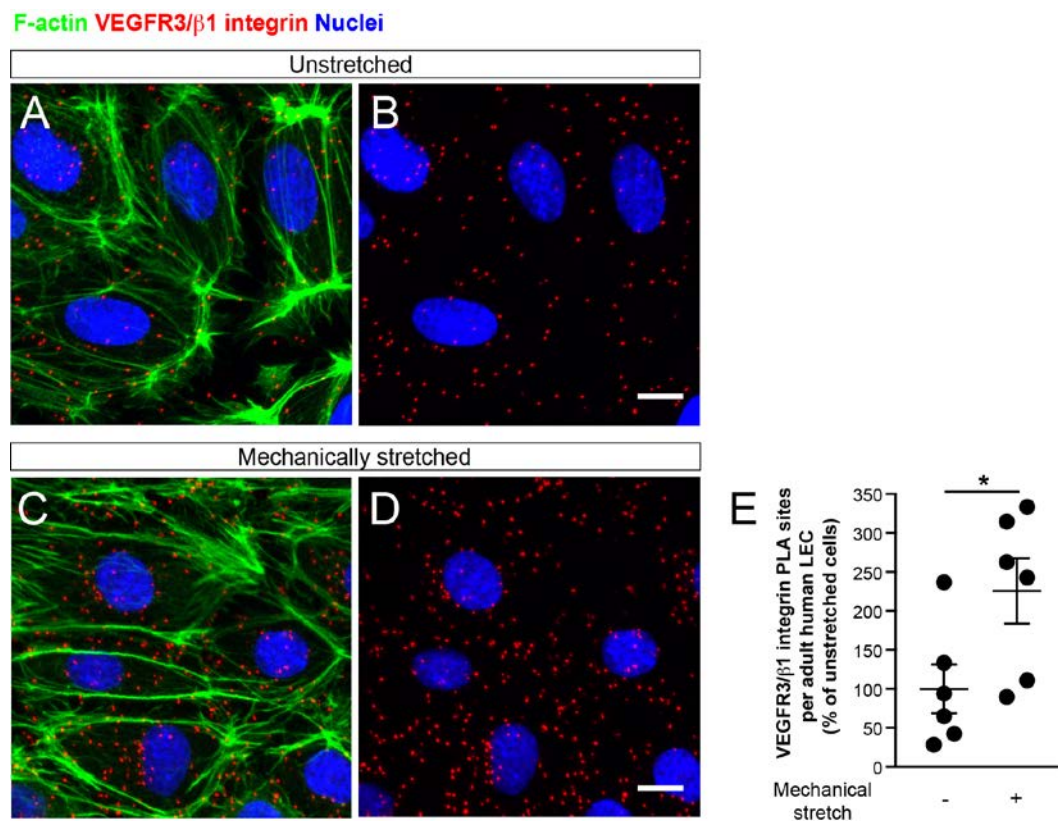


**Figure 30: Stretch of adult human LECs results in increased interactions between VEGFR3 and  $\beta$ 1 integrin.** (A-D) Representative LSM images of human LECs that were either kept unstretched (A, B) or were mechanically stretched for 30 minutes (C, D), showing VEGFR3/ $\beta$ 1 integrin proximity ligation assay (PLA) sites (red). A co-staining for F-actin (green) and nuclei (blue) is also shown. Scale bars, 10  $\mu$ m. (E) Quantifications of VEGFR3/ $\beta$ 1 integrin PLA sites per LEC; cells were unstretched or mechanically stretched; shown as percentage of unstretched cells. All values are shown as means  $\pm$  SEM with  $n = 6$  independent stretch experiments; statistical significance was determined by an unpaired two-tailed Student's  $t$ -test ( $*P < 0.05$ ). Sofia Uner and Laura Sophie Hilger performed the presented experiments.

Because both mechanical stimulations of LECs by stretch as well as *ILK* silencing by siRNAs resulted in increased VEGFR3 and  $\beta$ 1 integrin interactions, we next analyzed the interaction between *ILK* and  $\beta$ 1 integrin upon stretch by performing co-immunoprecipitation (Co-IP) assays. In this context, we transfected adult human LECs with a plasmid for expression of HA-tagged  $\beta$ 1 integrin, and used the HA-tag to precipitate  $\beta$ 1 integrin from LEC lysates. When analyzing how much *ILK* protein is associated with the precipitated HA-tagged  $\beta$ 1 integrin by Western Blotting, we found significantly less *ILK* protein in lysates of stretched

LECs, reduced by around 50% (Figure 31A, B). These results strongly suggest that ILK dissociates from  $\beta 1$  integrin upon mechanical stimulations of human LECs, such as stretch.

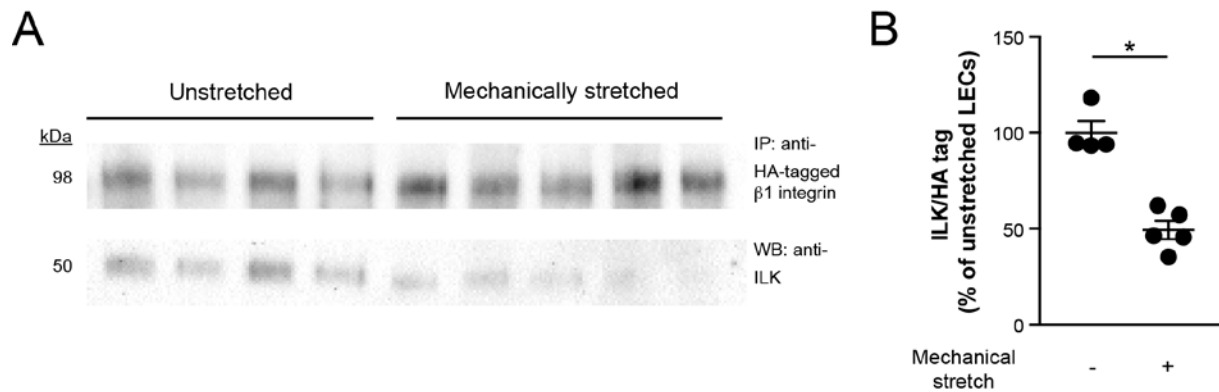


**Figure 31: Stretch of adult human LECs results in decreased interactions between ILK and  $\beta 1$  integrin.** (A) Representative Western Blot image of human LECs that were either kept unstretched or were mechanically stretched for 30 minutes, subsequently lysed and used for Immunoprecipitation (IP) of HA-tagged  $\beta 1$  integrin from whole cell lysates (by antibodies against HA-tag). Interacting ILK protein with immunoprecipitated HA-tagged  $\beta 1$  integrin was detected on the Western blot (WB) by antibodies against ILK. (B) Quantifications of the amount of detected ILK protein in immunoprecipitated lysates, normalized to the respective amount of HA-tagged  $\beta 1$  integrin in unstretched or mechanically stretched LECs; shown as percentage of unstretched LECs. All values are shown as means  $\pm$  SEM with  $n \geq 4$  independent stretch experiments; statistical significance was determined by an unpaired two-tailed Student's t-test (\* $P < 0.05$ ). Sofia Urner performed the presented experiments.

## 6. Discussion

### 6.1. Role of ILK in VEGFR3 signaling, LEC proliferation and lymphatic vascular growth

The aim of this study was first of all to determine the role of ILK in VEGFR3 signaling and lymphatic vascular growth. Therefore, we analyzed three different model systems, including mouse embryos, adult mice, as well as adult human LECs, and found ILK to be a critical inhibitor of VEGFR3 tyrosine phosphorylation, LEC proliferation and lymphatic vascular expansion during developmental, physiological and pathological processes.

#### 6.1.1. Role of ILK in regulating LEC proliferation and lymphatic vascular growth

We first analyzed the effect of endothelial cell-specific *Ilk* deletion on lymphatic vascular development during mouse embryogenesis. Interestingly, ILK K.O. embryos developed strong edema from around E13.0 onwards, which was also the same developmental stage, in which ILK K.O. embryos showed significantly increased LEC proliferation, followed by strongly upregulated LEC numbers and enlarged size of the jls/pTD at E13.5. These observations indicate that ILK inhibits lymphatic vascular expansion during embryogenesis, and that exaggerated LEC proliferation and lymphatic vascular overgrowth do not necessarily lead to the formation of functional lymphatic vessels, as demonstrated by edema development. Indeed, additional experiments, in which the skin vasculature of E14.5 embryos was analyzed by WMS (performed by Dr. Lara Planas-Paz as well as Sofia Urner), showed that ILK K.O. embryos developed strongly enlarged lymphatic vessels, which failed to form a proper lymphatic vascular network, indicated by significantly reduced lymphatic vascular branching. Interestingly, such observations of enlarged lymphatic vessel diameter and reduced branching complexity were previously suggested to be associated with a hyperplastic phenotype (Coxam et al. 2014). Also other embryonic studies indicate that critical regulation of lymphatic vascular expansion in order to prevent overgrowth is essential for proper lymphatic vascular development and its physiological function (Klein et al. 2014).

In addition to the inhibitory function of ILK in LEC proliferation and lymphatic vascular expansion during embryonic development, we also found ILK to be required to control lymphatic vascular growth in the adult. Strikingly, our results indicate that ILK is required to prevent lymphatic vascular growth into the usually avascular cornea. Interestingly, while

siRNA-mediated silencing of *Ilk* in the adult mouse cornea by trend showed increased length of corneal lymphatic vessels, tamoxifen-induced LEC-specific deletion of *Ilk* resulted in a significantly higher number of lymphatic vascular sprouts protruding into the cornea. Both results, however, suggest an ingrowth of lymphatic vessels into the cornea in the absence of *Ilk*. Strikingly, while siRNA-mediated *Ilk* silencing was indicative of lymphatic vascular growth, no blood vessels could be observed protruding into the cornea, indicating that ILK seems to have lymphatic vascular-specific regulatory functions. Importantly, the avascularity of the cornea is essential for proper vision, and previous studies provided evidence for the existence of endogenous lymphangiogenic inhibitors in the cornea, such as soluble VEGFR2 and soluble VEGFR3 (Albuquerque et al. 2009; Singh et al. 2013). In contrast, lymphangiogenic processes in the cornea are rather associated with inflammatory conditions (Cursiefen et al. 2004). Interestingly, the Schlemm's canal, which is a unique ring-shaped vessel with drainage functions surrounding the cornea, was recently shown to share close similarities with lymphatic vessels, such as the expression of Prox1 and responsive VEGFR3 (Aspelund et al. 2014). Since we used *Prox1-CreER<sup>T2</sup>* mice for our analyses, the tamoxifen-induced deletion of *Ilk* might also affect the proliferative response of cells within the Schlemm's canal. Therefore, further investigations including LEC proliferation analyses should be performed in order to determine whether pre-existing lymphatic vessels elongate from the corneal limbus region, or whether newly formed lymphatic vascular sprouts grow into the cornea.

To further evaluate the role of ILK in the adult lymphatic vasculature, we used adult ILK K.O. mice with tamoxifen-induced LEC-specific *Ilk* deletion to identify whether ILK is also important in mediating lymphatic vascular growth in established lymphatic vascular networks, such as in the skin. Notably, we observed significantly increased density of dermal lymphatic vessels in adult ILK K.O. mice, which was associated with significantly upregulated LEC proliferation. These results on the one hand demonstrate the relevance of ILK in regulating LEC proliferation in the adult, and on the other hand support that the observed proliferative phenotype in ILK K.O. embryos is LEC-specific. In addition, *in vitro* studies with adult human LECs further strengthen that ILK critically inhibits LEC proliferation. Interestingly, previous studies of adult mice suggest that hyperplasticity of lymphatic vessels is associated with progressive lymphatic vascular dysfunction (Rutkowski et al. 2006; Gousopoulos et al. 2016). For example, early stages of lymphedema are characterized by increased LEC proliferation, which results in strongly enlarged lymphatic vessels that are unable to drain and transport interstitial fluid (Gousopoulos et al. 2016). Therefore, it would be interesting to further analyze whether the excessive growth of dermal lymphatic vessels in adult ILK K.O. mice is also associated with changes in their functionality.

Our results provide strong evidence for the relevant role of ILK in regulating lymphatic vascular growth by inhibiting LEC proliferation. Interestingly, other reports, which analyzed the role of ILK in different cell types, also support that ILK is a critical regulator of proliferative processes. However, the reported effects of its deletion on cell proliferation are very diverse. For example, *Ilk* deletion in hepatocytes was shown to result in strongly increased cell proliferation soon after birth (Gkretsi et al. 2008), which is in line with our observations that ILK inhibits growth-related processes. Similar effects were described for *in vitro* analyses of vascular SMCs, which showed upregulated cell proliferation upon silencing of *ILK* (Ho et al. 2008). In contrast, *Ilk* deletion in tumor cells results in reduced proliferation, indicating that ILK promotes tumor growth (Serrano et al. 2013). Interestingly, while *in vivo* studies of endothelial cell-specific *Ilk* deletion have shown that ILK is strictly required for VEC survival (Friedrich et al. 2004), *ex vivo* experiments with embryonic stem cells revealed that *Ilk*-deficiency results in increased proliferation of MACS-sorted VECs (Malan et al. 2013). Therefore, the role of ILK in regulating cell proliferation might critically depend on the cell type, and we, for the first time, described its important function in LECs by using embryonic as well as adult mouse and human model systems.

### 6.1.2. Role of ILK in regulating VEGFR3 signaling

Because ILK K.O. embryos, adult ILK K.O. mice, and adult human LECs showed increased LEC proliferation, we aimed to analyze the underlying cellular mechanism, such as the role of RTK signaling. Particularly VEGFR3 and VEGFR2 have been described to be expressed in LECs, and to be involved in the induction of cell survival, migration and proliferation (Makinen et al. 2001b; Dixelius et al. 2003). Therefore, we analyzed the functional role of ILK in regulation of VEGFR3 and VEGFR2 signaling. Surprisingly, while VEGFR3 tyrosine phosphorylation in LECs within the jls/pTD region was strongly increased in ILK K.O. embryos at E13.5, we did not observe any changes in VEGFR2 tyrosine phosphorylation, suggesting that VEGFR3, but not VEGFR2 are important in mediating ILK-dependent effects. Notably, LEC-specific deletion of *Flk1* was previously shown to result in unchanged size of the jls/pTD at E14.5 (Dellinger et al. 2013). In addition, although these embryos showed a decreased lymphatic vessel density in the skin, no changes in LEC proliferation were detected at this embryonic stage, strongly indicating that VEGFR2 in LECs might be dispensable during early lymphatic vascular development (Dellinger et al. 2013). These observations are further supported by studies that showed that inducible endothelial cell-specific *Flk1*-deficiency also has no impact on postnatal lymphangiogenesis (Zarkada et

al. 2015), and adult mice with LEC-specific *Flk1* deletion show no functional defects in lymphatic drainage properties (Dellinger et al. 2013). Based on our observations, we conclude that ILK is required to specifically regulate VEGFR3 signaling in LECs during embryonic development. Furthermore, we could validate increased VEGFR3 phosphorylation in both adult ILK K.O. mice with tamoxifen-induced LEC-specific *Ilk* deletion as well as in adult human LECs, suggesting that ILK inhibits VEGFR3 tyrosine phosphorylation during developmental processes, but also during adulthood, and thereby controls LEC proliferation and lymphatic vascular expansion.

### 6.1.3. Role of ILK in regulating lymphatic vascular growth after MI

After having demonstrated an important role of ILK in regulating lymphatic vascular growth during embryonic development as well as in the adulthood, we next investigated whether ILK is also important in regulating lymphatic vascular growth during pathological conditions, such as MI. Several recent studies provided evidence that cardiac lymphatic vessels are involved in recovery processes after MI (Klotz et al. 2015; Henri et al. 2016; Tatin et al. 2017). In detail, MI was shown to result in a strong lymphangiogenic response, which is associated with lymphatic vascular remodeling and growth in certain regions of the heart (Ishikawa et al. 2007; Sun et al. 2012; Klotz et al. 2015; Henri et al. 2016; Tatin et al. 2017). For example, strongly enlarged lymphatic vessels have been observed close to the infarction zone around 2 weeks after MI in mouse hearts. Around 4 weeks later (6 weeks after MI), such dilated lymphatic vessels could be observed also in non-infarction zones, such as predominantly in epicardial regions (Tatin et al. 2017). However, on the molecular level, the highest lymphangiogenic effect in these mice was observed 4 weeks after MI, as demonstrated by highest VEGFR3 expression levels (Tatin et al. 2017). Therefore, we investigated the effect of tamoxifen-induced LEC-specific *Ilk* deletion on cardiac lymphatic vascular growth without MI, and 4 weeks after MI. In the absence of MI, we only found a trend towards an increased cardiac lymphatic vessel density in the hearts of adult ILK K.O. mice. Interestingly, we observed highly variable effects of *Ilk* deletion depending on the analyzed heart section region, which might be explained by the heterogeneous anatomy and morphology of the cardiac lymphatic vasculature (Norman and Riley 2016; Tatin et al. 2017). In contrast, we observed an increase in the overall cardiac lymphatic vessel density in adult ILK K.O. mice 4 weeks after MI. These data strongly indicate that ILK is important in controlling cardiac lymphatic vascular growth, particularly after MI.

Whether the cardiac lymphatic vessels in adult ILK K.O. mice are functional, needs to be further analyzed. Interestingly, the reported lymphangiogenic response after MI seems to result in disorganized, hyperplastic cardiac lymphatic vessels, which become leaky, and are associated with increased myocardial water accumulation, indicative of dysfunctional lymphatic vessels (Henri et al. 2016; Tatin et al. 2017). However, several studies showed that induction of cardiac lymphangiogenesis via therapeutically applied VEGF-C improves the outcome after MI because it induces growth of functional cardiac lymphatic vessels that seem to contribute to reduced fluid retention and improved inflammatory cell clearance (reviewed by (Goichberg 2016; Vuorio et al. 2017)). Furthermore, VEGF-C treatment after MI was shown to prevent development of cardiac fibrosis, and improve cardiac function (Klotz et al. 2015; Henri et al. 2016). Therefore, it would be interesting to determine in how far the increased lymph vessel density in the hearts of adult ILK K.O. mice after MI contributes to changes in cardiac function. In our experiments, we used the *Prox1* promoter for the analysis of *Ilk*-deficiency in LECs (*Prox1-CreER<sup>T2</sup>*). However, a recently published report about the use of these mice as reporter mice demonstrated that besides its LEC-specificity, *Prox1* seems to be also expressed in adult myocardium (Bianchi et al. 2015), as already previously reported for developmental processes of the heart (Risebro et al. 2009; Petchey et al. 2014). Since several studies exist on the relevance of ILK in cardiomyocytes (Hannigan et al. 1996; White et al. 2006; Ding et al. 2009; Traister et al. 2012), additional mouse lines should be considered for functional cardiac analyses to distinguish between the LEC-specific role of ILK and its function in the myocardium. However, the availability of inducible solely LEC-specific mouse lines is limited, so far.

## **6.2. Underlying mechanism of the regulatory function of ILK in VEGFR3 signaling and lymphatic vascular growth**

In order to understand how ILK inhibits VEGFR3 signaling and LEC proliferation, and thereby controls lymphatic vascular expansion, we used different genetically modified embryos to study the role of caveolin-1,  $\beta$ 1 integrin as well as  $\alpha$ -parvin in VEGFR3 signaling and lymphatic vascular growth. While we found that caveolin-1 is not required to control VEGFR3 signaling and LEC proliferation during lymphatic vascular development, we found that ILK controls  $\beta$ 1 integrin-mediated VEGFR3 signaling, and that  $\alpha$ -parvin is involved in controlling lymphatic vascular growth during embryonic development. We further used an *in vitro* system to study the role of mechanical stretch, and found that stretch of adult human LECs results in the dissociation of ILK from  $\beta$ 1 integrin, but leads to increased interaction

between VEGFR3 and  $\beta 1$  integrin, which have been previously described to result in increased VEGFR3 signaling.

### 6.2.1. Role of caveolin-1

We investigated the role of caveolin-1, which is the major component of caveolae, in VEGFR3 signaling and lymphatic vascular growth during embryonic development in order to see whether its deletion results in a phenocopy of *Ilk*-deficiency. Our hypothesis was based on previous studies that demonstrated the relevance of ILK in caveolae formation, and suggested an inhibitory function of caveolin-1 in VEGFR3 signaling (Galvagni et al. 2007; Wickstrom et al. 2010a; Malan et al. 2013). This raised the possibility that the phenotype we observed in ILK K.O. embryos might be due to reduced caveolae formation, which would result in increased VEGFR3 signaling. However, our analyses revealed that global *Cav1* deletion leads to unchanged VEGFR3 tyrosine phosphorylation, LEC proliferation and size of the jls/pTD in E13.5 embryos. In general, caveolin-1 is highly expressed in endothelial tissues, including LECs, indicating that it plays an important function in endothelial cell biology (Podgrabinska et al. 2002; Sohn et al. 2016). Indeed, several studies identified caveolae as general regulators of RTK signaling, particularly demonstrated in VECs (Drab et al. 2001; Razani et al. 2001). However, the inhibitory function of caveolin-1 in VEGFR3 signaling was so far only described *in vitro* for human umbilical vein endothelial cells (HUVECs) (Galvagni et al. 2007). Therefore, VEGFR3 signaling and LEC proliferation *in vivo*, at least during embryonic development, might not depend on regulatory functions via caveolae, or there might be any compensatory mechanisms in case of *Cav1*-deficiency.

### 6.2.2. Role of $\beta 1$ integrin

$\beta 1$  integrin is an essential part of full VEGFR3 signaling, and is required for lymphatic vascular development (Huang et al. 2000; Wang et al. 2001; Zhang et al. 2005; Galvagni et al. 2010; Planas-Paz et al. 2012). Because of the known interaction of ILK with  $\beta 1$  integrin (Hannigan et al. 1996), we analyzed whether  $\beta 1$  integrin plays a role in the upregulated VEGFR3 signaling and lymphatic vascular growth that we observed in ILK K.O. embryos.  $\beta 1$  integrin-mediated VEGFR3 signaling was previously described to be associated with either  $\beta 1$  integrin activation, or with increased interaction of  $\beta 1$  integrin with VEGFR3 (Wang et al. 2001; Zhang et al. 2005; Planas-Paz et al. 2012).

Activation of  $\beta 1$  integrin normally occurs upon a certain stimulus in the ECM, such as its swelling due to increased interstitial fluid pressure (Planas-Paz et al. 2012). We analyzed the role of ILK in  $\beta 1$  integrin activation in LECs *in vivo* and *in vitro* (performed by Dr. Lara Planas-Paz and Sofia Urner), but could not detect any changes in the absence of *Ilk*. These results strongly suggest that ILK is not required to control  $\beta 1$  integrin activation in LECs. Since ILK binds to the intracellular part of  $\beta 1$  integrin, its deletion might not have any effect on conformational changes in particularly the extracellular domain of  $\beta 1$  integrin, which are associated with its activation (Luo et al. 2007). Indeed, other  $\beta 1$  and  $\beta 3$  integrin-binding adaptor proteins, such as talin, kindlin-2 or kindlin-3 have been reported to be required for proper regulation of integrin activation, and therefore might have a more relevant role than ILK in regard of  $\beta 1$  integrin activation (Calderwood et al. 1999; Tadokoro et al. 2003; Montanez et al. 2008; Moser et al. 2008).

In contrast, our results rather indicate that ILK is required to prevent interactions between VEGFR3 and  $\beta 1$  integrin in LECs, as demonstrated by *in vivo* experiments using mouse embryos as well as by *in vitro* experiments using adult human LECs. The increased interactions observed upon *Ilk*-deficiency might explain the upregulated VEGFR3 tyrosine phosphorylation levels in the absence of *Ilk*. To test whether the increased interaction between VEGFR3 and  $\beta 1$  integrin is functional, we performed genetic rescue experiments by using mouse embryos with endothelial cell-specific homozygous deletion of *Ilk* and heterozygous deletion of *Itgb1*. These experiments strongly indicate that the increased VEGFR3 signaling and LEC proliferation in ILK K.O. embryos depends on the full presence of  $\beta 1$  integrin, since heterozygous deletion of *Itgb1* is sufficient to rescue the significant differences upon *Ilk*-deficiency only. We therefore conclude that ILK inhibits  $\beta 1$  integrin-mediated VEGFR3 signaling by blocking their interaction. Indeed, the molecular cross-talk between integrins and growth factor receptors in general seems to involve their physical interaction as well as formation of complexes at the plasma membrane in order to promote RTK signaling, as demonstrated for several growth factor receptors (Schneller et al. 1997; Moro et al. 1998; Wang et al. 2001). Interestingly, while  $\beta 3$  integrin was shown to interact with VEGFR2, and contributes to its signaling, no such interaction could be observed between  $\beta 1$  integrin and VEGFR2 (Soldi et al. 1999; Borges et al. 2000). In turn,  $\beta 1$  integrin associates with VEGFR3 in order to promote its signaling, while VEGFR3 could not be detected to interact with  $\beta 3$  integrin (Wang et al. 2001; Zhang et al. 2005), supporting the specific relevance of  $\beta 1$  integrin in VEGFR3 signaling. In addition, this might explain the different effects of *Ilk* deletion on VEGFR2 and VEGFR3 signaling, since our findings suggest that it involves  $\beta 1$  integrin-mediated signal transduction.

### 6.2.3. Role of $\alpha$ -parvin

The relevance of the actin cytoskeleton in  $\beta$ 1 integrin-mediated VEGFR3 signaling is demonstrated by experiments, in which inhibition of actin polymerization results in impaired ECM-induced VEGFR3 tyrosine phosphorylation (Wang et al. 2001). Since our previously performed experiments strongly suggest that ILK regulates  $\beta$ 1 integrin-mediated VEGFR3 signaling, we studied the role of  $\alpha$ -parvin in VEGFR3 signaling and lymphatic vascular growth, particularly because ILK connects  $\beta$ 1 integrin tails to F-actin filaments via  $\alpha$ -parvin (Olski et al. 2001; Tu et al. 2001). Indeed, we found  $\alpha$ -parvin to be involved in lymphatic vascular expansion, as demonstrated by analyses of embryos with endothelial cell-specific *Parva* deletion. Interestingly, while the number of proliferating LECs as well as the total LEC number within the jls/pTD region was significantly increased in E13.5  $\alpha$ -parvin K.O. embryos, VEGFR3 tyrosine phosphorylation was only increased by trend. This partial phenocopy of ILK K.O. embryos provides first evidence that  $\alpha$ -parvin controls lymphatic vascular growth, but might also indicate that it involves regulation of other RTK signaling pathways that we did not analyze during these studies. In addition, these results were gathered within primary experiments on  $\alpha$ -parvin, and therefore might aim for further investigations, including analyzing more  $\alpha$ -parvin K.O. embryos.

A very interesting fact about the IPP complex members is that loss of one IPP protein results in the degradation of the other complex members, strongly suggesting an interdependence of each other for complex stability (Fukuda et al. 2003; Xu et al. 2005). Further, preliminary *in vitro* data on adult human LECs (performed by Laura Sophie Hilger) showed that siRNA-mediated silencing of *ILK* results in complete downregulation of  $\alpha$ -parvin protein, while knockdown of *PARVA* barely leads to a reduction of ILK protein expression, strongly indicating that ILK as the central component of the IPP complex is essential for its existence. These experiments might provide an explanation for the significantly stronger phenotype of ILK K.O. embryos in contrast to  $\alpha$ -parvin K.O. embryos during lymphatic vascular development. However, further investigations should be performed in order to finally determine the exact role of  $\alpha$ -parvin in ILK-regulated VEGFR3 signaling and lymphatic vascular growth.

Moreover, since three isoforms of parvin and two isoforms of PINCH exist in eukaryotic cells, different cell types might form diverse IPP complex compositions (Legate et al. 2006). These could in turn have differential functions, and might be a possible explanation why deletion of an IPP complex member, such as *Ilk*, results in variable phenotypes regarding cell proliferation in different cell types.

#### 6.2.4. Role of mechanical stretch

We could so far provide evidence for the importance of ILK in  $\beta 1$  integrin-mediated VEGFR3 signaling, as well as for the involvement of  $\alpha$ -parvin, which provides the connection between  $\beta 1$  integrin-bound ILK and the F-actin cytoskeleton. Since both  $\beta 1$  integrin as well as its proper connection to the cytoskeleton are important for mechanotransduction, this raised the question of whether ILK might be involved in mechano-induced VEGFR3 signaling. Because of the highly established importance of  $\beta 1$  integrin and mechanical stimulations in VEGFR3 signaling and lymphatic vascular expansion, it is not surprising that VEGFR3 is reported as a highly mechano-responsive molecule (Planas-Paz et al. 2012; Baeyens et al. 2015; Coon et al. 2015; Choi et al. 2017). Indeed, *in vitro* studies, in which adult human LECs as well as HUVECs were analyzed in regard of their mechano-sensitive properties, strongly indicate that particularly the amount of VEGFR3 expression, which is higher in LECs, determines how fast these cells respond to mechanical stimulations (Baeyens et al. 2015). In general, the lymphatic vasculature is exposed to different mechanical forces, including flow-induced shear stress or circumferential stretch (reviewed in (Urner et al. in press 2017)). However, high shear stress levels were shown to reduce LEC identity, and therefore might be associated with diminished VEGFR3 signaling (Petrova et al. 2002; Chen et al. 2012; Sabine et al. 2016). In contrast, increased stretch of LECs results in the induction of VEGFR3 signaling and LEC proliferation, as demonstrated for developmental processes such as upon increased interstitial fluid pressure *in vivo* as well as for human LECs during mechanical stretch experiments *in vitro* (Planas-Paz et al. 2012). In addition, this response in VEGFR3 activity is dependent on  $\beta 1$  integrin (Planas-Paz et al. 2012). Because of our findings that ILK controls  $\beta 1$  integrin-mediated VEGFR3 signaling, we therefore focused on analyzing the role of mechanical stretch in regulating interactions between ILK and  $\beta 1$  integrin. Strikingly, we found that stretch of LECs results in dissociation of ILK from  $\beta 1$  integrin, while we observed increased interactions between  $\beta 1$  integrin and VEGFR3 upon stretch. Previous studies further showed that LEC stretch leads to increased  $\beta 1$  integrin-mediated VEGFR3 tyrosine phosphorylation (Planas-Paz et al. 2012). Therefore, our observations suggest that silencing of *ILK* mimics the signaling conditions, which LECs experience upon stretch. Consequently, these results implicate that ILK is a cell-autonomous inhibitor of  $\beta 1$  integrin-mediated VEGFR3 signaling by binding to  $\beta 1$  integrin, and preventing its interaction with VEGFR3 in the absence of mechanical stimulations, such as stretch.

### 6.3. Conclusion

Based on the results we obtained during my thesis, we propose the following model of how ILK acts as an endogenous regulator of VEGFR3 signaling and lymphatic vascular growth: We suggest that ILK prevents interactions between VEGFR3 and  $\beta 1$  integrin in non-stimulated LECs by tightly connecting  $\beta 1$  integrin tails to the F-actin cytoskeleton via  $\alpha$ -parvin as part of the IPP complex. VEGFR3 is still capable of ligand-induced activation (Figure 32A). Upon mechanical stimulations, such as stretch that LECs experience upon increased interstitial fluid pressure, ILK dissociates from  $\beta 1$  integrin, and thereby disrupts its connection with the actin cytoskeleton (Figure 32B). This allows  $\beta 1$  integrin to interact with VEGFR3 at the plasma membrane, and results in increased VEGFR3 tyrosine phosphorylation, LEC proliferation, and thus enhanced lymphatic vascular growth (Figure 32C). This model suggests a novel mechanism of how  $\beta 1$  integrin-mediated VEGFR3 signaling is regulated in order to prevent excessive lymphatic vascular growth.

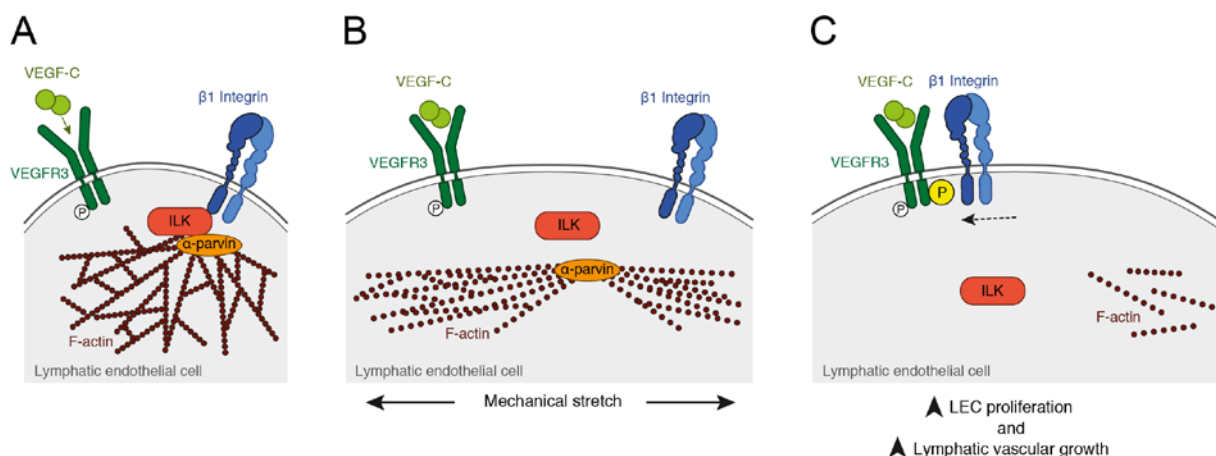


**Figure 32: Proposed model of how ILK regulates VEGFR3 signaling and lymphatic vascular growth. (A)** In non-stimulated LECs, ILK binds to  $\beta 1$  integrin, and connects it to F-actin filaments via  $\alpha$ -parvin, while VEGFR3 activity is predominantly modulated by ligand binding (such as VEGF-C). **(B)** Upon mechanical stretch of LECs, the complex of  $\beta 1$  integrin/ ILK/  $\alpha$ -parvin disrupts. **(C)** As a consequence, interactions between  $\beta 1$  integrin and VEGFR3 increase, and VEGFR3 tyrosine phosphorylation (yellow (P)) is enhanced, leading to increased LEC proliferation and lymphatic vascular growth. Figure was drafted by Sofia Uner, and illustrated by Yousun Koh.

## 7. Publications

Parts of this study will be used for a publication:

Urner S\*, Planas-Paz L\*, Hilger LS, Henning C, Branopolski A, Kelly-Goss M, Stanczuk L, Peirce SM, Mäkinen T, Flögel U and Lammert E (\* equally contributed).

**Identification of ILK as a critical regulator of VEGFR3 signaling and lymphatic vascular growth.** Publication in preparation (2017).

Other publications:

2017: Urner S, Kelly-Goss M, Peirce SM and Lammert E.

**Mechanotransduction in Blood and Lymphatic Vascular Development and Disease.**

Adv Pharmacol. In press, 2017.

Invited Review article.

2014: Neufeld S, Planas-Paz L and Lammert, E.

**Blood and lymphatic vascular tube formation in mouse.**

Semin Cell Dev Biol. 2014 Jul;31:115-23. doi: 10.1016/j.semcdb.2014.02.013.

Epub 2014 Mar 14.

Invited Review article.

## 8. References

- Achen MG, Jeltsch M, Kukk E, Makinen T, Vitali A, Wilks AF, Alitalo K, Stacker SA. 1998. Vascular endothelial growth factor D (VEGF-D) is a ligand for the tyrosine kinases VEGF receptor 2 (Flk1) and VEGF receptor 3 (Flt4). *Proc Natl Acad Sci U S A* **95**: 548-553.
- Alam A, Herault JP, Barron P, Favier B, Fons P, Delesque-Touchard N, Senegas I, Laboudie P, Bonnin J, Cassan C et al. 2004. Heterodimerization with vascular endothelial growth factor receptor-2 (VEGFR-2) is necessary for VEGFR-3 activity. *Biochem Biophys Res Commun* **324**: 909-915.
- Albuquerque RJ, Hayashi T, Cho WG, Kleinman ME, Dridi S, Takeda A, Baffi JZ, Yamada K, Kaneko H, Green MG et al. 2009. Alternatively spliced vascular endothelial growth factor receptor-2 is an essential endogenous inhibitor of lymphatic vessel growth. *Nat Med* **15**: 1023-1030.
- Alvarez-Aznar A, Muhl L, Gaengel K. 2017. VEGF Receptor Tyrosine Kinases: Key Regulators of Vascular Function. *Curr Top Dev Biol* **123**: 433-482.
- Aplin AE, Juliano RL. 1999. Integrin and cytoskeletal regulation of growth factor signaling to the MAP kinase pathway. *J Cell Sci* **112 ( Pt 5)**: 695-706.
- Aspelund A, Antila S, Proulx ST, Karlsten TV, Karaman S, Detmar M, Wiig H, Alitalo K. 2015. A dural lymphatic vascular system that drains brain interstitial fluid and macromolecules. *J Exp Med* **212**: 991-999.
- Aspelund A, Tammela T, Antila S, Nurmi H, Leppanen VM, Zarkada G, Stanczuk L, Francois M, Makinen T, Saharinen P et al. 2014. The Schlemm's canal is a VEGF-C/VEGFR-3-responsive lymphatic-like vessel. *J Clin Invest* **124**: 3975-3986.
- Baeyens N, Nicoli S, Coon BG, Ross TD, Van den Dries K, Han J, Lauridsen HM, Mejean CO, Eichmann A, Thomas JL et al. 2015. Vascular remodeling is governed by a VEGFR3-dependent fluid shear stress set point. *Elife* **4**.
- Baldwin ME, Halford MM, Roufail S, Williams RA, Hibbs ML, Grail D, Kubo H, Stacker SA, Achen MG. 2005. Vascular endothelial growth factor D is dispensable for development of the lymphatic system. *Mol Cell Biol* **25**: 2441-2449.
- Baluk P, Fuxe J, Hashizume H, Romano T, Lashnits E, Butz S, Vestweber D, Corada M, Molendini C, Dejana E et al. 2007. Functionally specialized junctions between endothelial cells of lymphatic vessels. *J Exp Med* **204**: 2349-2362.
- Banerji S, Ni J, Wang SX, Clasper S, Su J, Tammi R, Jones M, Jackson DG. 1999. LYVE-1, a new homologue of the CD44 glycoprotein, is a lymph-specific receptor for hyaluronan. *J Cell Biol* **144**: 789-801.
- Bazigou E, Lyons OT, Smith A, Venn GE, Cope C, Brown NA, Makinen T. 2011. Genes regulating lymphangiogenesis control venous valve formation and maintenance in mice. *J Clin Invest* **121**: 2984-2992.
- Bazigou E, Xie S, Chen C, Weston A, Miura N, Sorokin L, Adams R, Muro AF, Sheppard D, Makinen T. 2009. Integrin-alpha9 is required for fibronectin matrix assembly during lymphatic valve morphogenesis. *Dev Cell* **17**: 175-186.
- Benoit JN, Zawieja DC, Goodman AH, Granger HJ. 1989. Characterization of intact mesenteric lymphatic pump and its responsiveness to acute edemagenic stress. *Am J Physiol* **257**: H2059-2069.
- Bianchi R, Teijeira A, Proulx ST, Christiansen AJ, Seidel CD, Rulicke T, Makinen T, Hagerling R, Halin C, Detmar M. 2015. A transgenic Prox1-Cre-tdTomato reporter mouse for lymphatic vessel research. *PLoS One* **10**: e0122976.
- Borges E, Jan Y, Ruoslahti E. 2000. Platelet-derived growth factor receptor beta and vascular endothelial growth factor receptor 2 bind to the beta 3 integrin through its extracellular domain. *J Biol Chem* **275**: 39867-39873.
- Bos FL, Caunt M, Peterson-Maduro J, Planas-Paz L, Kowalski J, Karpanen T, van Impel A, Tong R, Ernst JA, Korving J et al. 2011. CCBE1 is essential for mammalian lymphatic vascular development and enhances the lymphangiogenic effect of vascular endothelial growth factor-C in vivo. *Circ Res* **109**: 486-491.
- Boudeau J, Miranda-Saavedra D, Barton GJ, Alessi DR. 2006. Emerging roles of pseudokinases. *Trends Cell Biol* **16**: 443-452.
- Braun A, Bordoy R, Stanichi F, Moser M, Kostka GG, Ehler E, Brandau O, Fassler R. 2003. PINCH2 is a new five LIM domain protein, homologous to PINCH and localized to focal adhesions. *Exp Cell Res* **284**: 239-250.
- Breslin JW. 2014. Mechanical forces and lymphatic transport. *Microvasc Res* **96**: 46-54.

- Calderwood DA, Zent R, Grant R, Rees DJ, Hynes RO, Ginsberg MH. 1999. The Talin head domain binds to integrin beta subunit cytoplasmic tails and regulates integrin activation. *J Biol Chem* **274**: 28071-28074.
- Cao R, Lim S, Ji H, Zhang Y, Yang Y, Honek J, Hedlund EM, Cao Y. 2011. Mouse corneal lymphangiogenesis model. *Nat Protoc* **6**: 817-826.
- Chen CY, Bertozzi C, Zou Z, Yuan L, Lee JS, Lu M, Stachelek SJ, Srinivasan S, Guo L, Vicente A et al. 2012. Blood flow reprograms lymphatic vessels to blood vessels. *J Clin Invest* **122**: 2006-2017.
- Chiswell BP, Zhang R, Murphy JW, Boggon TJ, Calderwood DA. 2008. The structural basis of integrin-linked kinase-PINCH interactions. *Proc Natl Acad Sci U S A* **105**: 20677-20682.
- Choe K, Jang JY, Park I, Kim Y, Ahn S, Park DY, Hong YK, Alitalo K, Koh GY, Kim P. 2015. Intravital imaging of intestinal lacteals unveils lipid drainage through contractility. *J Clin Invest* **125**: 4042-4052.
- Choi CK, Vicente-Manzanares M, Zareno J, Whitmore LA, Mogilner A, Horwitz AR. 2008. Actin and alpha-actinin orchestrate the assembly and maturation of nascent adhesions in a myosin II motor-independent manner. *Nat Cell Biol* **10**: 1039-1050.
- Choi D, Park E, Jung E, Seong YJ, Hong M, Lee S, Burford J, Gyarmati G, Peti-Peterdi J, Srikanth S et al. 2017. ORAI1 Activates Proliferation of Lymphatic Endothelial Cells in Response to Laminar Flow Through Kruppel-Like Factors 2 and 4. *Circ Res*.
- Chomczynski P, Sacchi N. 1987. Single-step method of RNA isolation by acid guanidinium thiocyanate-phenol-chloroform extraction. *Anal Biochem* **162**: 156-159.
- Clark EA, Brugge JS. 1995. Integrins and signal transduction pathways: the road taken. *Science* **268**: 233-239.
- Coon BG, Baeyens N, Han J, Budatha M, Ross TD, Fang JS, Yun S, Thomas JL, Schwartz MA. 2015. Intramembrane binding of VE-cadherin to VEGFR2 and VEGFR3 assembles the endothelial mechanosensory complex. *J Cell Biol* **208**: 975-986.
- Coso S, Zeng Y, Opeskin K, Williams ED. 2012. Vascular endothelial growth factor receptor-3 directly interacts with phosphatidylinositol 3-kinase to regulate lymphangiogenesis. *PLoS One* **7**: e39558.
- Coxam B, Sabine A, Bower NI, Smith KA, Pichol-Thievend C, Skoczylas R, Astin JW, Frampton E, Jaquet M, Crosier PS et al. 2014. Pkd1 regulates lymphatic vascular morphogenesis during development. *Cell Rep* **7**: 623-633.
- Cursiefen C, Chen L, Borges LP, Jackson D, Cao J, Radziejewski C, D'Amore PA, Dana MR, Wiegand SJ, Streilein JW. 2004. VEGF-A stimulates lymphangiogenesis and hemangiogenesis in inflammatory neovascularization via macrophage recruitment. *J Clin Invest* **113**: 1040-1050.
- Davis KL, Laine GA, Geissler HJ, Mehlhorn U, Brennan M, Allen SJ. 2000. Effects of myocardial edema on the development of myocardial interstitial fibrosis. *Microcirculation* **7**: 269-280.
- Davis MJ, Rahbar E, Gashev AA, Zawieja DC, Moore JE, Jr. 2011. Determinants of valve gating in collecting lymphatic vessels from rat mesentery. *Am J Physiol Heart Circ Physiol* **301**: H48-60.
- Dellinger MT, Meadows SM, Wynne K, Cleaver O, Brekken RA. 2013. Vascular endothelial growth factor receptor-2 promotes the development of the lymphatic vasculature. *PLoS One* **8**: e74686.
- Dieterich LC, Detmar M. 2016. Tumor lymphangiogenesis and new drug development. *Adv Drug Deliv Rev* **99**: 148-160.
- Ding L, Dong L, Chen X, Zhang L, Xu X, Ferro A, Xu B. 2009. Increased expression of integrin-linked kinase attenuates left ventricular remodeling and improves cardiac function after myocardial infarction. *Circulation* **120**: 764-773.
- Dixelius J, Makinen T, Wirzenius M, Karkkainen MJ, Wernstedt C, Alitalo K, Claesson-Welsh L. 2003. Ligand-induced vascular endothelial growth factor receptor-3 (VEGFR-3) heterodimerization with VEGFR-2 in primary lymphatic endothelial cells regulates tyrosine phosphorylation sites. *J Biol Chem* **278**: 40973-40979.
- Dobrev I, Fielding A, Foster LJ, Dedhar S. 2008. Mapping the integrin-linked kinase interactome using SILAC. *J Proteome Res* **7**: 1740-1749.
- Drab M, Verkade P, Elger M, Kasper M, Lohn M, Lauterbach B, Menne J, Lindschau C, Mende F, Luft FC et al. 2001. Loss of caveolae, vascular dysfunction, and pulmonary defects in caveolin-1 gene-disrupted mice. *Science* **293**: 2449-2452.
- Drake CJ, Fleming PA. 2000. Vasculogenesis in the day 6.5 to 9.5 mouse embryo. *Blood* **95**: 1671-1679.
- Dumont DJ, Jussila L, Taipale J, Lymboussaki A, Mustonen T, Pajusola K, Breitman M, Alitalo K. 1998. Cardiovascular failure in mouse embryos deficient in VEGF receptor-3. *Science* **282**: 946-949.

- Escobedo N, Proulx ST, Karaman S, Dillard ME, Johnson N, Detmar M, Oliver G. 2016. Restoration of lymphatic function rescues obesity in Prox1-haploinsufficient mice. *JCI Insight* **1**.
- Fassler R, Meyer M. 1995. Consequences of lack of beta 1 integrin gene expression in mice. *Genes Dev* **9**: 1896-1908.
- Favier B, Alam A, Barron P, Bonnin J, Laboudie P, Fons P, Mandron M, Herault JP, Neufeld G, Savi P et al. 2006. Neuropilin-2 interacts with VEGFR-2 and VEGFR-3 and promotes human endothelial cell survival and migration. *Blood* **108**: 1243-1250.
- Feng D, Nagy JA, Brekken RA, Pettersson A, Manseau EJ, Pyne K, Mulligan R, Thorpe PE, Dvorak HF, Dvorak AM. 2000. Ultrastructural localization of the vascular permeability factor/vascular endothelial growth factor (VPF/VEGF) receptor-2 (FLK-1, KDR) in normal mouse kidney and in the hyperpermeable vessels induced by VPF/VEGF-expressing tumors and adenoviral vectors. *J Histochem Cytochem* **48**: 545-556.
- Fong GH, Rossant J, Gertsenstein M, Breitman ML. 1995. Role of the Flt-1 receptor tyrosine kinase in regulating the assembly of vascular endothelium. *Nature* **376**: 66-70.
- Fraccaroli A, Pitter B, Taha AA, Seebach J, Huvneers S, Kirsch J, Casaroli-Marano RP, Zahler S, Pohl U, Gerhardt H et al. 2015. Endothelial alpha-parvin controls integrity of developing vasculature and is required for maintenance of cell-cell junctions. *Circ Res* **117**: 29-40.
- Francois M, Caprini A, Hosking B, Orsenigo F, Wilhelm D, Browne C, Paavonen K, Karnezis T, Shayan R, Downes M et al. 2008. Sox18 induces development of the lymphatic vasculature in mice. *Nature* **456**: 643-647.
- Francois M, Short K, Secker GA, Combes A, Schwarz Q, Davidson TL, Smyth I, Hong YK, Harvey NL, Koopman P. 2012. Segmental territories along the cardinal veins generate lymph sacs via a ballooning mechanism during embryonic lymphangiogenesis in mice. *Dev Biol* **364**: 89-98.
- Friedrich EB, Liu E, Sinha S, Cook S, Milstone DS, MacRae CA, Mariotti M, Kuhlencordt PJ, Force T, Rosenzweig A et al. 2004. Integrin-linked kinase regulates endothelial cell survival and vascular development. *Mol Cell Biol* **24**: 8134-8144.
- Fukuda K, Gupta S, Chen K, Wu C, Qin J. 2009. The pseudoactive site of ILK is essential for its binding to alpha-Parvin and localization to focal adhesions. *Mol Cell* **36**: 819-830.
- Fukuda T, Chen K, Shi X, Wu C. 2003. PINCH-1 is an obligate partner of integrin-linked kinase (ILK) functioning in cell shape modulation, motility, and survival. *J Biol Chem* **278**: 51324-51333.
- Gale NW, Prevo R, Espinosa J, Ferguson DJ, Dominguez MG, Yancopoulos GD, Thurston G, Jackson DG. 2007. Normal lymphatic development and function in mice deficient for the lymphatic hyaluronan receptor LYVE-1. *Mol Cell Biol* **27**: 595-604.
- Galvagni F, Anselmi F, Salameh A, Orlandini M, Rocchigiani M, Oliviero S. 2007. Vascular endothelial growth factor receptor-3 activity is modulated by its association with caveolin-1 on endothelial membrane. *Biochemistry* **46**: 3998-4005.
- Galvagni F, Pennacchini S, Salameh A, Rocchigiani M, Neri F, Orlandini M, Petraglia F, Gotta S, Sardone GL, Matteucci G et al. 2010. Endothelial cell adhesion to the extracellular matrix induces c-Src-dependent VEGFR-3 phosphorylation without the activation of the receptor intrinsic kinase activity. *Circ Res* **106**: 1839-1848.
- Garmy-Susini B, Avraamides CJ, Schmid MC, Foubert P, Ellies LG, Barnes L, Feral C, Papayannopoulou T, Lowy A, Blair SL et al. 2010. Integrin alpha4beta1 signaling is required for lymphangiogenesis and tumor metastasis. *Cancer Res* **70**: 3042-3051.
- Geng X, Cha B, Mahamud MR, Lim KC, Silasi-Mansat R, Uddin MK, Miura N, Xia L, Simon AM, Engel JD et al. 2016. Multiple mouse models of primary lymphedema exhibit distinct defects in lymphovenous valve development. *Dev Biol* **409**: 218-233.
- Gerli R, Solito R, Weber E, Agliano M. 2000. Specific adhesion molecules bind anchoring filaments and endothelial cells in human skin initial lymphatics. *Lymphology* **33**: 148-157.
- Ghalamkarpour A, Morlot S, Raas-Rothschild A, Utkus A, Mulliken JB, Boon LM, Vikkula M. 2006. Hereditary lymphedema type I associated with VEGFR3 mutation: the first de novo case and atypical presentations. *Clin Genet* **70**: 330-335.
- Gkretsi V, Apte U, Mars WM, Bowen WC, Luo JH, Yang Y, Yu YP, Orr A, St-Arnaud R, Dedhar S et al. 2008. Liver-specific ablation of integrin-linked kinase in mice results in abnormal histology, enhanced cell proliferation, and hepatomegaly. *Hepatology* **48**: 1932-1941.
- Goichberg P. 2016. Therapeutic lymphangiogenesis after myocardial infarction: vascular endothelial growth factor-C paves the way. *J Thorac Dis* **8**: 1904-1907.
- Gousopoulos E, Proulx ST, Scholl J, Uecker M, Detmar M. 2016. Prominent Lymphatic Vessel Hyperplasia with Progressive Dysfunction and Distinct Immune Cell Infiltration in Lymphedema. *Am J Pathol* **186**: 2193-2203.
- Hagerling R, Pollmann C, Andreas M, Schmidt C, Nurmi H, Adams RH, Alitalo K, Andresen V, Schulte-Merker S, Kiefer F. 2013. A novel multistep mechanism for initial lymphangiogenesis in mouse embryos based on ultramicroscopy. *EMBO J* **32**: 629-644.

- Haiko P, Makinen T, Keskkitalo S, Taipale J, Karkkainen MJ, Baldwin ME, Stacker SA, Achen MG, Alitalo K. 2008. Deletion of vascular endothelial growth factor C (VEGF-C) and VEGF-D is not equivalent to VEGF receptor 3 deletion in mouse embryos. *Mol Cell Biol* **28**: 4843-4850.
- Hanks SK, Quinn AM, Hunter T. 1988. The protein kinase family: conserved features and deduced phylogeny of the catalytic domains. *Science* **241**: 42-52.
- Hannigan GE, Leung-Hagesteijn C, Fitz-Gibbon L, Coppelino MG, Radeva G, Filmus J, Bell JC, Dedhar S. 1996. Regulation of cell adhesion and anchorage-dependent growth by a new beta 1-integrin-linked protein kinase. *Nature* **379**: 91-96.
- Hannigan GE, McDonald PC, Walsh MP, Dedhar S. 2011. Integrin-linked kinase: not so 'pseudo' after all. *Oncogene* **30**: 4375-4385.
- Harvey NL, Srinivasan RS, Dillard ME, Johnson NC, Witte MH, Boyd K, Sleeman MW, Oliver G. 2005. Lymphatic vascular defects promoted by Prox1 haploinsufficiency cause adult-onset obesity. *Nat Genet* **37**: 1072-1081.
- Hattori K, Heissig B, Wu Y, Dias S, Tejada R, Ferris B, Hicklin DJ, Zhu Z, Bohlen P, Witte L et al. 2002. Placental growth factor reconstitutes hematopoiesis by recruiting VEGFR1(+) stem cells from bone-marrow microenvironment. *Nat Med* **8**: 841-849.
- Henri O, Pouehe C, Houssari M, Galas L, Nicol L, Edwards-Levy F, Henry JP, Dumesnil A, Boukhalfa I, Banquet S et al. 2016. Selective Stimulation of Cardiac Lymphangiogenesis Reduces Myocardial Edema and Fibrosis Leading to Improved Cardiac Function Following Myocardial Infarction. *Circulation* **133**: 1484-1497; discussion 1497.
- Hiratsuka S, Minowa O, Kuno J, Noda T, Shibuya M. 1998. Flt-1 lacking the tyrosine kinase domain is sufficient for normal development and angiogenesis in mice. *Proc Natl Acad Sci U S A* **95**: 9349-9354.
- Ho B, Hou G, Pickering JG, Hannigan G, Langille BL, Bendeck MP. 2008. Integrin-linked kinase in the vascular smooth muscle cell response to injury. *Am J Pathol* **173**: 278-288.
- Hong YK, Harvey N, Noh YH, Schacht V, Hirakawa S, Detmar M, Oliver G. 2002. Prox1 is a master control gene in the program specifying lymphatic endothelial cell fate. *Dev Dyn* **225**: 351-357.
- Huang XZ, Wu JF, Ferrando R, Lee JH, Wang YL, Farese RV, Jr., Sheppard D. 2000. Fatal bilateral chylothorax in mice lacking the integrin alpha9beta1. *Mol Cell Biol* **20**: 5208-5215.
- Humphries JD, Byron A, Humphries MJ. 2006. Integrin ligands at a glance. *J Cell Sci* **119**: 3901-3903.
- Hynes RO. 2002. Integrins: bidirectional, allosteric signaling machines. *Cell* **110**: 673-687.
- Irrthum A, Karkkainen MJ, Devriendt K, Alitalo K, Vikkula M. 2000. Congenital hereditary lymphedema caused by a mutation that inactivates VEGFR3 tyrosine kinase. *Am J Hum Genet* **67**: 295-301.
- Ishikawa Y, Akishima-Fukasawa Y, Ito K, Akasaka Y, Tanaka M, Shimokawa R, Kimura-Matsumoto M, Morita H, Sato S, Kamata I et al. 2007. Lymphangiogenesis in myocardial remodelling after infarction. *Histopathology* **51**: 345-353.
- Iskratsch T, Yu CH, Mathur A, Liu S, Stevenin V, Dwyer J, Hone J, Ehler E, Sheetz M. 2013. FHOD1 is needed for directed forces and adhesion maturation during cell spreading and migration. *Dev Cell* **27**: 545-559.
- Jeltsch M, Kaipainen A, Joukov V, Meng X, Lakso M, Rauvala H, Swartz M, Fukumura D, Jain RK, Alitalo K. 1997. Hyperplasia of lymphatic vessels in VEGF-C transgenic mice. *Science* **276**: 1423-1425.
- Johnson NC, Dillard ME, Baluk P, McDonald DM, Harvey NL, Frase SL, Oliver G. 2008. Lymphatic endothelial cell identity is reversible and its maintenance requires Prox1 activity. *Genes Dev* **22**: 3282-3291.
- Joukov V, Kumar V, Sorsa T, Arighi E, Weich H, Saksela O, Alitalo K. 1998. A recombinant mutant vascular endothelial growth factor-C that has lost vascular endothelial growth factor receptor-2 binding, activation, and vascular permeability activities. *J Biol Chem* **273**: 6599-6602.
- Joukov V, Pajusola K, Kaipainen A, Chilov D, Lahtinen I, Kukk E, Saksela O, Kalkkinen N, Alitalo K. 1996. A novel vascular endothelial growth factor, VEGF-C, is a ligand for the Flt4 (VEGFR-3) and KDR (VEGFR-2) receptor tyrosine kinases. *EMBO J* **15**: 1751.
- Kaipainen A, Korhonen J, Mustonen T, van Hinsbergh VW, Fang GH, Dumont D, Breitman M, Alitalo K. 1995. Expression of the fms-like tyrosine kinase 4 gene becomes restricted to lymphatic endothelium during development. *Proc Natl Acad Sci U S A* **92**: 3566-3570.
- Karaman S, Detmar M. 2014. Mechanisms of lymphatic metastasis. *J Clin Invest* **124**: 922-928.
- Karkkainen MJ, Ferrell RE, Lawrence EC, Kimak MA, Levinson KL, McTigue MA, Alitalo K, Finegold DN. 2000. Missense mutations interfere with VEGFR-3 signalling in primary lymphoedema. *Nat Genet* **25**: 153-159.
- Karkkainen MJ, Haiko P, Sainio K, Partanen J, Taipale J, Petrova TV, Jeltsch M, Jackson DG, Talikka M, Rauvala H et al. 2004. Vascular endothelial growth factor C is required for sprouting of the first lymphatic vessels from embryonic veins. *Nat Immunol* **5**: 74-80.

- Karkkainen MJ, Saaristo A, Jussila L, Karila KA, Lawrence EC, Pajusola K, Bueler H, Eichmann A, Kauppinen R, Kettunen MI et al. 2001. A model for gene therapy of human hereditary lymphedema. *Proc Natl Acad Sci U S A* **98**: 12677-12682.
- Katoh O, Tauchi H, Kawaishi K, Kimura A, Satow Y. 1995. Expression of the vascular endothelial growth factor (VEGF) receptor gene, KDR, in hematopoietic cells and inhibitory effect of VEGF on apoptotic cell death caused by ionizing radiation. *Cancer Res* **55**: 5687-5692.
- Kisanuki YY, Hammer RE, Miyazaki J, Williams SC, Richardson JA, Yanagisawa M. 2001. Tie2-Cre transgenic mice: a new model for endothelial cell-lineage analysis in vivo. *Dev Biol* **230**: 230-242.
- Klein KR, Karpnich NO, Espenschied ST, Willcockson HH, Dunworth WP, Hoopes SL, Kushner EJ, Bautch VL, Caron KM. 2014. Decoy receptor CXCR7 modulates adrenomedullin-mediated cardiac and lymphatic vascular development. *Dev Cell* **30**: 528-540.
- Klotz L, Norman S, Vieira JM, Masters M, Rohling M, Dube KN, Bollini S, Matsuzaki F, Carr CA, Riley PR. 2015. Cardiac lymphatics are heterogeneous in origin and respond to injury. *Nature* **522**: 62-67.
- Koltowska K, Betterman KL, Harvey NL, Hogan BM. 2013. Getting out and about: the emergence and morphogenesis of the vertebrate lymphatic vasculature. *Development* **140**: 1857-1870.
- Korenbaum E, Olski TM, Noegel AA. 2001. Genomic organization and expression profile of the parvin family of focal adhesion proteins in mice and humans. *Gene* **279**: 69-79.
- Kukk E, Lymboussaki A, Taira S, Kaipainen A, Jeltsch M, Joukov V, Alitalo K. 1996. VEGF-C receptor binding and pattern of expression with VEGFR-3 suggests a role in lymphatic vascular development. *Development* **122**: 3829-3837.
- Lampugnani MG, Orsenigo F, Gagliani MC, Tacchetti C, Dejana E. 2006. Vascular endothelial cadherin controls VEGFR-2 internalization and signaling from intracellular compartments. *J Cell Biol* **174**: 593-604.
- Lange A, Wickstrom SA, Jakobson M, Zent R, Sainio K, Fassler R. 2009. Integrin-linked kinase is an adaptor with essential functions during mouse development. *Nature* **461**: 1002-1006.
- Le Bras B, Barallobre MJ, Homman-Ludiye J, Ny A, Wyns S, Tammela T, Haiko P, Karkkainen MJ, Yuan L, Muriel MP et al. 2006. VEGF-C is a trophic factor for neural progenitors in the vertebrate embryonic brain. *Nat Neurosci* **9**: 340-348.
- Leak LV. 1970. Electron microscopic observations on lymphatic capillaries and the structural components of the connective tissue-lymph interface. *Microvasc Res* **2**: 361-391.
- . 1976. The structure of lymphatic capillaries in lymph formation. *Fed Proc* **35**: 1863-1871.
- Leak LV, Burke JF. 1968. Ultrastructural studies on the lymphatic anchoring filaments. *J Cell Biol* **36**: 129-149.
- Lee J, Gray A, Yuan J, Luoh SM, Avraham H, Wood WI. 1996. Vascular endothelial growth factor-related protein: a ligand and specific activator of the tyrosine kinase receptor Flt4. *Proc Natl Acad Sci U S A* **93**: 1988-1992.
- Legate KR, Montanez E, Kudlacek O, Fassler R. 2006. ILK, PINCH and parvin: the tIPP of integrin signalling. *Nat Rev Mol Cell Biol* **7**: 20-31.
- Lemmon MA, Schlessinger J. 2010. Cell signaling by receptor tyrosine kinases. *Cell* **141**: 1117-1134.
- Li F, Zhang Y, Wu C. 1999. Integrin-linked kinase is localized to cell-matrix focal adhesions but not cell-cell adhesion sites and the focal adhesion localization of integrin-linked kinase is regulated by the PINCH-binding ANK repeats. *J Cell Sci* **112 ( Pt 24)**: 4589-4599.
- Li S, Bordoy R, Stanchi F, Moser M, Braun A, Kudlacek O, Wewer UM, Yurchenco PD, Fassler R. 2005. PINCH1 regulates cell-matrix and cell-cell adhesions, cell polarity and cell survival during the peri-implantation stage. *J Cell Sci* **118**: 2913-2921.
- Liang X, Zhou Q, Li X, Sun Y, Lu M, Dalton N, Ross J, Jr., Chen J. 2005. PINCH1 plays an essential role in early murine embryonic development but is dispensable in ventricular cardiomyocytes. *Mol Cell Biol* **25**: 3056-3062.
- Licht AH, Raab S, Hofmann U, Breier G. 2004. Endothelium-specific Cre recombinase activity in flk-1-Cre transgenic mice. *Dev Dyn* **229**: 312-318.
- Lim HY, Thiam CH, Yeo KP, Bisioendial R, Hii CS, McGrath KC, Tan KW, Heather A, Alexander JS, Angeli V. 2013. Lymphatic vessels are essential for the removal of cholesterol from peripheral tissues by SR-BI-mediated transport of HDL. *Cell Metab* **17**: 671-684.
- Lin FJ, Chen X, Qin J, Hong YK, Tsai MJ, Tsai SY. 2010. Direct transcriptional regulation of neuropilin-2 by COUP-TFII modulates multiple steps in murine lymphatic vessel development. *J Clin Invest* **120**: 1694-1707.
- Livak KJ, Schmittgen TD. 2001. Analysis of relative gene expression data using real-time quantitative PCR and the 2(-Delta Delta C(T)) Method. *Methods* **25**: 402-408.

- Louveau A, Smirnov I, Keyes TJ, Eccles JD, Rouhani SJ, Peske JD, Derecki NC, Castle D, Mandell JW, Lee KS et al. 2015. Structural and functional features of central nervous system lymphatic vessels. *Nature* **523**: 337-341.
- Luo BH, Carman CV, Springer TA. 2007. Structural basis of integrin regulation and signaling. *Annu Rev Immunol* **25**: 619-647.
- Ly CL, Kataru RP, Mehrara BJ. 2017. Inflammatory Manifestations of Lymphedema. *Int J Mol Sci* **18**.
- Mackinnon AC, Qadota H, Norman KR, Moerman DG, Williams BD. 2002. C. elegans PAT-4/ILK functions as an adaptor protein within integrin adhesion complexes. *Curr Biol* **12**: 787-797.
- Mahadevan A, Welsh IC, Sivakumar A, Gludish DW, Shilvock AR, Noden DM, Huss D, Lansford R, Kurpios NA. 2014. The left-right Pitx2 pathway drives organ-specific arterial and lymphatic development in the intestine. *Dev Cell* **31**: 690-706.
- Makinen T, Adams RH, Bailey J, Lu Q, Ziemiecki A, Alitalo K, Klein R, Wilkinson GA. 2005. PDZ interaction site in ephrinB2 is required for the remodeling of lymphatic vasculature. *Genes Dev* **19**: 397-410.
- Makinen T, Jussila L, Veikkola T, Karpanen T, Kettunen MI, Pulkkanen KJ, Kauppinen R, Jackson DG, Kubo H, Nishikawa S et al. 2001a. Inhibition of lymphangiogenesis with resulting lymphedema in transgenic mice expressing soluble VEGF receptor-3. *Nat Med* **7**: 199-205.
- Makinen T, Veikkola T, Mustjoki S, Karpanen T, Catimel B, Nice EC, Wise L, Mercer A, Kowalski H, Kerjaschki D et al. 2001b. Isolated lymphatic endothelial cells transduce growth, survival and migratory signals via the VEGF-C/D receptor VEGFR-3. *EMBO J* **20**: 4762-4773.
- Malan D, Elischer A, Hesse M, Wickstrom SA, Fleischmann BK, Bloch W. 2013. Deletion of integrin linked kinase in endothelial cells results in defective RTK signaling caused by caveolin 1 mislocalization. *Development* **140**: 987-995.
- Martel C, Li W, Fulp B, Platt AM, Gautier EL, Westerterp M, Bittman R, Tall AR, Chen SH, Thomas MJ et al. 2013. Lymphatic vasculature mediates macrophage reverse cholesterol transport in mice. *J Clin Invest* **123**: 1571-1579.
- Martinez-Corral I, Ulvmar MH, Stanczuk L, Tatin F, Kizhatil K, John SW, Alitalo K, Ortega S, Makinen T. 2015. Nonvenous origin of dermal lymphatic vasculature. *Circ Res* **116**: 1649-1654.
- Merx MW, Gorressen S, van de Sandt AM, Cortese-Krott MM, Ohlig J, Stern M, Rassaf T, Godecke A, Gladwin MT, Kelm M. 2014. Depletion of circulating blood NOS3 increases severity of myocardial infarction and left ventricular dysfunction. *Basic Res Cardiol* **109**: 398.
- Miyamoto S, Teramoto H, Gutkind JS, Yamada KM. 1996. Integrins can collaborate with growth factors for phosphorylation of receptor tyrosine kinases and MAP kinase activation: roles of integrin aggregation and occupancy of receptors. *J Cell Biol* **135**: 1633-1642.
- Montanez E, Ussar S, Schifferer M, Bosl M, Zent R, Moser M, Fassler R. 2008. Kindlin-2 controls bidirectional signaling of integrins. *Genes Dev* **22**: 1325-1330.
- Montanez E, Wickstrom SA, Altstatter J, Chu H, Fassler R. 2009. Alpha-parvin controls vascular mural cell recruitment to vessel wall by regulating RhoA/ROCK signalling. *EMBO J* **28**: 3132-3144.
- Moro L, Venturino M, Bozzo C, Silengo L, Altruda F, Beguinot L, Tarone G, Defilippi P. 1998. Integrins induce activation of EGF receptor: role in MAP kinase induction and adhesion-dependent cell survival. *EMBO J* **17**: 6622-6632.
- Mortimer PS, Rockson SG. 2014. New developments in clinical aspects of lymphatic disease. *J Clin Invest* **124**: 915-921.
- Moser M, Nieswandt B, Ussar S, Pozgajova M, Fassler R. 2008. Kindlin-3 is essential for integrin activation and platelet aggregation. *Nat Med* **14**: 325-330.
- Murfee WL, Rappleye JW, Ceballos M, Schmid-Schonbein GW. 2007. Discontinuous expression of endothelial cell adhesion molecules along initial lymphatic vessels in mesentery: the primary valve structure. *Lymphat Res Biol* **5**: 81-89.
- Nagy JA, Vasile E, Feng D, Sundberg C, Brown LF, Detmar MJ, Lawitts JA, Benjamin L, Tan X, Manseau EJ et al. 2002. Vascular permeability factor/vascular endothelial growth factor induces lymphangiogenesis as well as angiogenesis. *J Exp Med* **196**: 1497-1506.
- Nakao S, Hafezi-Moghadam A, Ishibashi T. 2012. Lymphatics and lymphangiogenesis in the eye. *J Ophthalmol* **2012**: 783163.
- Nakayama M, Nakayama A, van Lessen M, Yamamoto H, Hoffmann S, Drexler HC, Itoh N, Hirose T, Breier G, Vestweber D et al. 2013. Spatial regulation of VEGF receptor endocytosis in angiogenesis. *Nat Cell Biol* **15**: 249-260.
- Neufeld S, Planas-Paz L, Lammert E. 2014. Blood and lymphatic vascular tube formation in mouse. *Semin Cell Dev Biol* **31**: 115-123.
- Nikolopoulos SN, Turner CE. 2000. Actopaxin, a new focal adhesion protein that binds paxillin LD motifs and actin and regulates cell adhesion. *J Cell Biol* **151**: 1435-1448.

- Nilsson I, Bahram F, Li X, Gualandi L, Koch S, Jarvius M, Soderberg O, Anisimov A, Kholova I, Pytowski B et al. 2010. VEGF receptor 2/3 heterodimers detected in situ by proximity ligation on angiogenic sprouts. *EMBO J* **29**: 1377-1388.
- Norman S, Riley PR. 2016. Anatomy and development of the cardiac lymphatic vasculature: Its role in injury and disease. *Clin Anat* **29**: 305-315.
- Nossuli TO, Lakshminarayanan V, Baumgarten G, Taffet GE, Ballantyne CM, Michael LH, Entman ML. 2000. A chronic mouse model of myocardial ischemia-reperfusion: essential in cytokine studies. *Am J Physiol Heart Circ Physiol* **278**: H1049-1055.
- Okazaki T, Ni A, Ayeni OA, Baluk P, Yao LC, Vossmeier D, Zischinsky G, Zahn G, Knolle J, Christner C et al. 2009. alpha5beta1 Integrin blockade inhibits lymphangiogenesis in airway inflammation. *Am J Pathol* **174**: 2378-2387.
- Oliver G. 2004. Lymphatic vasculature development. *Nat Rev Immunol* **4**: 35-45.
- Oliver G, Detmar M. 2002. The rediscovery of the lymphatic system: old and new insights into the development and biological function of the lymphatic vasculature. *Genes Dev* **16**: 773-783.
- Olski TM, Noegel AA, Korenbaum E. 2001. Parvin, a 42 kDa focal adhesion protein, related to the alpha-actinin superfamily. *J Cell Sci* **114**: 525-538.
- Orlandini M, Spreafico A, Bardelli M, Rocchigiani M, Salameh A, Nucciotti S, Capperucci C, Frediani B, Oliviero S. 2006. Vascular endothelial growth factor-D activates VEGFR-3 expressed in osteoblasts inducing their differentiation. *J Biol Chem* **281**: 17961-17967.
- Pajusola K, Aprelikova O, Korhonen J, Kaipainen A, Pertovaara L, Alitalo R, Alitalo K. 1992. FLT4 receptor tyrosine kinase contains seven immunoglobulin-like loops and is expressed in multiple human tissues and cell lines. *Cancer Res* **52**: 5738-5743.
- Partanen TA, Arola J, Saaristo A, Jussila L, Ora A, Miettinen M, Stacker SA, Achen MG, Alitalo K. 2000. VEGF-C and VEGF-D expression in neuroendocrine cells and their receptor, VEGFR-3, in fenestrated blood vessels in human tissues. *FASEB J* **14**: 2087-2096.
- Parton RG, Simons K. 2007. The multiple faces of caveolae. *Nat Rev Mol Cell Biol* **8**: 185-194.
- Pasquet JM, Noury M, Nurden AT. 2002. Evidence that the platelet integrin alphaIIb beta3 is regulated by the integrin-linked kinase, ILK, in a PI3-kinase dependent pathway. *Thromb Haemost* **88**: 115-122.
- Petchey LK, Risebro CA, Vieira JM, Roberts T, Bryson JB, Greensmith L, Lythgoe MF, Riley PR. 2014. Loss of Prox1 in striated muscle causes slow to fast skeletal muscle fiber conversion and dilated cardiomyopathy. *Proc Natl Acad Sci U S A* **111**: 9515-9520.
- Petrova TV, Makinen T, Makela TP, Saarela J, Virtanen I, Ferrell RE, Finegold DN, Kerjaschki D, Yla-Herttuala S, Alitalo K. 2002. Lymphatic endothelial reprogramming of vascular endothelial cells by the Prox-1 homeobox transcription factor. *EMBO J* **21**: 4593-4599.
- Planas-Paz L, Lammert E. 2013. Mechanical forces in lymphatic vascular development and disease. *Cell Mol Life Sci* **70**: 4341-4354.
- . 2014. Mechanosensing in developing lymphatic vessels. *Adv Anat Embryol Cell Biol* **214**: 23-40.
- Planas-Paz L, Strlic B, Goedecke A, Breier G, Fassler R, Lammert E. 2012. Mechanoinduction of lymph vessel expansion. *EMBO J* **31**: 788-804.
- Podgrabinska S, Braun P, Velasco P, Kloos B, Pepper MS, Skobe M. 2002. Molecular characterization of lymphatic endothelial cells. *Proc Natl Acad Sci U S A* **99**: 16069-16074.
- Potocnik AJ, Brakebusch C, Fassler R. 2000. Fetal and adult hematopoietic stem cells require beta1 integrin function for colonizing fetal liver, spleen, and bone marrow. *Immunity* **12**: 653-663.
- Qin J, Wu C. 2012. ILK: a pseudokinase in the center stage of cell-matrix adhesion and signaling. *Curr Opin Cell Biol* **24**: 607-613.
- Randolph GJ, Ivanov S, Zinselmeyer BH, Scallan JP. 2017. The Lymphatic System: Integral Roles in Immunity. *Annu Rev Immunol* **35**: 31-52.
- Razani B, Engelman JA, Wang XB, Schubert W, Zhang XL, Marks CB, Macaluso F, Russell RG, Li M, Pestell RG et al. 2001. Caveolin-1 null mice are viable but show evidence of hyperproliferative and vascular abnormalities. *J Biol Chem* **276**: 38121-38138.
- Regenfuss B, Bock F, Cursiefen C. 2012. Corneal angiogenesis and lymphangiogenesis. *Curr Opin Allergy Clin Immunol* **12**: 548-554.
- Ren S, Zhang F, Li C, Jia C, Li S, Xi H, Zhang H, Yang L, Wang Y. 2010. Selection of housekeeping genes for use in quantitative reverse transcription PCR assays on the murine cornea. *Mol Vis* **16**: 1076-1086.
- Renshaw MW, Price LS, Schwartz MA. 1999. Focal adhesion kinase mediates the integrin signaling requirement for growth factor activation of MAP kinase. *J Cell Biol* **147**: 611-618.
- Risebro CA, Searles RG, Melville AA, Ehler E, Jina N, Shah S, Pallas J, Hubank M, Dillard M, Harvey NL et al. 2009. Prox1 maintains muscle structure and growth in the developing heart. *Development* **136**: 495-505.
- Rockson SG. 2001. Lymphedema. *Am J Med* **110**: 288-295.

- Rutkowski JM, Moya M, Johannes J, Goldman J, Swartz MA. 2006. Secondary lymphedema in the mouse tail: Lymphatic hyperplasia, VEGF-C upregulation, and the protective role of MMP-9. *Microvasc Res* **72**: 161-171.
- Sabin F. 1902. On the origin of the lymphatic system from the veins and the development of the lymphatic hearts and thoracic duct in the pig. *Am J Anat* **1(3)**: 367-391.
- Sabine A, Agalarov Y, Maby-El Hajjami H, Jaquet M, Hagerling R, Pollmann C, Bebbler D, Pfenniger A, Miura N, Dormond O et al. 2012. Mechanotransduction, PROX1, and FOXC2 cooperate to control connexin37 and calcineurin during lymphatic-valve formation. *Dev Cell* **22**: 430-445.
- Sabine A, Saygili Demir C, Petrova TV. 2016. Endothelial Cell Responses to Biomechanical Forces in Lymphatic Vessels. *Antioxid Redox Signal* **25**: 451-465.
- Saito Y, Nakagami H, Kaneda Y, Morishita R. 2013. Lymphedema and therapeutic lymphangiogenesis. *Biomed Res Int* **2013**: 804675.
- Sakai T, Li S, Docheva D, Grashoff C, Sakai K, Kostka G, Braun A, Pfeifer A, Yurchenco PD, Fassler R. 2003. Integrin-linked kinase (ILK) is required for polarizing the epiblast, cell adhesion, and controlling actin accumulation. *Genes Dev* **17**: 926-940.
- Salameh A, Galvagni F, Bardelli M, Bussolino F, Oliviero S. 2005. Direct recruitment of CRK and GRB2 to VEGFR-3 induces proliferation, migration, and survival of endothelial cells through the activation of ERK, AKT, and JNK pathways. *Blood* **106**: 3423-3431.
- Scallan JP, Wolpers JH, Muthuchamy M, Zawieja DC, Gashev AA, Davis MJ. 2012. Independent and interactive effects of preload and afterload on the pump function of the isolated lymphangion. *Am J Physiol Heart Circ Physiol* **303**: H809-824.
- Schacht V, Ramirez MI, Hong YK, Hirakawa S, Feng D, Harvey N, Williams M, Dvorak AM, Dvorak HF, Oliver G et al. 2003. T1alpha/podoplanin deficiency disrupts normal lymphatic vasculature formation and causes lymphedema. *EMBO J* **22**: 3546-3556.
- Schiller HB, Friedel CC, Boulegue C, Fassler R. 2011. Quantitative proteomics of the integrin adhesome show a myosin II-dependent recruitment of LIM domain proteins. *EMBO Rep* **12**: 259-266.
- Schmeisser A, Christoph M, Augstein A, Marquetant R, Kasper M, Braun-Dullaeus RC, Strasser RH. 2006. Apoptosis of human macrophages by Flt-4 signaling: implications for atherosclerotic plaque pathology. *Cardiovasc Res* **71**: 774-784.
- Schmittgen TD, Livak KJ. 2008. Analyzing real-time PCR data by the comparative C(T) method. *Nat Protoc* **3**: 1101-1108.
- Schneller M, Vuori K, Ruoslahti E. 1997. Alphavbeta3 integrin associates with activated insulin and PDGFbeta receptors and potentiates the biological activity of PDGF. *EMBO J* **16**: 5600-5607.
- Schoenwaelder SM, Burridge K. 1999. Bidirectional signaling between the cytoskeleton and integrins. *Curr Opin Cell Biol* **11**: 274-286.
- Schulte-Merker S, Sabine A, Petrova TV. 2011. Lymphatic vascular morphogenesis in development, physiology, and disease. *J Cell Biol* **193**: 607-618.
- Serrano I, McDonald PC, Lock F, Muller WJ, Dedhar S. 2013. Inactivation of the Hippo tumour suppressor pathway by integrin-linked kinase. *Nat Commun* **4**: 2976.
- Shalaby F, Rossant J, Yamaguchi TP, Gertsenstein M, Wu XF, Breitman ML, Schuh AC. 1995. Failure of blood-island formation and vasculogenesis in Flk-1-deficient mice. *Nature* **376**: 62-66.
- Simons M, Gordon E, Claesson-Welsh L. 2016. Mechanisms and regulation of endothelial VEGF receptor signalling. *Nat Rev Mol Cell Biol* **17**: 611-625.
- Singh N, Tiem M, Watkins R, Cho YK, Wang Y, Olsen T, Uehara H, Mamalis C, Luo L, Oakey Z et al. 2013. Soluble vascular endothelial growth factor receptor 3 is essential for corneal alymphaticity. *Blood* **121**: 4242-4249.
- Soderberg O, Gullberg M, Jarvius M, Ridderstrale K, Leuchowius KJ, Jarvius J, Wester K, Hydbring P, Bahram F, Larsson LG et al. 2006. Direct observation of individual endogenous protein complexes in situ by proximity ligation. *Nat Methods* **3**: 995-1000.
- Sohn J, Brick RM, Tuan RS. 2016. From embryonic development to human diseases: The functional role of caveolae/caveolin. *Birth Defects Res C Embryo Today* **108**: 45-64.
- Soldi R, Mitola S, Strasly M, Defilippi P, Tarone G, Bussolino F. 1999. Role of alphavbeta3 integrin in the activation of vascular endothelial growth factor receptor-2. *EMBO J* **18**: 882-892.
- Srinivasan RS, Dillard ME, Lagutin OV, Lin FJ, Tsai S, Tsai MJ, Samokhvalov IM, Oliver G. 2007. Lineage tracing demonstrates the venous origin of the mammalian lymphatic vasculature. *Genes Dev* **21**: 2422-2432.
- Srinivasan RS, Geng X, Yang Y, Wang Y, Mukatira S, Studer M, Porto MP, Lagutin O, Oliver G. 2010. The nuclear hormone receptor Coup-TFII is required for the initiation and early maintenance of Prox1 expression in lymphatic endothelial cells. *Genes Dev* **24**: 696-707.
- Stanchi F, Bordoy R, Kudlacek O, Braun A, Pfeifer A, Moser M, Fassler R. 2005. Consequences of loss of PINCH2 expression in mice. *J Cell Sci* **118**: 5899-5910.

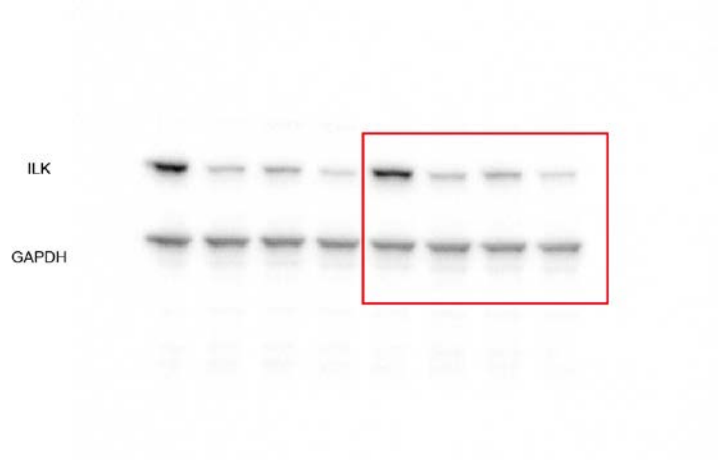
- Stanczuk L, Martinez-Corral I, Ulvmar MH, Zhang Y, Lavina B, Fruttiger M, Adams RH, Saur D, Betsholtz C, Ortega S et al. 2015. cKit Lineage Hemogenic Endothelium-Derived Cells Contribute to Mesenteric Lymphatic Vessels. *Cell Rep*.
- Stephens LE, Sutherland AE, Klimanskaya IV, Andrieux A, Meneses J, Pedersen RA, Damsky CH. 1995. Deletion of beta 1 integrins in mice results in inner cell mass failure and peri-implantation lethality. *Genes Dev* **9**: 1883-1895.
- Su Y, Xia W, Li J, Walz T, Humphries MJ, Vestweber D, Cabanas C, Lu C, Springer TA. 2016. Relating conformation to function in integrin alpha5beta1. *Proc Natl Acad Sci U S A* **113**: E3872-3881.
- Sun QN, Wang YF, Guo ZK. 2012. Reconstitution of myocardial lymphatic vessels after acute infarction of rat heart. *Lymphology* **45**: 80-86.
- Sun Z, Guo SS, Fassler R. 2016. Integrin-mediated mechanotransduction. *J Cell Biol* **215**: 445-456.
- Sundberg C, Rubin K. 1996. Stimulation of beta1 integrins on fibroblasts induces PDGF independent tyrosine phosphorylation of PDGF beta-receptors. *J Cell Biol* **132**: 741-752.
- Tadokoro S, Shattil SJ, Eto K, Tai V, Liddington RC, de Pereda JM, Ginsberg MH, Calderwood DA. 2003. Talin binding to integrin beta tails: a final common step in integrin activation. *Science* **302**: 103-106.
- Takahashi H, Shibuya M. 2005. The vascular endothelial growth factor (VEGF)/VEGF receptor system and its role under physiological and pathological conditions. *Clin Sci (Lond)* **109**: 227-241.
- Tammela T, Zarkada G, Wallgard E, Murtomaki A, Suchting S, Wirzenius M, Waltari M, Hellstrom M, Schomber T, Peltonen R et al. 2008. Blocking VEGFR-3 suppresses angiogenic sprouting and vascular network formation. *Nature* **454**: 656-660.
- Tatin F, Renaud-Gabardos E, Godet AC, Hantelys F, Pujol F, Morfousse F, Calise D, Viars F, Valet P, Masri B et al. 2017. Apelin modulates pathological remodeling of lymphatic endothelium after myocardial infarction. *JCI Insight* **2**.
- Tatin F, Taddei A, Weston A, Fuchs E, Devenport D, Tissir F, Makinen T. 2013. Planar cell polarity protein Celsr1 regulates endothelial adherens junctions and directed cell rearrangements during valve morphogenesis. *Dev Cell* **26**: 31-44.
- Terman BI, Carrion ME, Kovacs E, Rasmussen BA, Eddy RL, Shows TB. 1991. Identification of a new endothelial cell growth factor receptor tyrosine kinase. *Oncogene* **6**: 1677-1683.
- Terman BI, Dougher-Vermazen M, Carrion ME, Dimitrov D, Armellino DC, Gospodarowicz D, Bohlen P. 1992. Identification of the KDR tyrosine kinase as a receptor for vascular endothelial cell growth factor. *Biochem Biophys Res Commun* **187**: 1579-1586.
- Thomson BR, Heinen S, Jeansson M, Ghosh AK, Fatima A, Sung HK, Onay T, Chen H, Yamaguchi S, Economides AN et al. 2014. A lymphatic defect causes ocular hypertension and glaucoma in mice. *J Clin Invest* **124**: 4320-4324.
- Traister A, Aafaqi S, Masse S, Dai X, Li M, Hinek A, Nanthakumar K, Hannigan G, Coles JG. 2012. ILK induces cardiomyogenesis in the human heart. *PLoS One* **7**: e37802.
- Tu Y, Huang Y, Zhang Y, Hua Y, Wu C. 2001. A new focal adhesion protein that interacts with integrin-linked kinase and regulates cell adhesion and spreading. *J Cell Biol* **153**: 585-598.
- Tu Y, Li F, Goicoechea S, Wu C. 1999. The LIM-only protein PINCH directly interacts with integrin-linked kinase and is recruited to integrin-rich sites in spreading cells. *Mol Cell Biol* **19**: 2425-2434.
- Ulvmar MH, Martinez-Corral I, Stanczuk L, Makinen T. 2016. Pdgfrb-Cre targets lymphatic endothelial cells of both venous and non-venous origins. *Genesis* **54**: 350-358.
- Urner S, Kelly-Goss, Peirce SM, Lammert. 2017. Mechanotransduction in blood and lymphatic vascular development and disease. *Adv Pharmacol*. In press.
- Veikkola T, Jussila L, Makinen T, Karpanen T, Jeltsch M, Petrova TV, Kubo H, Thurston G, McDonald DM, Achen MG et al. 2001. Signalling via vascular endothelial growth factor receptor-3 is sufficient for lymphangiogenesis in transgenic mice. *EMBO J* **20**: 1223-1231.
- Velyvis A, Yang Y, Wu C, Qin J. 2001. Solution structure of the focal adhesion adaptor PINCH LIM1 domain and characterization of its interaction with the integrin-linked kinase ankyrin repeat domain. *J Biol Chem* **276**: 4932-4939.
- von der Weid PY, Zawieja DC. 2004. Lymphatic smooth muscle: the motor unit of lymph drainage. *Int J Biochem Cell Biol* **36**: 1147-1153.
- Vuorio T, Nurmi H, Moulton K, Kurkipuro J, Robciuc MR, Ohman M, Heinonen SE, Samaranyake H, Heikura T, Alitalo K et al. 2014. Lymphatic vessel insufficiency in hypercholesterolemic mice alters lipoprotein levels and promotes atherosclerosis. *Arterioscler Thromb Vasc Biol* **34**: 1162-1170.
- Vuorio T, Tirronen A, Yla-Herttuala S. 2017. Cardiac Lymphatics - A New Avenue for Therapeutics? *Trends Endocrinol Metab* **28**: 285-296.

- Walls JR, Coultas L, Rossant J, Henkelman RM. 2008. Three-dimensional analysis of vascular development in the mouse embryo. *PLoS One* **3**: e2853.
- Wang JF, Zhang XF, Groopman JE. 2001. Stimulation of beta 1 integrin induces tyrosine phosphorylation of vascular endothelial growth factor receptor-3 and modulates cell migration. *J Biol Chem* **276**: 41950-41957.
- Wang Y, Nakayama M, Pitulescu ME, Schmidt TS, Bochenek ML, Sakakibara A, Adams S, Davy A, Deutsch U, Luthi U et al. 2010. Ephrin-B2 controls VEGF-induced angiogenesis and lymphangiogenesis. *Nature* **465**: 483-486.
- White DE, Coutu P, Shi YF, Tardif JC, Nattel S, St Arnaud R, Dedhar S, Muller WJ. 2006. Targeted ablation of ILK from the murine heart results in dilated cardiomyopathy and spontaneous heart failure. *Genes Dev* **20**: 2355-2360.
- Wickstrom SA, Lange A, Hess MW, Polleux J, Spatz JP, Kruger M, Pfaller K, Lambacher A, Bloch W, Mann M et al. 2010a. Integrin-linked kinase controls microtubule dynamics required for plasma membrane targeting of caveolae. *Dev Cell* **19**: 574-588.
- Wickstrom SA, Lange A, Montanez E, Fassler R. 2010b. The ILK/PINCH/parvin complex: the kinase is dead, long live the pseudokinase! *EMBO J* **29**: 281-291.
- Widmaier M, Rognoni E, Radovanac K, Azimifar SB, Fassler R. 2012. Integrin-linked kinase at a glance. *J Cell Sci* **125**: 1839-1843.
- Wigle JT, Harvey N, Detmar M, Lagutina I, Grosveld G, Gunn MD, Jackson DG, Oliver G. 2002. An essential role for Prox1 in the induction of the lymphatic endothelial cell phenotype. *EMBO J* **21**: 1505-1513.
- Wigle JT, Oliver G. 1999. Prox1 function is required for the development of the murine lymphatic system. *Cell* **98**: 769-778.
- Wiig H, Swartz MA. 2012. Interstitial fluid and lymph formation and transport: physiological regulation and roles in inflammation and cancer. *Physiol Rev* **92**: 1005-1060.
- Xu Y, Yuan L, Mak J, Pardanaud L, Caunt M, Kasman I, Larrivee B, Del Toro R, Suchting S, Medvinsky A et al. 2010. Neuropilin-2 mediates VEGF-C-induced lymphatic sprouting together with VEGFR3. *J Cell Biol* **188**: 115-130.
- Xu Z, Fukuda T, Li Y, Zha X, Qin J, Wu C. 2005. Molecular dissection of PINCH-1 reveals a mechanism of coupling and uncoupling of cell shape modulation and survival. *J Biol Chem* **280**: 27631-27637.
- Yamaji S, Suzuki A, Kanamori H, Mishima W, Yoshimi R, Takasaki H, Takabayashi M, Fujimaki K, Fujisawa S, Ohno S et al. 2004. Affixin interacts with alpha-actinin and mediates integrin signaling for reorganization of F-actin induced by initial cell-substrate interaction. *J Cell Biol* **165**: 539-551.
- Yamaji S, Suzuki A, Sugiyama Y, Koide Y, Yoshida M, Kanamori H, Mohri H, Ohno S, Ishigatsubo Y. 2001. A novel integrin-linked kinase-binding protein, affixin, is involved in the early stage of cell-substrate interaction. *J Cell Biol* **153**: 1251-1264.
- Yang Y, Garcia-Verdugo JM, Soriano-Navarro M, Srinivasan RS, Scallan JP, Singh MK, Epstein JA, Oliver G. 2012. Lymphatic endothelial progenitors bud from the cardinal vein and intersomitic vessels in mammalian embryos. *Blood* **120**: 2340-2348.
- Yang Y, Oliver G. 2014. Development of the mammalian lymphatic vasculature. *J Clin Invest* **124**: 888-897.
- Yang Y, Wang X, Hawkins CA, Chen K, Vaynberg J, Mao X, Tu Y, Zuo X, Wang J, Wang YX et al. 2009. Structural basis of focal adhesion localization of LIM-only adaptor PINCH by integrin-linked kinase. *J Biol Chem* **284**: 5836-5844.
- Yao LC, Baluk P, Srinivasan RS, Oliver G, McDonald DM. 2012. Plasticity of button-like junctions in the endothelium of airway lymphatics in development and inflammation. *Am J Pathol* **180**: 2561-2575.
- Yuan L, Moyon D, Pardanaud L, Breant C, Karkkainen MJ, Alitalo K, Eichmann A. 2002. Abnormal lymphatic vessel development in neuropilin 2 mutant mice. *Development* **129**: 4797-4806.
- Zarkada G, Heinolainen K, Makinen T, Kubota Y, Alitalo K. 2015. VEGFR3 does not sustain retinal angiogenesis without VEGFR2. *Proc Natl Acad Sci U S A* **112**: 761-766.
- Zawieja DC. 2009. Contractile physiology of lymphatics. *Lymphat Res Biol* **7**: 87-96.
- Zeeb M, Axnick J, Planas-Paz L, Hartmann T, Strilic B, Lammert E. 2012. Pharmacological manipulation of blood and lymphatic vascularization in ex vivo-cultured mouse embryos. *Nat Protoc* **7**: 1970-1982.
- Zervas CG, Gregory SL, Brown NH. 2001. Drosophila integrin-linked kinase is required at sites of integrin adhesion to link the cytoskeleton to the plasma membrane. *J Cell Biol* **152**: 1007-1018.
- Zhang X, Groopman JE, Wang JF. 2005. Extracellular matrix regulates endothelial functions through interaction of VEGFR-3 and integrin alpha5beta1. *J Cell Physiol* **202**: 205-214.

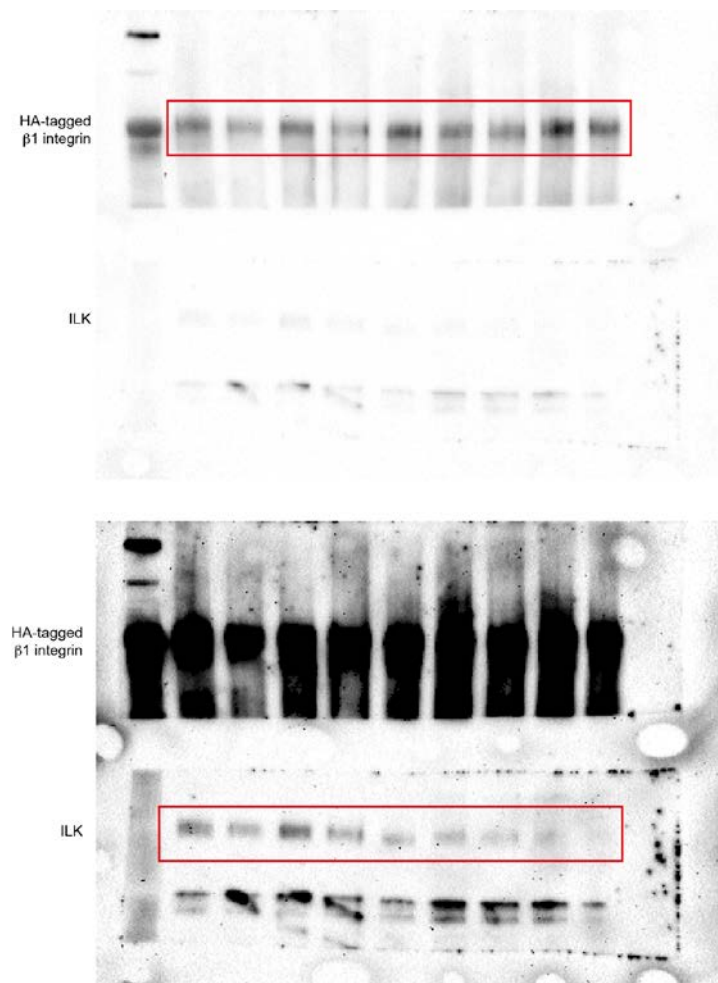
- Zhang Y, Chen K, Guo L, Wu C. 2002a. Characterization of PINCH-2, a new focal adhesion protein that regulates the PINCH-1-ILK interaction, cell spreading, and migration. *J Biol Chem* **277**: 38328-38338.
- Zhang Y, Chen K, Tu Y, Velyvis A, Yang Y, Qin J, Wu C. 2002b. Assembly of the PINCH-ILK-CH-ILKBP complex precedes and is essential for localization of each component to cell-matrix adhesion sites. *J Cell Sci* **115**: 4777-4786.
- Zhou F, Chang Z, Zhang L, Hong YK, Shen B, Wang B, Zhang F, Lu G, Tvorogov D, Alitalo K et al. 2010. Akt/Protein kinase B is required for lymphatic network formation, remodeling, and valve development. *Am J Pathol* **177**: 2124-2133.
- Zong H, Bastie CC, Xu J, Fassler R, Campbell KP, Kurland IJ, Pessin JE. 2009. Insulin resistance in striated muscle-specific integrin receptor beta1-deficient mice. *J Biol Chem* **284**: 4679-4688.

## 9. Supplementary information

Fully unedited gel images used for representative Western Blot images in this thesis:



**Supplementary Figure 1: Unedited gel used for Figure 27.** Cropped region used for representative image is indicated by red framing.



**Supplementary Figure 2: Unedited gel used for Figure 31.** Cropped regions used for representative image are indicated by red framing.

## Statutory declaration

I hereby declare that I wrote the dissertation "Role of integrin-linked kinase (ILK) in VEGFR3 signaling and lymphatic vascular growth" independently and without other resources as indicated in compliance with "Grundsätze zur Sicherung guter wissenschaftlicher Praxis an der Heinrich-Heine Universität Düsseldorf".

Furthermore, I declare that I did not submit this dissertation, either in full or in part, to any other academic institution and did not absolve any promotion trials before.

Düsseldorf,

---

Sofia Urner

## Eidesstattliche Erklärung

Ich versichere an Eides Statt, dass die Dissertation „Rolle der integrin-linked kinase (ILK) in der Signalaktivierung von VEGFR3 sowie im Lymphgefäßwachstum“ von mir selbstständig und ohne unzulässige fremde Hilfe unter Beachtung der „Grundsätze zur Sicherung guter wissenschaftlicher Praxis an der Heinrich-Heine Universität Düsseldorf“ erstellt worden ist.

Darüber hinaus versichere ich, dass ich die Dissertation weder in der hier vorgelegten noch in einer ähnlichen Form bei einem anderen Institut eingereicht habe und bisher keine Promotionsversuche unternommen habe.

Düsseldorf, den

---

Sofia Urner

## Danksagung

Abschließend möchte ich mich recht herzlich bei meinem Doktorvater Ecki bedanken, der mir die Möglichkeit gegeben hat, diese Arbeit in seinem Institut anzufertigen. Vielen Dank für die jahrelange Unterstützung und die fachlichen Anregungen sowie für die Gelegenheit, dass ich mich wissenschaftlich sowie menschlich mit seiner Unterstützung weiterentwickeln konnte.

Ich danke Axel für die Übernahme des Zweitgutachters sowie für die zahlreichen wissenschaftlichen Diskussionen und dafür, dass er immer ein offenes Ohr hatte.

Außerdem möchte ich mich bei allen aktuellen und ehemaligen Mitgliedern des Instituts für Stoffwechselphysiologie bedanken, die mir stets mit Rat und Tat zur Seite standen und die den Laboralltag so angenehm gemacht haben. Besonders danken möchte ich Silke und Barbara für ihre technische Unterstützung, sowie Daniel für seine fachlichen Beratungen. Ich danke Jessi für die regelmäßigen spätabendlichen Besprechungen. Vielen Dank auch an Anna und Carina für ihre Hilfe. Und ganz besonders möchte ich mich bei Lara und Laura für die tolle Zusammenarbeit bedanken!

I would also like to thank Shayn and the Department for Biomedical Engineering for the great research stay at the UVA in Charlottesville, and for making me feel being part of the lab. Thanks also to Anthony who always helped me with technical issues. Especially, I would like to thank Molly for such a great collaboration and for having so much fun in lab - but also for being such a wonderful friend!

Ich möchte mich bei dem gesamten IRTG1902 bedanken für die Möglichkeit, ein Teil dieses großartigen Austauschprogramms zu sein. Mein besonderer Dank gilt Sandra für ihre Unterstützung!

Ich möchte mich weiterhin besonders bei Nicky und Nenja bedanken, die mir über die Forschung hinaus als wundervolle Freunde jederzeit zur Seite standen! Vielen Dank für die wundervolle Zeit, die wir zusammen in Düsseldorf als auch in Charlottesville verbracht haben!

Ein besonderer Dank gilt allen meinen Freunden und ganz besonders Irene für ihre jahrelange Freundschaft und Unterstützung.

Zuletzt möchte ich mich aus tiefstem Herzen bei meinem Ehemann Marc und meiner Familie, ganz besonders bei meiner Mutter bedanken! Danke, dass ihr mich so bedingungslos unterstützt habt, mich motiviert habt und immer an mich geglaubt habt!